SYNTHESIS AND CHARACTERIZATION OF Fe_3O_4 LOADED CALCIUM SILICATE HYDRATE COMPOSITE FOR REMOVAL OF NITRATE FROM WATER

Shimeles Nigussie Abate

A Thesis Submitted to the Department of Chemical Engineering
School of Mechanical, Chemical and Materials Engineering

Presented in Partial Fulfillment of the Requirement for the Degree of Master's in Chemical Engineering (Specialization in Process Engineering)

Office of Graduate Studies
Adama Science and Technology University

February, 2022
Adama, Ethiopia

SYNTHESIS AND CHARACTERIZATION OF Fe_3O_4 LOADED CALCIUM SILICATE HYDRATE COMPOSITE FOR REMOVAL OF NITRATE FROM WATER

Shimeles Nigussie Abate

Advisors: 1. Dr. Mulugeta Yilma

2. Dr. Melaku Tesfaye

A Thesis Submitted to the Department of Chemical Engineering
School of Mechanical, Chemical and Materials Engineering

Presented in Partial Fulfillment of the Requirement for the Degree of Master's in Chemical Engineering (Specialization in Process Engineering)

Office of Graduate Studies
Adama Science and Technology University

February, 2022
Adama, Ethiopia

Declaration

I hereby declare that this Master Thesis entitled **"Synthesis and characterization of Fe_3O_4 loaded Calcium Silicate Hydrate composite for removal of Nitrate from Water"** is my original work. That is, it has not been submitted for the award of any academic degree, diploma, or certificate in any other university. All sources of materials that are used for this thesis have been duly acknowledged through citation.

Shimeles Nigussie Abate _____ _____

Name of the Student Signature Date

Recommendation

We, the advisors of this thesis, hereby certify that we have read the revised version of the thesis entitled "**Synthesis and characterization of Fe_3O_4 loaded Calcium Silicate Hydrate composite for removal of Nitrate from Water"** prepared under our guidance by Shimeles Nigussie Abate submitted in partial fulfillment of the requirements for the degree of Mater's of Science in Chemical Engineering. Therefore, we recommend the submission of the revised version of the thesis to the department following the applicable procedures.

Mulugeta Yilma (PhD)	_____	_____
Major Advisor	Signature	Date
Melaku Tesfaye (PhD)	_____	_____
Co-advisor	Signature	Date

Approval Page of M.Sc. Thesis

We, the advisors of the thesis entitled **" Synthesis and characterization of Fe_3O_4 loaded Calcium Silicate Hydrate composite for removal of Nitrate from water''** and developed by Shimeles Nigussie Abate, hereby certify that the recommendation and suggestions made by the board of examiners are appropriately incorporated into the final version of the thesis.

Mulugeta Yilma (PhD)	_____	_____
Major Advisor	Signature	Date
Melaku Tesfaye (PhD)	_____	_____
Co-advisor	Signature	Date

We, the undersigned, members of the Board of Examiners of the thesis by Shimeles Nigussie Abate have read and evaluated the thesis entitled **"Synthesis and characterization of Fe_3O_4 loaded Calcium Silicate Hydrate composite for removal of Nitrate from Water''** and examined the candidate during the open defense. This is, therefore, to certify that the thesis is accepted for partial fulfillment of the requirement of the degree of Master of Science in Chemical Engineering.

_____	_____	_____
Chairperson	Signature	Date
_____	_____	_____
Internal Examiner	Signature	Date
Dr. Wondalem Misganaw	_____	14-03-2022
External Examiner	Signature	Date

Finally, approval and acceptance of the thesis is contingent upon submission of its final Copy to the Office of Postgraduate Studies (OPGS) through the Department Graduate Council (DGC) and School Graduate Committee (SGC).

_____	_____	_____
Department Head	Signature	Date
_____	_____	_____
School Dean	Signature	Date
_____	_____	_____
Office of Postgraduate Studies, Dean	**Signature**	**Date**

DEDICATION

This Thesis is dedicated to in loving memory of my beloved brother Lieutenant Colonel Abu Nigussie who gave his life for his country. My hero you are always in my heart. I also dedicate this research work to my beloved mother Birki Koru Yadete and my father Nigussie Abate. Your endless support, encouragement, appreciated sacrifice, and constant love have sustained me in success throughout my life.

AKNOWLEDGMENT

First of all, I would love to provide my immensely thanks to Almighty God for blessing me with achievements throughout my study, and for granting me with strength, power, and good health to attain my ambition. I would really like to express my genuine gratitude to my advisors Dr. Mulugeta Yilma and Dr. Melaku Tesfaye for their continuous guidance, indispensable comments, encouragement, support and excellent supervision throughout my research work. Thank you for generously sharing your time, and for all your support to succeed this research.

I would like to extend my acknowledgment to my brother Kebede Abu for unreserved help and useful advice throughout this study. I would like to thank Alemu Gizaw (PhD candidate) for his valuable guidance, and kindly support me in completing the laboratory analysis work at Addis Ababa University. My thanks to all Academic and Research Assistants of Chemical engineering department, Mr. Demeke from Material science and engineering at Adama science and Technology University, and Mr. Alebel Abebawu from Bahir Dar University. This thesis would not have been possible without the inspiration and support of a number of wonderful individuals. Thank you all of my friends for being part of this journey and making this thesis possible.

Finally, my deep and sincere gratitude to my family as whole for their continuous support, unparalleled love, help, and understanding me during thesis work. I am grateful to my beloved brothers Meketaw Nigussie and Lieutenant Colonel Abu Nigussie for always there for me, thank you for everything you have done for me.

Table of Contents

LIST OF TABLES

LIST OF FIGURES

LIST OF ABREVATIONS

AAS	Atomic Absorption Spectroscopy
BAT	Best Available Technology
CCD	Central Composite Design
CSH	Calcium Silicate Hydrate
DTG	Derivative Thermogravimetric
ED	Electrodialysis
Fe_3O_4	Magnetite (Ferrous-ferric Oxide)
FTIR	Fourier-Transform Infrared Spectroscopy
FWHM	Full Width at Half Maximum
IX	Ion Exchange
MCL	Maximum Contaminated Level
MCSH	Magnetic Calcium Silicate Hydrate
MNP	Magnetic Nano particle
nZVI	Nano Scale Zero-valent
ONE	Organic Nitrogen Elimination
RO	Reverse Osmosis
RSM	Response Surface Methodology
SBA	Strong Base Anion
SEM	Scanning Electron Microscopy
SWR	Solid Waste Residue
TGA	Thermogravimetric analysis
XRD	X- Ray Diffraction

ABSTRACTS

The presence of an excess nitrate ion in the human body leads to various health problems. The increased nitrate level may be a result of different human activities such as the huge amount of fertilizer in agriculture activities, industrial and household wastewaters. Therefore, the removal of nitrate ions to the lowest concentration in drinking water and wastewater is crucial. Physical and Biological technologies have been used for nitrate removal. However, those treatment technologies have limitations regarding cost and complex operations in achieving the required concentration level. The adsorption process is the best among other technologies due to simple design, versatile, lowest cost for instrumentation, easy operation, sludge free, environmentally friendly, and regeneration. Hence, the aim of this work was synthesis and characterization of Fe_3O_4 loaded CSH composite for removal of nitrate ion from water. XRD, FTIR, SEM, BET, and TGA were used to characterize the crystalline structure, specific functional groups, morphological properties, specific surface area, and thermal stability. The chemical composition and structure of Fe_3O_4 loaded CSH and the successful surface loading of hydroxyl functional groups were confirmed. The BET specific surface area of CSH and Fe_3O_4 loaded CSH composite are determined to be 91m^2/g and 163 m^2/g respectively. Adsorption increase with the increase in the surface area of the adsorbent. Moreover, the optimization effects of adsorption parameters such as contact time, adsorbent dose, pH, and initial nitrate concentration have been carried out. The result confirmed that 92.71% of nitrate ion was removed from wastewater at optimum 150 min, 2.4 g adsorbent dose, the pH level of 6.3, and 85 mg/L of initial nitrate concentration. Furthermore, the adsorption parameters such as equilibrium isotherm, kinetics, and thermodynamic properties were conducted. The adsorption isotherm data were best fitted to the Langmuir with a maximum adsorption capacity of 27.93 mg/g. In addition, the result of the kinetic model proved that pseudo-second-order provided a good description of the experimental data with a maximum R^2 of 0.999. The result of the thermodynamic parameters demonstrated that the adsorption process is spontaneous and endothermic. The removal efficiency of 68.73% of nitrate ion was found after 4 cycles of desorption/adsorption cycles, which indicates wonderful reusability of the adsorbent. The result illustrates that Fe_3O_4 loaded CSH is an excellent promising adsorbent for the removal of nitrate ions.

Key Words: *Adsorption, Magnetic calcium silicate hydrate, Kinetics, Isotherm, nitrate*

CHAPTER ONE

INTRODUCTION

1.1. Background

Water is the greatest plentiful compound, which plays a substantial role in maintaining the well-being and welfare of human beings (Abegaz & Midekssa, 2021). Water is one of the foremost necessary substances on earth. All plants and animals should have water to survive. If there were no water, there would be no life exists on earth. It covers 71% of the Earth's surface, and is important for all famed kinds of life. However solely 2.5% of the Earth's water is freshwater (Rajasulochana & Preethy, 2016). However, its quality and appropriateness for use can be determined by its sense of taste, odor, color, and the concentration of organic and inorganic substances that originate in it.

The foundations of water contamination might be geological, industrial, and agricultural activities. In another way, these contaminants are further categorized as microorganisms, inorganics, organics, and radionuclides. They can disturb the quality of water and then human health before appropriate treatment. (Abegaz & Midekssa, 2021). Water bodies are those centered easily polluted by using the industries. Industrial effluents are the number one purpose for the pollution of water. Wastewater is not only best harmful to aquatic lifestyles but also even more dangerous to human existence. So, they are in a kingdom to be effectively handled before letting into the environment (Velusamy et al., 2021).

The increment in the world population growth, development of industrialization, agricultural activities, and excessive use of chemical products provide the environmental pollution. Organic, inorganic, and biological waste produced by human activities has resulted in a huge amount of water contamination which directly harms human and other living things (Sadegh et al., 2019). Since the end of the last century, there have been many products, such as medicines, laundry detergents, surfactants, pesticides, dyes, paints, preservatives, food additives, and personal care products, which have been released from chemical and pharmaceutical industries threatening the environment and human health. The removal of emerging contaminants of concern is now, as ever important in the production of safe drinking water and the environmentally responsible release of wastewater (Grassi et al., 2012). The major sources of nitrates in both surface and groundwater include using fertilizers for agricultural activities, industrial and household

wastewaters (Battas et al., 2019). Nitrate contamination of drinking water sources, particularly groundwater, primarily from agricultural activities (including excessive use of nitrogen fertilizers and manure), wastewater treatment, and the oxidation of nitrogen waste in human and animal waste, including septic tanks, has become an important global problem(Rezvani et al., 2019). Ground and surface water are extremely polluted by different nitrogen compounds like nitrites and nitrates. The contamination of groundwater by nitrate has become a serious environmental problem that has increased since 1970 (El Ouardi et al., 2015).

Over the years, many parts of the world have faced the problem of environmental nitrogen pollution. As you know, the main forms of nitrogen are ammonia (NH_3), nitrate (NO_3^-), and nitrite (NO_2). The huge release of nitrogen compounds into the environment is one of the greatest problems of this time. Nitrogen compounds such as nitrogen oxides and ammonia pollute the environment in many complex ways and threaten human health. Eutrophication and acidification of nitrogen are contributing factors to the loss of biodiversity. Atmospheric nitrogen oxides contribute to surface ozone, forming ammonia and harmful particulates that will directly affect human health. Nitrates in beverages and food pose a threat to human health. Nitrosamine is suspected to be carcinogenic. Nitrous oxide destroys the ozone layer and leads to climate change (German et al., 2015).

Nitrate is the most stable form of nitrogen in the water, so almost all aqueous nitrogen sources tend to be converted to nitrate. Nitrate (NO_3^-) is the most concerned topic in the world. Due to its high solubility in water, Nitrate may be the most widely distributed groundwater pollutant in the world, posing a serious threat to the drinking water supply and promoting eutrophication. The increased NO_3^- level may be related to various human activities, especially the large-scale use of chemical fertilizers in agriculture, leading to high nitrate contamination of ground and surface water sources (Ganesan et al., 2013).

Nitrate ions are needed to nourish plants, but when they occur excessively, they present serious environmental problems. Eutrophication may be accelerated in the presence of high concentrations of nitrate in groundwater and surface water together. Eutrophication is the excessive nutrient enrichment of rivers and lakes that stimulates the growth of birds and aquatic plants with roots. Eutrophication can alter the overall aquatic ecosystem, reducing light penetration into the water, and reducing vegetation in deeper waters. The higher concentration of nitrate in the water, the more the dissolved oxygen tends to

decrease. Therefore, it has a negative impact on the lives of aquatic organisms such as fish and shrimp, and requires oxygen in the water(Hai & Bui, 2013).

Protecting the environment is the first preoccupation for every society. Specifically, the problems of water contamination have become the task of all professionals, researchers, industry, scientists as well as national and international decision-makers. The contamination of water by various pollutants like nitrates calls for numerous treatment methods which are not only technologically feasible but also effective and economical (Crini et al., 2019). Adsorption process is considered to be the best method of water purification process due to its very simple design, ease of operation, convenient maintenance, easy repair, and advances in construction technology for high-capacity adsorbents (Asl et al., 2016).

1.2. Statement of the Problem

The occurrence of huge concentrations of nitrate in potable water has gotten to be a genuine concern around the world. In water it creates inorganic compounds; mainly nitrate ions, nitrite, and ammonium. In these forms, it occurs in drinking water as well as in the surface or underground water (Gierak & Łazarska, 2017). The presence of nitrogen ions in excess in different forms results in negative effects on the ecosystem, and can damage human health, and even kill (Ganesan et al., 2013). It leads to various health problems such as cancer, stomach problem, gastrointestinal, birth defects, abortion, methemoglobinemia or blue baby syndrome, increase infant mortality, and deterioration of immune system (Brindha et al., 2017). If babies under six months of age drink water with a high content of nitrate, this nitrate could be reduced to nitrite, and nitrite will combine with hemoglobin in the blood to form methemoglobin. This in turn leads to a health condition commonly referred to as "Blue Baby Syndrome"(Ruiz-Beviá & Fernández-Torres, 2019).

As a result, numerous organizations have set allowable contamination level for the nitrate content material in drinking water. For example, the United States of America Environmental protection agency (USEPA) has installed a maximum contaminant level (MCL) of 10 mg nitrate-nitrogen (NO_3− –N)/L. In the other case, the world Health Organization (WHO) and European Economic Network (EEC) have set up 11.3 mg NO_3^- –N/L limit (Rezvani et al., 2019). The study of nitrate in the drinking water showed maximum concentration of 69.6 and 327.3 mg/L in spring and well water in Addis Ababa

respectively. In addition, groundwater contamination by nitrates at African scale reported that 117-260 NO_3^- (mg/L) concentration at central and south east of Ethiopia (Temesgen Getahun, 2019).

Different physiochemical techniques have been employed to remove nitrates from the water. Adsorption proved to be the best technique among all due to its low cost, ease of operation, highest removal efficiency, fantastic reusability performance, and efficient method (Alagha et al., 2020). Nowadays, Fe_3O_4 loaded calcium silicate hydrate is used as a functional material, particularly adsorbent because of their high specific surface area and huge structural sites with porous structures. Previous studies reports the magnetic Calcium Silicate Hydrate synthesized using a Tetraethyl orthosilicate (TEOS), white carbon black (SiO_2), and sodium silicate purchased from the market as a source of silicate material. In addition, Magnetic calcium silicate hydrate adsorbent was used for phosphate, and uranium removal from aqueous systems (Zhang et al., 2015), (Peng et al., 2017). However, in this work Aluminium sulfate solid waste residue of Awash Melkassa Chemical Factory was used as a silicate source, which is low-cost, abundant, and locally available. There is no work reported on Fe_3O_4 loaded CSH composite for nitrate removal from water.

1.3. Basic Research Questions

1. Is it possible to convert Aluminium sulfate solid waste residue of Awash Melkassa Chemical factory into valuable products particularly adsorbent?

2. What is the best Fe_3O_4 to CSH composite composition to develop a novel adsorbent that gives maximum nitrate removal from wastewater?

3. Is loading of Fe_3O_4 to Calcium Silicate Hydrate adsorbent become helpful for nitrate removal from water?

4. What are the optimum parameters such as pH, adsorbent dose, contact time, and initial nitrate concentration for nitrate removal?

1.4. Objectives

1.4.1. General Objective

The main objectives of this thesis was synthesis and characterization of Fe_3O_4 loaded Calcium Silicates Hydrate composite as an Adsorbent for Nitrates removal from water.

1.4.2. Specific Objectives

- Synthesis and Characterization of CSH using XRD, FTIR,BET, and SEM
- Investigation of the effect of adsorbent dose, initial Nitrate concentration, pH of the solution, and contact time on nitrates removal using calcium silicate hydrate adsorbent.
- Synthesis and characterize Fe_3O_4 Loaded calcium silicate hydrate composite using XRD, BET, SEM, TGA, FTIR and investigate adsorption capacity for nitrate removal
- Explore the adsorption kinetics, equilibrium isotherm, and thermodynamics effect using batch adsorption experimental data
- To study adsorbent regeneration, and coexisting of ions within nitrate in wastewater

1.5. Significance of the Study

Industrial waste residue, produced during the manufacturing of Aluminium sulfate (alum) from kaolin by the presence of sulfuric acid is highly acidic (pH about 3) and is considered hazardous. A large amount of solid waste residue is estimated as 4500-5000 tonnes of waste accumulated in Awash Melkassa Chemical Factory, Ethiopia(Nigussie et al., 2007). The advantage of this research was converting this byproduct to valuable products, particularly adsorbent.

In this study aluminium sulfate solid waste residue, which exists in Awash Melkassa Chemical Factory, is used as raw material to produce calcium silicate hydrate as an adsorbent. Fe_3O_4 loaded CSH composite adsorbent was produced by utilizing Alum factory solid waste residue, which has an excellent removal efficiency and adsorption capacity of nitrates that can exist in waters. The study provides basic information about the adsorption of nitrate ions from water. The removal of nitrate ions by using low-cost adsorbents from industrial waste residue is found to be promising in the long term due to the adsorbent product obtained from material locally and abundantly available in Ethiopia. The other benefit of this study is replacing the expensive commercial adsorbents with easily available and low-cost adsorbents.

1.6. Scope of the study

This thesis focused on the synthesis and characterization of Fe_3O_4 loaded calcium silicate hydrate as an adsorbent for the removal of nitrates from water. The XRD, SEM, TGA, BET, and FTIR were used to characterize the Fe_3O_4 loaded calcium silicate hydrate. Furthermore, adsorption studies of various effects such as adsorbent dose, initial nitrate concentration, pH, and contact time on nitrate removal by CSH were investigated. In addition, adsorption kinetics, adsorption isotherm, adsorption thermodynamics, and regeneration were conducted. Not only the effect of co-existing ion within nitrate ion but also the performance of Fe_3O_4 loaded calcium silicate hydrate composite for real wastewater studied in this work.

CHAPTER TWO

LITERATURE REVIEW

2.1. Nitrate ions

Nitrates are inorganic compounds that occur in a variety of conditions in the environment, both in nature and synthetically. Nitrate is made up of one nitrogen atom (N) and three oxygen atoms (O), and the chemical symbol for nitrate is NO_3. Nitrite (NO_2) is formed from nitrates by a chemical process called reduction. The anion is the conjugate base of nitric acid, producing one central nitrogen atom surrounded by three similar bonded oxygen atoms in a triangular planar arrangement. The nitrate ion has a type -1 charge. This charge arises from the combination of the formal charge carrying the three oxygen +2/3 charges, but with the nitrogen +1 charge, all this becomes the formal charge of the polyatomic nitrate ion (Dey et al., 2021).

Nitrate is an example of a worldwide pollutant because it is repelled by negatively charged colloids and has high solubility. If its concentration is not appropriate for water resources, it poses many health and ecological threats (I. Ibrahim & Bsharat, 2018). Nitrates are one among the most common groundwater pollutants in rural areas. The quality of drinking water is primarily prescribed because excessive amounts can cause methemoglobinemia or "blue baby" disease. Nitrates in groundwater mainly come from fertilizers, septic tanks, fertilizer storage, or diffusion operations. Potential cancer risks from nitrates (or nitrites) in water and food have been reported. Nitrates can react with amines or amides in the body to form nitrosamines, which are known to cause cancer. Nitrate must be converted to nitrite before forming nitrosamine. The magnitude of cancer risk from nitrates in drinking water is unknown. As Nitrate, Phosphate affect the growth of aquatic plants, it has the same effect on water quality. Plant and algae are stimulated to feed the fish. This has the potential to increase the fish population. However, with severe algae, the oxygen level in the water decreases along with the growth, and the fish die (Dey et al., 2021).

Pollution with nitrite (NO_2^-) and nitrate (NO_3^-) predominantly arises from the overuse of ammonia-primarily based totally fertilizers for meals production. Because of their agricultural use and the water-soluble nature of nitrate, the worst nitrate pollutants are in rural areas, wherein ingesting water structures are small-scale or man or woman groundwater wells. Nitrate run-off in floor waters contributes to eutrophication and the

boom of massive algal blooms, which damage water quality, make contributions to cyanobacteria boom, effect leisure activities, and creates hypoxic lifeless zones (Heck et al., 2019). Nitrate contamination in both surface and groundwater is a serious problem all over the globe (Sun et al., 2020). Due to its high-water solubility, it is widespread as a groundwater contaminant in the world which imposes a threat to drinking water supplies, and promotes eutrophication (El Ouardi et al., 2015). The natural nitrate in groundwater depends on the nature of the soil and geology (Fewtrell, 2004).

2.2. Major Uses and sources of Nitrates

The main sources of nutrient contamination are fertilizer, animal manure, wastewater from sewage treatment plants, detergents, storm water runoff, breakdowns in automobiles and power plants, septic tanks, and pet excrement. Nitrate is mainly used for inorganic fertilizers and in the production of oxidants and explosives, and refined saltpeter (potassium nitrate) is use in the production of glass. Sodium nitrite is especially used as a food preservative for preserved meat. In addition, sometimes nitrate can be added to food and acts as a reservoir for nitrite. Nitrate occurs naturally in plants, which are the main nutrients. Nitrates and nitrites formed endogenously in mammals, including humans. Nitrate is salivated and converted to nitrite by the oral microbial flora(Velusamy et al., 2021).

Meat products make up less than 10% of the nitrates in the diet, but between 60 and 90% of the nitrites are consumed. This is mainly due to the addition of sodium nitrite to foods such as hot dogs, bacon, and ham. Fruits, grains, and dairy products give very little nitrates and nitrites to people's diets. It is often difficult to specify a source of nitrate because there are so many possibilities. Sources of nitrogen and nitrates can include runoff or infiltration from fertile farmland, municipal and industrial wastewater, garbage disposal plants, animal septic tanks, private sewage purification systems, municipal wastewater, and decaying plant debris. Stratum and groundwater flow direction also affect nitrate concentration(Dey et al., 2021).

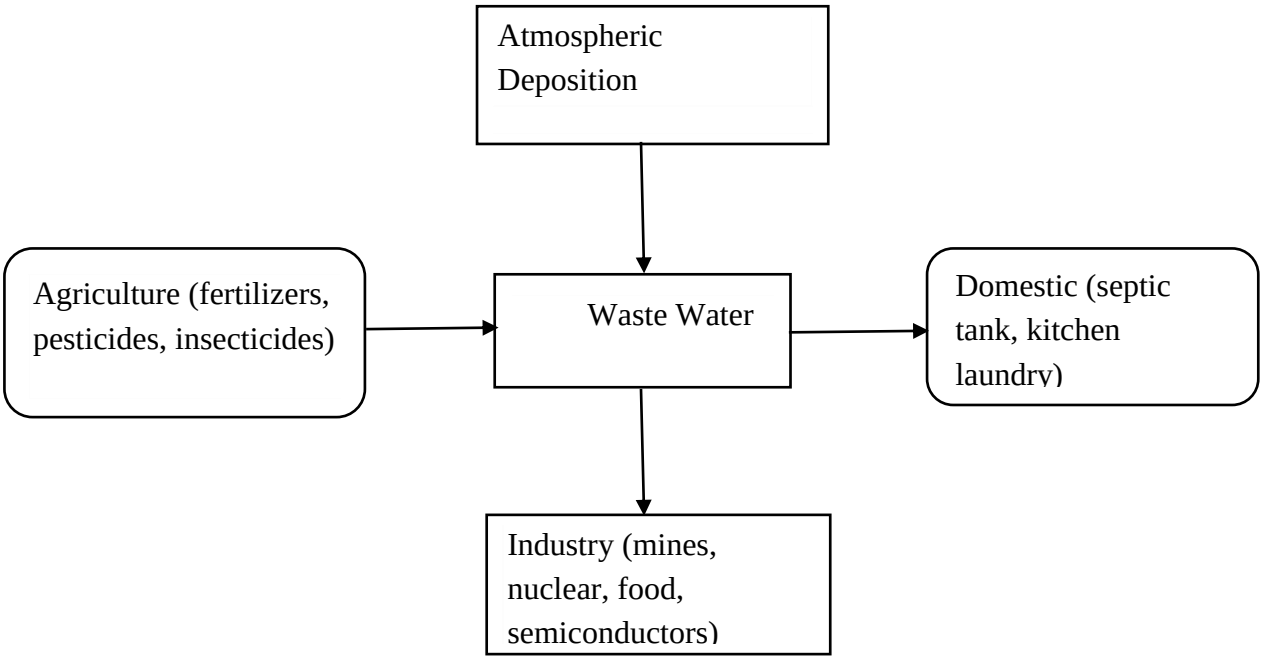

Figure 2. 1: Four main sources of wastewater

Domestic wastewaters encompass wastes, which can be generated in all sorts of family works along with washing, cleaning, bathing, sewage machine, septic device, and trash scrapyards. Business wastewaters include effluents coming from industries together with mining and smelting, pigment and dye, metallurgy, tannery, electroplating, galvanizing, paint, petrochemical, pharmaceutical, biochemical, textile, leather-based, steel completing, processing of meat and dairy merchandise, nuclear and car exhaust and construct structures. Moreover, agricultural wastewaters come from animal waste, irrigation, fodder used for animals, manures, use of fertilizers, pesticides, herbicides, insecticides on stay inventory farms, and food flora and wood preservatives(Velusamy et al., 2021). Atmospheric deposition consists of the decomposition of decaying organic matters and hurricane runoffs.

Nitrogen is plenteous on soil, making up about 80 % of our air as N_2 gas and most plants cannot utilize nitrogen in a vaporous frame. Nevertheless, Bluegreen algae and vegetables have the capacity to convert N_2 gas into nitrate (NO_3^-), which can be utilized by plants. Plants utilize nitrate to construct protein, and animals that eat plants to utilize natural nitrogen to build protein. When plants and creatures kick the bucket or excrete squander, this nitrogen is discharged into the environment as NH_4^+ (ammonium). Ammonium is eventually oxidized into nitrite (NO_2^-) by microbes, and at that point into nitrate, which is

liberally found in a freshwater oceanic biological systems. US EPA gives 10 mg/L as the greatest concentration permitted in human drinking water, As per BIS IS 10500: 2012, of India, the worthy constrain of nitrate in drinking water is 45 mg/L and no unwinding for nitrate within the nonattendance of substitute sources. The World Wellbeing organization and the European Standards have endorsed 50 mg/L of acceptable nitrate levels in drinking water (Rakshitha R, 2017).

2.3. Health effects of Nitrate

Nitrates are a wide range of contaminants for their high solubility and pose a threat to human health. High concentrations of nitrates can cause several health problems, including blue baby syndrome in infants and methemoglobinemia, bloody or urinating, abdominal pain, weakness, mental depression, vomiting, diabetes, diarrhea, high blood pressure, disruption of the immune system, and increased infant mortality. There are also spontaneous abortions and respiratory infections In addition, Elevated nitrate levels in drinking water can also cause various types of cancer in humans (Nabhan, 2019).

2.4. Nitrate Pollution in Ethiopia

The highest concentration of nitrate in the water samples could be due to contamination from agricultural runoff, refuse dumps, human and animal waste. These days, nitrate contamination in groundwater has become a widely worried environmental problem in Ethiopia and the spatial distribution of nitrate indicated that the southeast and south part of the study area has the most nitrate concentration of 88 mg/L at Dire Dawa city administration (Temesgen Getahun, 2019). The highest concentration of nitrate was found in the water samples collected from Dire Dewa, Harari, Afar and some water samples collected from Addis Ababa, Amhara, and Oromia. Nitrate concentration in the water samples reached the maximum level of 1295.00 mg/L throughout the country (Teklu, 2018).

2.5. Methods of nitrate removal

Removing nitrates from drinking water using traditional treatment methods such as coagulation and filtration is nearly impossible due to the high stability and solubility of nitrates and the low likelihood of coprecipitation or adsorption in water. Industrial techniques for saltwater treatment include the removal of dissolved salt ions from wastewater, as different types of pollution of water and wastewater require different

strategies to remove the pollution. These techniques, known as separation-based methods and applied to remove nitrates from other types of water. However, these techniques cannot remove all ions in the medium and selectively remove nitrates. Industrial bio nutrient removal (called removal technology), which is applied to remove biodegradable organic matter from wastewater, can also be used as a method for selectively removing nitrates during the multipurpose treatment of water (Rezvani et al., 2019). World Health Organization (WHO) has suggested biological denitrification and IX as nitrate removal methods; whereas the US EPA endorses IX, RO, and ED are the Best Available Technologies (BAT) to treat NO_3^- sullied water. Nevertheless, currently available advances for NO_3^- expulsion have their own quality and restrictions, which are found to be expensive, less effective, and create extra byproducts. However, these traditional technologies do not illuminate the issue related to the excess of NO_3^- within the environment; in turn, they generate NO_3^- concentrated squander streams that pose a transfer issue due to the high saline substance (Rakshitha R, 2017).

2.5.1. Separation-based technologies for nitrate removal

Different techniques have been applied to remove nitrate. The traditional methods of removing nitrogen from wastewater are biological denitrification processes, ion exchange (IX), reverse osmosis (RO), Electrodialysis (ED), and chemical denitrification. The first four of these methods have been applied to the industry(Hai & Bui, 2013).

2.5.1.1. Reverse osmosis

Reverse osmosis (RO) can be used to simultaneously combat multiple contaminants, including ionic (nitrate, arsenic, sodium, chloride, fluoride, etc.), particulate (such as asbestos and protozoan cysto), and organic components (such as some pesticides). In this process, water is forced through the semipermeable membrane under pressure and allows water to pass through the membrane without selection obstructs contaminants. The required pressure depends on the concentration of solute in the water supply. However, the collected concentrate contains high levels of nitrates and other rejected components (salt) and requires proper disposal (Rezvani et al., 2019).

Reverse osmosis (RO) is a physical process that removes contaminants by passing water molecules through a semipermeable membrane while retaining most of the dissolved minerals in raw water by applying pressure. For low-pressure (less than 100 psi) applications, only 10 to 25 percent of the raw water is produced as a finished product.

High-pressure systems can achieve more than 85% water efficiency, but this level of efficiency requires dedicated pumps and significant energy. RO is one of the most expensive forms of intensive care, removing multiple contaminants and the demand for beverages is very low.

In reverse osmosis (RO), water begins to go with the flow inside the reverse path with the application of pressure (750 psi) better than the price of osmotic pressure. The pressure required to force the permeation via the membrane is dictated by the osmotic pressure of the feed stream. Membranes are normally manufactured from materials consisting of cellulose acetate, polyamides, and composite materials. In actual practice, the process has been set with difficulties usually due to membrane fouling, high-priced power, large capital costs, and calls for treatment or disposal of concentrate. Similarly, some nitrate and phosphate ions escape through the membrane (performance approximately 65–95 %). The benefits of this technique are proper for waters with excessive TDS content, not by using merchandise, non-unfavorable (Ranjan et al., 2016).

2.5.1.2. Ion exchange

Conventional ion exchange (IX (the most common method of nitrate removal)) uses a strong base anion (SBA) exchange resin. During this process, the raw water is pretreated to remove suspended solids and other components that can contaminate the resin column. The receiving process flow enters the ion exchange vessel. After contact with the resin, the nitrates displace the chlorides in the surface area and remove the nitrates from the water. The drained resin is regenerate using a concentrated solution of sodium chloride or baking soda(Rezvani et al., 2019)**.**

Ion exchange technology is technically simpler than other common methods, and has the advantage of being able to efficiently remove even trace impurities from the solution, enabling high processing power, high removal efficiency, and high-speed kinetics. It can be applied to various industrial wastewaters to remove harmful substances. Ion exchange techniques depend on toxic or unwanted ions, which are replace by other ions. There are two types of ion exchange, which can classified as cation exchange and anion exchanger. Ion exchange is a natural or synthetic resin with an active site on its surface. Synthetic resins are widely preferred because of their ability to remove heavy metals from wastewater. Several resins are most commonly used to remove harmful ions from wastewater, including zeolites, sodium silicates, acrylics, and metha-crylic resins.

Reversible processes and low energy requirements are the most important advantages of this method. This method can reduce organic and inorganic pollutants by about 95%, but if the wastewater contains oil or grease, pretreatment may be required (Ince, 2019).

2.5.1.3. Electrodialysis

Electrodialysis (ED) is a desalination process driven by a potential difference between two oppositely charged electrodes. ED combines the advantages of selectivity and lower chemical demand than RO chemical demand. Like RO, ED cannot selectively isolate nitrates and requires post-treatment for remineralization. Removal of nitrate is accomplished by applying an electrical current through a series or stack of anion and cation exchange membranes, as result of which nitrate ions move from the feed solution into the concentrated waste stream. The voltage applied to the membrane cell determines the degree of desalination and removes nitrates. Although ED can be used to produce drinking water in nitrate-rich water, high concentrations of nitrogen nitrate remain in the process (Rezvani et al., 2019).

In the Electrodialysis (ED) process, ions migrate via ion-selective semipermeable membranes due to electrically charged membrane surfaces. A positive electrode (cathode) and a negative electrode (anode) are used to fee the membrane surfaces and entice oppositely charged ions. Through this process, ions consisting of nitrate are eliminated from the uncooked water. In Electrodialysis Reversal (EDR), the fee at the membranes is reversed periodically to decrease scale development. Several methods have been used to remove various ions and other contaminants from wastewater that seriously affect the environment. Electrodialysis technology may be one of the most effective of these techniques for recent advances in membrane technology. Electrodialysis, a membrane separation technique, relies on a potential difference used to promote the movement of ions towards an oppositely charged electrode. In this process, water-soluble ions are passed through the membrane as an ion exchange material under the influence of an electric current. Removal of dissolved solids requires attention to certain factors such as the nature of the contaminant, the applied amperage, temperature, pH, etc. This method was used to produce drinking water in cardinal numbers and reduce water sources (Ince, 2019).

2.5.2. Elimination-Based Technologies for Nitrate Removal

2.5.2.1. Chemical denitrification process

Denitrification is one of the key techniques in the organic nitrogen elimination (ONR) from water and wastewater. Through denitrification, oxidized forms of nitrogen, together with NO_3^- and nitrite (NO_2^-), are transformed to dinitrogen (N_2) and, to a lesser quantity, N_2O gasoline. Denitrification is an anaerobic procedure that is achieved via denitrifying microorganism, which converts nitrate to dinitrogen in the subsequent sequence.

Chemical methods for degrading nitrates can be divided into two groups: non-specific methods and methods designed for nitrate decomposition. There is no easy chemical way to reduce nitrates to nitrogen gas at low temperatures and pressures. It is relatively easy to reduce nitric acid to ammonia, but it is much more difficult to stop the reduction with molecular nitrogen. Many metals like magnesium, manganese, Zn, chromium, iron, cadmium, tin, aluminum, and lead reduce nitrates. The final reduction product is affected by temperature, pH, and the metal used (Ince, 2019).

2.5.2.2. Biological denitrification process

The biological denitrification process has been used for many years in wastewater treatment. Biological denitrification is highly selective for the removal of nitric acid. The efficiency of the process is very high and can reach almost 100%. This is incomparable to other methods that can be used to reduce nitric acid. The main drawback is the potential bacterial contamination of treated water. This risk is very legal and requires subsequent treatment and disinfection to meet current drinking water standards. Many heterotrophic bacteria can switch to using nitrate as an alternative electron acceptor if no dissolved molecular oxygen is available for respiration. This process of desorption obtains the result that nitric acid is reduced to the next nitrogen gas that was first reduced to nitrite. However, denitrification is only effective at low dissolved oxygen concentrations, as energy yields are lower than oxygen respiration. An external carbon source is also required for maximum kinetics, but processing is done at a rate reduced by "intrinsic respiration". The carbon atoms used include precipitated wastewater and carbohydrate waste, but methanol may be preferred for nitrogen removal as it is relatively inexpensive, readily available, and easier to control the process (S. P. Burghate1, 2014).

$$6NO_3^- + 2CH_3OH \rightarrow 6NO_2^- + 2CO_2 + 4H_2O \qquad 2.1$$

$$6NO_2^- + 3CH_3OH \rightarrow 3N_2 + 3CO_2 + 3H_2O + OH^- \quad 2.2$$

Overall energy reaction:

$$6NO_3^- + 5CH_3OH \rightarrow 6N_2 + 5CO_2 + 7H_2O + OH^- \quad 2.3$$

On this technique, nitrate is converted to nitrogen gas through denitrifying bacteria in the absence of oxygen ($NO_3 \rightarrow NO_2 \rightarrow NO \rightarrow N_2O \rightarrow N_2$). with a view to fulfill the growth and energy necessities of the bacteria, methanol in extra of 25–35 % have to be introduced as a source of carbon. The elimination efficiency levels from 60 to 95 %. The most important advantage to anaerobic denitrification is that there are not any waste merchandise requiring disposal, produces a non-toxic by product (N_2), appropriate for massive applications, can manage high concentrations, and destructive approach. The nitrate removal from wastewater by using the biological denitrification technology the usage of immobilized Pseudomonas Stutzeri bacteria in a fluidized bed bioreactor with different initial nitrate concentrations (150, 180 and 200 ppm). The result discovered that the nitrogen removal performance accomplished become maximum (96 %) with methanol as carbon source, followed through ethanol (seventy seven %) and methane (70 %) throughout the duration 6–8 hr. (Ranjan et al., 2016).

2.5.2.3. Catalytic reduction

Catalytic reduction is one of a suitable technology for removal of nitrate from water. The process uses H_2 as reactant in the presence of bimetallic catalyst containing a noble metal from group VIII usually palladium, and transition metals such as copper as a catalytic promoter for conversion of NO_3^- to N_2. The advantages of NO_3^- catalytic reduction includes no brine production, no biohazard risks, stability and ease of fine-tuning and start up. Most studies about 75% concluded that Pd is the most active phase to reduce NO_2^- on catalytic reduction of NO_3^-. Moreover, Pd is more preferable to produce N_2 than Rh, Ru or Pt catalysts (Pizarro et al., 2018). Catalytic reduction of NO_3^- appears as an interesting and economically sound for water polluted. To remove NO_3^- the process carried out through heterogeneous catalytic hydrogenation to nitrogen. The main drawbacks of the process are the formation of nitrite as intermediate and ammonia (NH_4^+) as by-product, which is undesirable in drinking water (Soares, 2020).

2.6. Adsorption

Adsorption is a surface phenomenon in which it is characterized by chemical species (adsorbate) from its vapor or liquid solution phase onto or near the surface of solid (adsorbent). The presence of excess surface occurs when the attractive energy of a substance with the solid surface that is adhesive work is higher than that of cohesive energy of the substance (Chiou, 2003). Adsorption is the mass transfer operation of solute (adsorbate) exists in a fluid phase to the surface of solid phase (adsorbent) due to the existent of high molecular interaction between them. It is a process of the interface in which a film of adsorbates is created on the surface of the adsorbents of material. Thus, it is the result of surface energy (Machado et al., 2011). Adsorption is commonly employed as a polishing step to remove organic and inorganic contaminants in water and wastewater treatment. The surface area or active sites, the lack of selectivity, and the adsorption kinetics usually limit the efficiency of conventional adsorbents (Qu et al., 2013). Adsorption is a term used to describe the metal or organic substances in solution attached to a solid adsorbent at low, medium, and high coverage(Al-anber, 2011). Adsorption as a separation process is widely applied in our manufacturing economy and daily life. The adsorption process takes advantage of the ability of a particular solid to preferentially concentrate a particular substance in a solution (gas or liquid) on the surface. Therefore, the required purpose of purification or separation can be achieved by contacting the fluid with such a solid.

Adsorption can be categorized into physical adsorption (physisorption) and chemical adsorption (chemisorption) in nature. Physical adsorption has relatively weak intermolecular forces. It does not allow the sharing or transfer of electrons. Hence always maintains as individuality of interacting species. Even though the process is slow due to the occurrence of diffusion of molecules, the interactions are fully reversible which enables desorption to occur at a similar temperature. Not only the adsorbed molecules are free to move and cover the entire surface, but also have low heat in the case of physical adsorption (Aly, 1987).

The main characteristic of chemical adsorption is the large interaction potential, which leads to a high heat of adsorption close to the value of the chemical bond. This fact, combined with other spectroscopy, electron spin resonance, and susceptibility measurements, confirms that chemical adsorption involves the transfer of electrons and the formation of true chemical bonds between the adsorbate and the solid surface. Because

chemisorption involves chemical bonding, it often occurs at high temperatures and is generally, related to the activation energy. Furthermore, the adsorbed molecules are located in specific locations and therefore cannot freely migrate to the surface. Table 2.1 Comparison of physical and chemical adsorption. Generally, adsorption can occur at any interface. That is either gas-solid interface or liquid-solid interface (Abdalla et al., 2020).

Table 2. 1: The difference between chemical and Physical Adsorption

Parameters	Chemical Adsorption	Physical Adsorption
Force of Attraction	Strong attraction forces or chemical bond such as ionic bonds	Weak inter particle bond as van der waal forces
Temperature	Higher heat of adsorption	Low heat of adsorption
Electron transfer	electron transfer leading to bond formation between sorbate and surface	Not involve electron transfer, although polarization of sorbate may occur.
Adsorption layer	Monolayer only	Monolayer or multilayer
Kinetics Adsorption	Activated, may be slow and irreversible	Rapid, non- activated and fully reversible
Adsorption sites	Site specific, adsorbed molecule are fixed at specific sites	Not site specific, the adsorbed molecules are free to cover the entire surface

The most literature studies showed that adsorption process could considered an efficient treatment method for the removal of emerging compounds from water. It allows reaching good removal percentage. In addition, a process does not imply by-products formation, which could be more toxic than parent compounds. It is obvious that adsorption process encompassed in an integrated treatment system, which involves many factors, such as available space for the construction of treatment facilities, waste disposal constraints, desired finished water quality, and capital and operating costs. All these factors imply the achievement of the optimal operating conditions for low-cost high efficiencies (Grassi et al., 2012).

2.7. Mechanism of Adsorption

The molecules diffuse into the bulk through the extreme planes of the laminar layer around the solid particles to the turbulent flow as result of the concentration gradient given by the four diffusion mechanisms that tends to be natural. The first is the diffusion of molecular-scale adsorbed water into the liquid film that surrounds the adsorbent molecules in bulk. The second film diffusion is the diffusion of adsorbed water on the surface sites of the adsorbent molecules in a liquid film. On the third, a pore diffusion of intraparticle diffusion of adsorbed water in the interstices of the adsorbent. Lastly, the adsorption of adsorbed water on the inner surface of the adsorbent (Kaushal, 2017).

In the context of adsorption, the main challenge is to select the most promising types of adsorbents, mainly in terms of low cost, high capacity (often expressed as q_{max} values) high adsorption rates, high selectivity, and fast kinetic adsorption mechanisms, especially adsorbents/adsorbates interactions that occur at interfaces. This is an important topic because the adsorption mechanisms involved in the collection of contaminants are what dictate the design of desorption strategies (e.g., the recovery of certain contaminants, such as "precious" metal ions, is also an important parameter for the economics of the process (Crini et al., 2019).

The basic principle of adsorption: The preferred concentration of seeds on the surface of the adsorbed solid operates in two different processes. That is, chromatography, and ion exchange. In fact, adsorption, ion exchange, and chromatography can often be grouped together in engineering textbooks. Chromatography, like most adsorption operations, operates in fixed layer mode. It is designed to intermittently feed the solution to separate, and then pass through the eluate to separate the liquid mixture. The solid material used in ion exchange contains charged groups that interact with the charged ions present in the liquid solution. Looking at adsorption during an exchange process involving virtual seeds reveals the equivalence between adsorption and ion exchange. In fact, most of the information presented in this book is also applicable to ion exchange(“Chi Tei,” 2019).

Table 2. 2: Comparison of nitrate removal technologies

Technologies	Advantages	Drawbacks
Adsorption	- Requires saturation adsorbent disposal - pH and temperature effects are important - Post-treatment is not commonly required - low cost, ease of operation and fantastic reusability performance	- Requires high TDs disposal - Removal efficiency differs with various adsorbents
Reverse Osmosis	- PH and temperature effects are not important - > 95% efficiency can be achieved	- Post-treatment is required due to the corrosivity of product water - High operational cost
Ion Exchange	- pH and temperature effect are not important. - Approximate 90% of efficiency can be achieved. - Medium operational cost	- Requires waste brine disposal. - Post treatment is required due to the corrosivity of product water
Electro dialysis	- Requires lesser acid dosages - Higher water recovery rates - Requires pre-treatment systems and close monitoring	- High operational cost - Requires waste disposal
Chemical denitrification	- No waste disposal is required - pH and temperature effect are important - Maximum efficiency > 60~70%	- Post-treatment is required due to the product of by-product - High operational cost
Biological denitrification	- > 99% efficiency can be achieved - Medium operational cost - Temperature effect is important (low limit of operation is 2- 6 ℃)	- Requires biomass waste disposal - Post-treatment is required due to microorganisms

2.8. Calcium Silicate Hydrate (C-S-H)

Calcium silicate can be present in a variety of forms with a variety of chemical compositions. The most commonly used forms are $CaSiO_3$, Ca_2SiO_4, Ca_3SiO_5, etc. It occurs in a hydrated form with other proportions of water crystallization. Calcium silicate hydrate (CSH) has a surprising level of structural complexity at various Ca/ Si ratios. The CSH has more than 30 known crystalline phases(Y. J. Zhu & Sham, 2014). Calcium silicate hydrate ($CaO.\ SiO_2.nH_2O$, CSH) is a hydration product especially in cement-based materials processing which accounts for about 70%. It increases its early strength and shortens the concrete setting time (S. Zhu et al., 2019). The Ca/Si molar ratio of CSH gel which is free of both $Ca(OH)_2$ and silica can vary between 0.66 to 1.5 (Wu et al., 2013).

Today, calcium silicate hydrate is being used as an adsorbent, especially as a functional material in general for its high specific surface area and multiple structural sites of porous structures. Many studies have been tailored to the scavenging ability of natural and synthetic crystalline CSH against heavy metal ions (Zeng & Yang, 2015). Numerous studies have demonstrated that Calcium Silicate Hydrate (CSH) has excellent adsorption properties. However, most synthetic phosphorus removal adsorbents, including CSH are used as powders with a particle size of 100 μm or less. CSH can be lost to drainage due to its small particle size, the utilization efficiency of the adsorbent is reduced, and the environment is polluted. CSH, a common synthetic silicate adsorbent, has been widely used due to its large specific surface area and unique ability to release Ca^{2+} and OH^-. CSH is synthesized using calcium oxide and silicon oxide materials (Ding et al., 2018).

CSH is a porous gel with an unfixed composition (calcium to silicon ratio) ranging from 0.6 to 2.0. This reveals an amorphous nanostructure with pores at the center of the particles. Because particles at 35 nm are randomly charged, the atoms are arranged in long-range disorder and short-range order. The calcium sheet attracts the defective silicate sheet and constitutes the backbone of the hierarchical CSH molecular structure, and free calcium ions and water molecules are charged in the middle layer region. Occurrence of multiple pores and defects in CSH nanostructures pure calcium silicate hydrate has a layered structure. Well-aligned calcium sheets attract silicate sheets, where silicate tetrahedral are linked together, aligned in chains, and form a skeleton. Between adjacent calcium silicate sheets, water molecules and calcium ions form a distributed middle-layer region. In light of different chemical environments, calcium ions can be classified into two categories: structural calcium ions and interlaminar calcium ions. The former simply

represents stuff on the backbone bound to the silicate tetrahedral chain, and it attracts oxygen atoms from silicate tetrahedron to and provides a specific coordination structure. The latter is located in the interlayer region and is distinguished from the housing of water molecules. Similarly, the calcium and oxygen atoms of water molecules are attracted by electrostatic forces (Y. Zhou et al., 2020).

According to (Sato, 2016) have been studied, the C-S-H structure when the Ca/Si ratio varies from 0.6 to 1.5. With a low Ca/Si ratio C-S-H is a turbostratic nanocrystalline tobamoratolite, with Si chains free from defects in the precision of the method used. As the Ca/Si ratio increases, the main structural evolution is the gradual depolymerization of the Si chains by the gradual selection of Si cross-linked tetrahedral and the gradual incorporation of interlayer Ca to catch up on the resulting layer charge. With the highest Ca/Si ratio, interlayer Ca probably polymerizes in the interlayer space to form a structure with many structural similarities to $Ca(OH)_2$. The formation of the $Ca(OH_)2$ phase is supported by the fact that Ca is in excess in the structure.

Based on the extraordinary structure and fabulous performance, CSH has appeared amazing potential within the safe transfer of low and intermediate-level waste. CSH comprises silica chains connected to CaO sheets and a number of Ca atoms that will be found within the interlayers between the Ca-silicate sheets. The preferences of this adsorbent are as follows: firstly, a high surface area containing surface hydroxyl groups and hydrated Ca^{2+} ions to which different chemical substances can be connected or used for ion-exchanged. On the second CSH may control the long-term discharge of radionuclides due to its long-term stability and high immobilization potential for cations. Finally, its low cost, accessibility, innocuity, and environment-friendly nature. Up to date, expanding interest has been focused on the advancement of mesoporous CSH due to its larger specific surface area and higher adsorption capacity. For illustration, the CSH spheres have a well-defined 3D arrange structure built up by nano- sheets, which show ultra-high medicate loading capacities(Zhang et al., 2015). Calcium silicate hydrate (CSH) has been broadly explored for crystallization due to its greatly moderate Ca^{2+} release, alkalinity supply capacity, special morphology, and great adsorption properties. In a seeded crystallization preparation process, appropriate seed materials with an isomorphic crystal plane initiate and advance the deposition of calcium phosphate (Ca-P) onto the surface of seeds at a low saturation record by removing the energy boundary. CSH could be a hydration item of physical and chemical binding between siliceous and calcareous

substrates, and it usually coexists with other crystal stages such as calcium hydroxide ($Ca(OH)_2$) and unreacted phases(Peng et al., 2017).

According to (Zhang et al., 2015) studied calcium silicate hydrate consists of silica chains related to CaO sheets and a number of Ca atoms that may be located inside the interlayers between the Ca-silicate sheets. The adsorbent includes not only a high surface area containing surface hydroxyl groups and hydrated Ca^{2+} ions to which numerous chemical entities can be attached or used for ion-exchanged, but also CSH may also manage the lengthy-time period release of radionuclides due to its long-term stability and excessive immobilization capability for cations. In addition, its low cost, availability, and environmentally friendly nature. Currently, an increasing interest has been centered on the development of mesoporous CSH because of its large specific surface area and higher adsorption capability.

2.8.1. Methods of Calcium Silicate Synthesis

2.8.1.1. Sol gel method

This technique revolves around hydroxylation and condensation of molecular precursors in solution. Acquired "sol" from nanometric particles is then dried or ''gelled'' both by way of solvent elimination or through a chemical reaction to gain a three-dimensional metallic oxide network. The solvent used is water, but the precursors may be hydrolyzed using an acid or a base. Basic catalysis yields a colloidal gel, while acid catalysis formulates a polymeric gel. The reaction is carried out at room temperature; but, heat treatment is required to achieve the final crystalline state (Zia et al., 2016)**.**

Sol-gel materials are metastable solids that form in kinetically controlled reactions in molecular precursors and constitute the building blocks of later materials. The direct result will have a decisive influence on all reaction parameters, including the properties of the precursor, the structure, and hence the properties of the sol material. Sol is a stable suspension of liquid colloidal particles (nanoparticles). The particles structure cannot only be categorized into amorphous or crystalline, but also dense, porous or polymeric substructure. The latter can be due to the aggregation of sub colloidal chemical units. The gel consists of a porous three-dimensional continuous solid network that surrounds and supports a continuous liquid phase ("wet gel"). In general, the formation of sol-gel systems for the synthesis of oxide materials, gelation (ie, gelation formation) is due to the creation of covalent bonds among a sol particle. Gel formation can be reversible if it

involves other bonds such as van der Waals forces or hydrogen bonds. The structure of the gel network is highly dependent on the size and shape of the sol particles (Zayat, 2005).

The easy agglomeration or aggregation of particulates (sol particles) occurs due to attractive van der Waals forces, minimization of the total surface energy or interfacial energy of the system. To prevent agglomeration (i.e., to stabilize the sol), a repulsive force of equal magnitude is required that must be overcome during the gel. Stabilization can be achieved by adsorbing organic layers ("steric barriers") or by generating electrostatic repulsion forces between particles. This demonstrates the large influence of organic additives, especially ionic species, on the gelation behavior to be discussed in more detail later. The stability of the sol and the coagulation sol chemistry are of paramount importance. Gelation can also be induced by rapid evaporation of solvents that are particularly important in the production of films or fibers.

2.8.1.2. Hydrothermal method

Hydrothermal synthesis can be defined as a technique of synthesis of different materials in hot water under excessive pressure, generally in autoclaves at temperatures above 100 °C and pressures above 1 atm. The benefits of hydrothermal synthesis encompass low-temperature synthesis, easy reactions, cost-effectiveness, excessive purity of the products, and precise water solubility or water dispensability of the products (Li et al., 2014). The hydrothermal method is one of the most vital tools for advanced materials processing, especially owing to its benefits within the processing of nano-structural materials for a wide kind of technological applications including electronics, optoelectronics, catalysis, ceramics, magnetic information storage, biomedical, bio photonics, and many others. The hydrothermal method not only the best facilitates in the processing of mono-dispersed and incredibly homogeneous nanoparticles, but also acts as one of the most appealing techniques for processing nano-hybrid and nanocomposite materials. The term 'hydrothermal' is only of geological origin. It became first utilized by the British geologist, Sir Roderick Murchison (1792–1871) to explain the action of water at increased temperature and pressure, in bringing about changes in the earth's crust leading to the formation of numerous rocks and minerals (Ranjan et al., 2016).

2.9. Magnetic Nano Particles (MNPs)

Nowadays, the development witnessed within the nanotechnology area has contributed to the improvement and revolutionizing of various fields. The listing of advantages and

applications of nanotechnology is developing unexpectedly. Substances at the nanoscale, normally called “nanomaterials,” have usually grabbed the eye of researchers for hundreds of years. amongst those unique types of nanomaterials, magnetic nanomaterials have been the focal point of considerable interest over the past many years as evidenced by an extraordinary increase in the wide variety of research papers focusing on these materials (Gul et al., 2019).

Nanoparticles (NPs) are small particles that exist in an average size between 1 and 100 nm that distinguish them from their parental bulky materials and lead them to perfect for numerous applications. Among them, magnetic nanoparticles (MNPs), a nanoscale material, with unique magnetic properties were widely used in extraordinary fields inclusive of biomedical, energy, engineering, and environmental applications. The MNPs have become an area of intensive research inside the recent beyond due to their particular and outstanding properties which make their potential application in biomedicine, catalysis, agriculture, and the environment (Ali et al., 2021).

Magnetic nanoparticles (MNPs) have appeared promising execution in toxin evacuation or poisonous quality relief (Mohammed et al., 2017). Many studies have been reported on newly developed magnetic adsorbents, such as magnetic zeolites for removing dyes and synthetic magnetite for removing radioactive elements. Not only can all magnetic adsorbents effectively remove adsorbed water, but also they easily separated from the solution under a magnetic field. Magnetic nanoparticle adsorbents are of great interest because they can be easily separated from water by an external magnetic field, can be used repeatedly, and are of great interest(Lai et al., 2016)**.**

According to (Jiang et al., 2017) report, Magnetic technology has been developed as an alternative to water treatment, especially for adsorption processes. After adsorption of contaminants by using magnetic adsorbent with two characteristics of magnetic adsorption, without using centrifugation and filtration, contaminants can be removed from solution by magnetic separation technology. To this end, Fe_3O_4 has been widely used as a magnetic carrier to prepare novel adsorbents according to its unique magnetic properties.

In spite of the fact that there are numerous unadulterated phases of iron oxide in nature, the foremost prevalent MNPs are the nanoscale zero-valent iron (nZVI), Fe_3O_4 and γ-Fe_2O_3. Among them, magnetite (Fe_3O_4), which could be a ferromagnetic black color iron oxide of both Fe(II) and Fe(III), has been the foremost broadly considered. Magnetite is

the favored sort since of the nearness of the Fe^{2+} state with the potential of acting as an electron giver. (Mohammed et al., 2017)

Over the past decades, magnetic nanoparticles (MNPs, particularly magnetite (Fe_3O_4) have gotten considerable attention for their interesting nano-sized and morphology-dependent physicochemical properties, and for their biocompatibility, magnetic properties, and strong binding affinity and capacity. However, due to high surface free energy Fe_3O_4 MNPs with fewer functional groups are susceptible to air oxidation and undergoes leaching under acidic conditions and prone to aggregation in aqueous solution which reduce the ion removal capacities and restricts the ranges of applications (Peng et al., 2017).

2.9.1. Synthesis of Magnetic Iron Oxide

A large number of researchers studied the synthesis of magnetic iron oxide nanoparticles with versatile compositions and phases. Synthetic routes were selected to manipulate the shape, stability, and dispersion tendencies of iron oxide magnetic nanoparticles. Great quality iron oxide magnetic nanoparticles can be synthesized with the aid of adopting flexible synthetic techniques consisting of thermal decomposition, co-precipitation, micelle formation, hydrothermal, and laser pyrolysis techniques. It turned hard for us to bring together all this literature and we have been attempted to give every synthetic technique by giving a few examples in conjunction with the corresponding formation mechanism (Gul et al., 2019).

2.9.1.1. Co-precipitation Methods

Co-precipitation is perhaps a greater suitable approach to prepare magnetic iron oxide nanoparticles from an aqueous solution containing Fe (II) and Fe (III) by including a base under the anaerobic situations at ambient or high temperatures. However, there are certain factors just like the type of iron salts, Fe(II): Fe(III) ratio, the temperature of the reaction, pH of the medium, volume, and ionic strength of the solution that markedly have an effect on size, shape, and composition of the magnetic iron oxide nanoparticles. In the co-precipitation method, once the synthetic situations are met high quality of the magnetic iron oxide nanoparticles are efficiently produced (Gul et al., 2019).

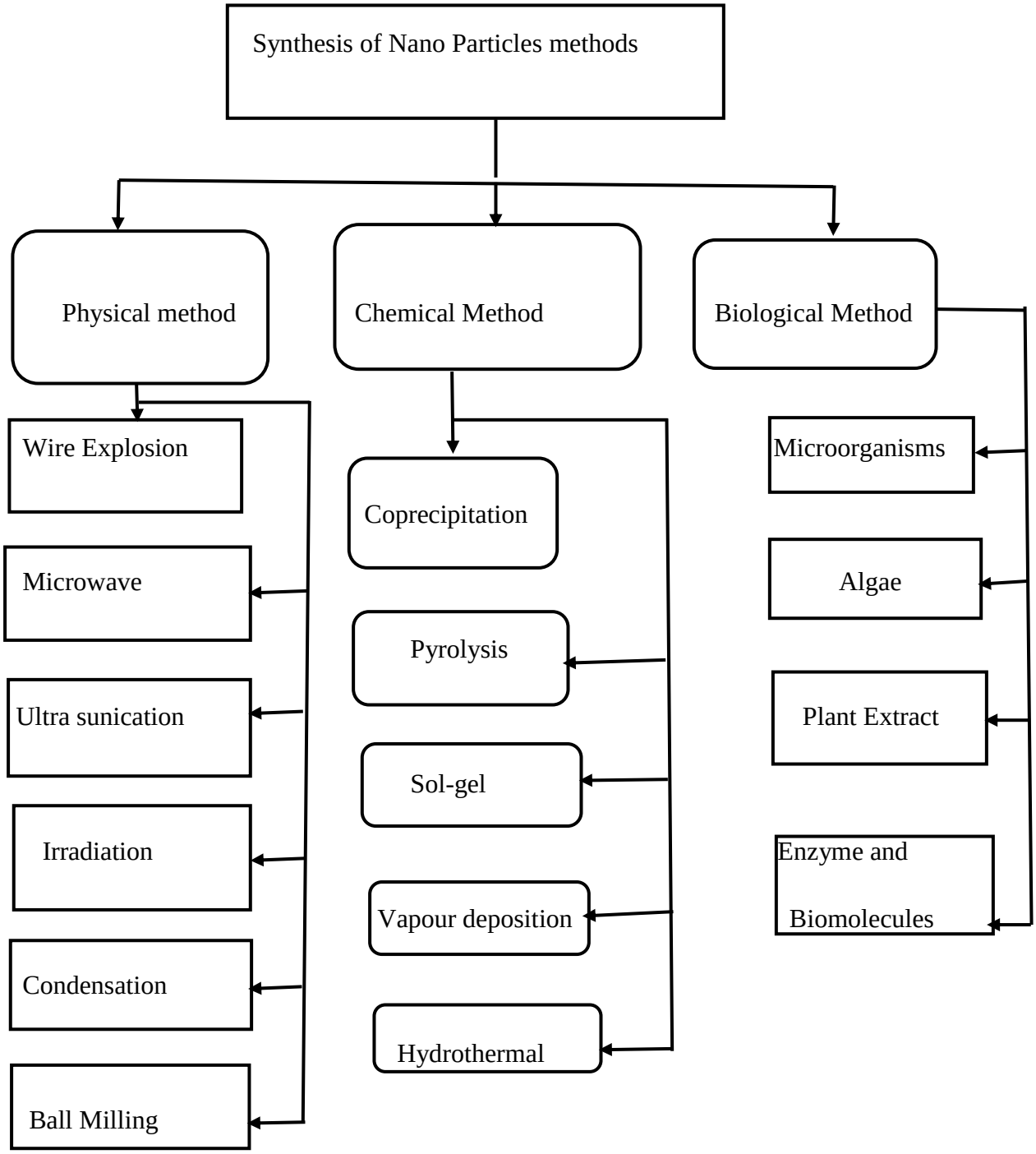

Figure 2. 2: Synthesis methods of Magnetic Nano particles

2.9.1.2. Microemulsion Synthesis

Water-in-oil Microemulsion includes Nano sized water droplets dispersed within the oil phase that might be stabilized with surfactant molecules. The process undergoes lemmatize particle growth, nucleation, as well as agglomeration. The sort of NPS because of surfactant, nature, physiological conditions, and plenty of others is the primary benefit

of this method. For the synthesis of magnetite NPs, nanoemulsions containing iron sources from salts and sodium hydroxide are blend together and at the end of the reaction washed with acetone to remove the surfactant, and washed with ethanol. Commonly, the colloidal NPs exhibit superparamagnetic behavior with excessive magnetization values (Zia et al., 2016). While two immiscible solvents are mixed collectively, a thermodynamically strong isotropic dispersion is formed that is described as Microemulsion with the presence of an interfacial layer of surfactant's molecules. Surfactants molecules commonly bearing hydrophilic heads soluble in water and hydrophobic tails soluble in oil segment form a monolayer on the interface of the two immiscible liquids (water-oil). Surfactant is an amphiphilic molecule playing a position to decrease the water-oil interfacial anxiety to provide a transparent solution. The Microemulsion method has numerous benefits in comparison with other synthetic techniques. For instance, with the use of a simple device, an awesome kind of nanomaterials may be synthesized with exceptional manipulate over size, shape, and composition, favored crystalline structure and excessive unique surface area, simple synthetic situations at ambient/close to ambient temperatures, and pressures (Gul et al., 2019).

2.9.1.3. Hydrothermal Route

The hydrothermal or solvothermal path is one of the most successful methods to put together with magnetic nanoparticles and ultrafine powders. Hydrothermal synthesis accompanies higher temperatures (125–250°C) at very excessive pressures (0.3–4 MPa). Powdery iron oxide magnetic nanoparticles with 40 nm diameter had been reported the use of hydrothermal course (140°C) and a saturation magnetization of 85.8 emu. g^{-1}, which is some distance lower than that of the bulk iron oxide(Gul et al., 2019).

According to (Ali et al., 2021) reported, under the hydrothermal method, hydrolysis and oxidation reaction takes place to provide MNPs. The crystal formation relies upon the extent of the solubility of minerals within the water. Particles of numerous magnetic nanomaterials of uniform size are acquired through this technique. For example, Fe_3O_4 NPs of length 15 nm and spherical shape were acquired. In addition, Chitosan-coated Fe_3O_4 NPs of 25 nm length were prepared, and carried out in enzyme immobilization. The morphology and crystallinity of synthesized MNPs depend upon the correct mixing of solvent, time, amount of pressure, and temperature.

2.10. Magnetic Calcium silicate Hydrate (Fe_3O_4 Loaded CSH Composite)

CSH is usually a kind of superfine powder, which is simple to lose within the processes of adsorption and difficult to partitioned from aqueous systems after batch adsorption tests. Therefore, magnetical materials have attracted broad interest due to their fast and successful separation from the treated water. Among magnetic adsorbents, magnetic mesoporous nanostructures are great adsorption materials, since they are not only showed a high specific surface area owing to the plenteous intraparticle spaces or intraparticle pores but also too have superior attractive properties than powder adsorbents due to weaker Brownian movement(Zhang et al., 2015).

Having fast kinetic, large surface area, a specific affinity for adsorbate, and giving minimal environmental impact metal-based CSH are advantageous both technologically as well as economically. In addition, metal oxides can be characterized by having short intraparticle diffusion distance, high adsorptivity, super magnetic, and easily regenerated. Nowadays, some of the metal oxides like ferric oxides and ferric magnetite used to eliminate the anions in water. These oxides have proven a high affinity towards nitrate ions where the sorption is specially controlled with the aid of complexation of hydroxide in solution, and subsequently acidic dissociation at the solid-solution interface that creates positively charged surface sites at the adsorbent, and as a result, adsorb the nitrate ions (Suzaimi et al., 2019).

2.11. Adsorption equilibrium isotherms

Isotherm refers to the relationship between the equilibrium adsorbate concentrations in the liquid-phase and the equilibrium adsorption amount on the solid-phase at a certain temperature. Sorption equilibria deliver fundamental physicochemical data for assessing the relevance of sorption processes as a unit operation. Sorption equilibrium is normally described by an isotherm equation whose parameters express the surface properties and affinity of the sorbent, at a constant temperature and pH. Therefore an accurate mathematical description of the equilibrium isotherm, preferably based on a correct sorption mechanism, is essential to the effective design of sorption systems (Ho et al., 2002). We can model the equilibrium adsorption data by the isotherms, and investigate the adsorption information, such as the adsorption mechanisms, the maximum adsorption capacity, as well as the properties of adsorbents by the isotherms (J. Wang & Guo, 2020). According to the paper, studied by (Berkessa et al., 2019) adsorption isotherm can be

described as a curve that explains the phenomenon governing the retention (release) or mobility of a substance to a solid at constant temperature and pH in an aqueous porous medium or aquatic environment.

Adsorption isotherm gives an idea about relation between the adsorbate and the extent of adsorbate adsorbed on the surface of adsorbent at fixed temperature (Mor et al., 2016). The adsorption equilibrium has continuously been clarified by the isotherm equations such that their parameters demonstrate the surface characteristics and affinity of the adsorbent toward the adsorbate(Ghadiri et al., 2017). The two popular isotherms are Langmuir and Freundlich isotherms which have been used to explain the equilibrium of an adsorption system (Nsami & Mbadcam, 2013).

2.11.1. Langmuir isotherm

Langmuir isotherm decides the adsorption of ions on the surface of the adsorbent on the monolayer and comparable destinations on the surface (Mor et al., 2016). According to Langmuir isotherm, assumptions can be taken based on adsorption that occurs at specific homogeneous sites within the adsorbent (Nsami & Mbadcam, 2013).

2.11.2. The Freundlich adsorption Isotherm

The Freundlich isotherm is an empirical equation employed to describe the heterogeneous system. This empirical model can be applied to non-uniform surface adsorption heat and non-uniform distribution of affinity and multi-layer adsorption. Historically, this was developed for the adsorption of animal charcoal, and indicates that the proportion of adsorbed water in the adsorbent in a given mass of solute is not constant at other solution concentrations. From these perspectives, the amount adsorbed is the sum of the adsorptions of all sites (with their respective binding energies) until the adsorption energy decreases exponentially when the adsorption process is complete, and the stronger binding sites are occupied first(Foo & Hameed, 2010).

At present, Freundlich isotherm is universally applied in varied systems especially for organic syntheses or considerably interactive species on triggered carbon and molecular sieves. The slope ranges between 0 and 1 is a measure of adsorption intensity or surface variousness, turning better heterogeneous as its value gets closer to zero. Whereas, a value below unity implies a chemisorption process where 1/ n above one is indicative of collaborative adsorption (Ho et al., 2002).

2.12. Adsorption Kinetics studies

Adsorption kinetics reflects the evolution of the adsorption process as a function of time. This is an important parameter to consider when choosing an adsorbent. Fast adsorption is recommended for treatment methods that use adsorption as a purification process. Several models have been developed that describe the diffusion of solutes on the surface of particles and within pores (such as film distribution models, intra-particle diffusion models, out-of-particle diffusion models, and pore diffusion models). In the case of nitrates removal, simplified models such as pseudo-first-order kinetics and pseudo-secondary kinetics were common (Battas et al., 2019).

The adsorption dynamic is one of the foremost imperative issues for understanding both the mechanisms of adsorption and the evaluation of persuasive factors on the reaction rate. Kinetics explains solute take-up rates additionally characterize the residence time of the adsorbate at the solid-liquid interface. Kinetic modeling was used to investigate the adsorption mechanism and potential velocity control processes (Ghadiri et al., 2017)**.**

2.13. Adsorption Thermodynamics

Another important factor characterizing adsorption is the enthalpy of adsorption. During adsorption, the residual forces on the surface always decrease. In other words, the surface energy, which appears as heat, is reduced. Therefore, adsorption is always an exothermic process. That is, the enthalpy of adsorption (ΔH) is always negative. When a gas or liquid is adsorbed, the freedom of movement of its molecules is limited. This corresponds to a reduce in entropy of the adsorbed molecule after adsorption. For the process to be spontaneous, the thermodynamic requirement is that ΔG, must be added at a constant temperature and pressure, i.e. the Gibbs energy decreases. According to the equation, $\Delta G = \Delta H - T\Delta S$, if ΔH has a sufficiently high negative value - ΔG can be negative because TΔS is positive. Therefore, the spontaneous adsorption process is a combination of these two factors is added ΔG. As adsorption proceeds, ΔH becomes increasingly negative, eventually ΔH becomes equal to TΔS, and ΔG becomes zero (Ibrahim & Bsharat, 2018).

Generally, these parameters indicate whether the adsorption process is spontaneous as well as it also indicates whether it is exothermic or endothermic. The standard enthalpy changes (ΔH^o) in the adsorption process are: (i) Positive values indicate that the process is endothermic in nature. (ii) Negative values indicate that the process is heat generating in

nature and that the amount of heat given when the metal ions on the adsorbent surface bind are released. This can be obtained with an adsorption rate (Cads) vs. temperature (T) plot. The adsorption rate increases as the temperature rises. This shows the endothermic process and the reverse phenomenon of fits. When the value of (ΔS^o) becomes positive, it shows an increment of the degree of freedom (or disorder) of the adsorbed species (Al-anber, 2011).

2.14. Factors Affecting Adsorption

2.14.1. pH of Solution

The pH of the solution affects the degree of adsorption, as the distribution of the surface charge of the adsorbent is likely to change. This is due to the composition of the raw material and the activation technology, so the degree of adsorption is different depending on the functional group of the adsorbate. (Berkessa et al., 2019) reported that the effect of initial solution pH on nitrate removal increased with pH increasing to 2-7 and decreased over pH 7. According to the studies above, the decrease in nitrate removal above pH 7 may be due to stronger competition with hydroxide ions, and the low removal below pH 7 may be due to the instability of SWR oxides at lower pH**.** The pH of the solution controls the electrostatic interactions between the adsorbent and the adsorbate.

According to (Helard et al., 2018) investigated that the adsorption of nitrate on natural pumice is strongly pH-based. The removal efficiency and nitrate uptake were reduced with increasing pH and the most effective pH value for nitrate removal became four. At lower pH values the quantity of H^+ ions inside the answer are more than OH^- ions. This brought about the reduction of the negative charge at the surface due to the extra protons within the solution and as a result, the number of positively charged sites increased. A positively charged surface site on the adsorbent favors the adsorption of the nitrate anions because of electrostatic attraction. On the other side, a pointy decline in removal efficiency of nitrate happened at higher pH that may be because of electrostatic repulsion of anionic nitrate by way of the negatively charged adsorbent's surface. The decrease in sorption ability on the higher pH (pH > four) may be due to the competition for the active sites' anionic nitrate by means of the negatively charged surface of natural pumice.

2.14.2. Effect of adsorbent dose

According to (Berkessa et al., 2019) reported that when the dose of adsorbent was changed between doses 4-32 g/L, the nitrate removal rate increased from 22.34 to 32.20% when the dose of adsorbent was increased. When the dose was changed from 4 and 32 g, the clearance increased from 24.3% to 32.2%. There is a slight increase in the removal rate of nitrate with increasing SWR dose, presumably because there is no appreciable increase in effective surface area due to the exchange particle conglomerates on the SWR surface. The adsorption effectiveness increments with the adsorbent dosage. Nevertheless, a dosage of nano-particle beyond the consistent state does not move forward adsorption due to covering of active sites. At lower measurement of adsorbents, there are deficiently active sites that the adsorbate can effectively possess(Temesgen Getahun, 2019).

2.14.3. Effect of initial concentration

Effect of adsorbate concentration on adsorption investigated by (Berkessa et al., 2019) with initial concentrations of nitrogen nitrate in the range of 3 to 19 mg/L. The results of this paper showed that the nitrate removal rate decreased from 26.33 to 6.53% with increasing nitrate-nitrogen concentration. A decrease in nitrate adsorption may suggest a lack of available space required for high initial concentrations of nitrate. The high congestion of low concentrations of nitrate is likely due to the availability of more space on the surface of the adsorbent for fewer adsorbent species**.**

2.14.4. Contact Time or residence time

The longer the residence time, the more complete the adsorption. Therefore, the contact time required to complete the settlement is important to provide insight into the settlement process. It also provides information on the minimum time required for significant adsorption to occur and the possible diffusion control mechanism of the adsorbent(Al-anber, 2011). Contact time is considered to be an important factor influencing adsorption. Based on the literature review, removal efficiency is greater with longer contact times. This is due to the longer contact between the solid and the liquid, which enables better interaction between the medium and the adsorbate (Nabhan, 2019).

By changing the contact time from 0 minutes to 120 minutes, and by stirring the mixture in a 250 ml plastic bottle, 100 ml of the test solution containing 5.14 mg/L NO_3-N in a dose of 20 g SWR is adsorbed to determine the equilibrium time at 150 revolutions per

minute. The results showed that the nitrate removal rate increased over time and reached a maximum value (0.071 NO_3- N mg/g) at 60 minutes and then stabilized (Berkessa et al., 2019).

2.14.5. Effect of Particle size

The smaller particle size reduces the restriction of internal diffusion and mass transfer and allows the adsorbate inside the adsorbent to penetrate (i.e., the equilibrium can be more easily achieved and almost full adsorption capacity can be achieved). According to (Al-anber, 2011) studied, the removal efficiency of Fe^{3+} ions by natural zeolites through three different particle sizes of (45, 125, and 250 µm). It is observed that the maximum adsorption efficiency is achieved with a particle size of 45 micrometers. This is because most of the inner surface of these particles can be used for adsorption. The smaller the particle size, the faster the adsorption rate, and the shorter the path for Fe^{3+} ions to move inside the zeolite pore structure with a smaller particle size.

2.15. Adsorption of Nitrates Ions

The efficiency of the adsorption process relies upon on the different adsorbents. The adsorbent should have excessive adsorption capability, a high rate of adsorption, low value, and easy regeneration (Hai & Bui, 2013). The adsorption of nitrate ions can be performed using different adsorbents. For instance, the sorption of nitrate ion on biochar made from several agricultural, and forest such as pinewood, bamboo, wheat straw, mustard straw, corn Stover, and sugarcane bagasse. The result of these adsorbents demonstrated that effective biochar-based sorbents for removal of nitrate ions from aqueous solutions (Zhao et al., 2018).

According to the study reported by (Moaaz K. Seliem, 2013) there are many materials and technologies that have been developed for the removal of nitrate, including sepiolite, sepiolite activated by HCl, slag and powdered activated carbon, pulsing potential electrolysis, red mud, modified wheat residue, ammonium-functionalized MCM-48, bio-electrochemical, Chitosan hydrogel beads, cross-linked Chitosan beads conditioned with sodium bisulfate, aquatic macrophytes, activated carbon prepared from sugar beet, Zn/Al chloride layered double hydroxide, and organic surfactants modified clay minerals. In addition, zero-valent iron and magnesium, nano bimetallic, and catalytic methods are also used for the removal of nitrates but have drawbacks of high cost and low yield (Halil Ibrahim Uzun, 2019).

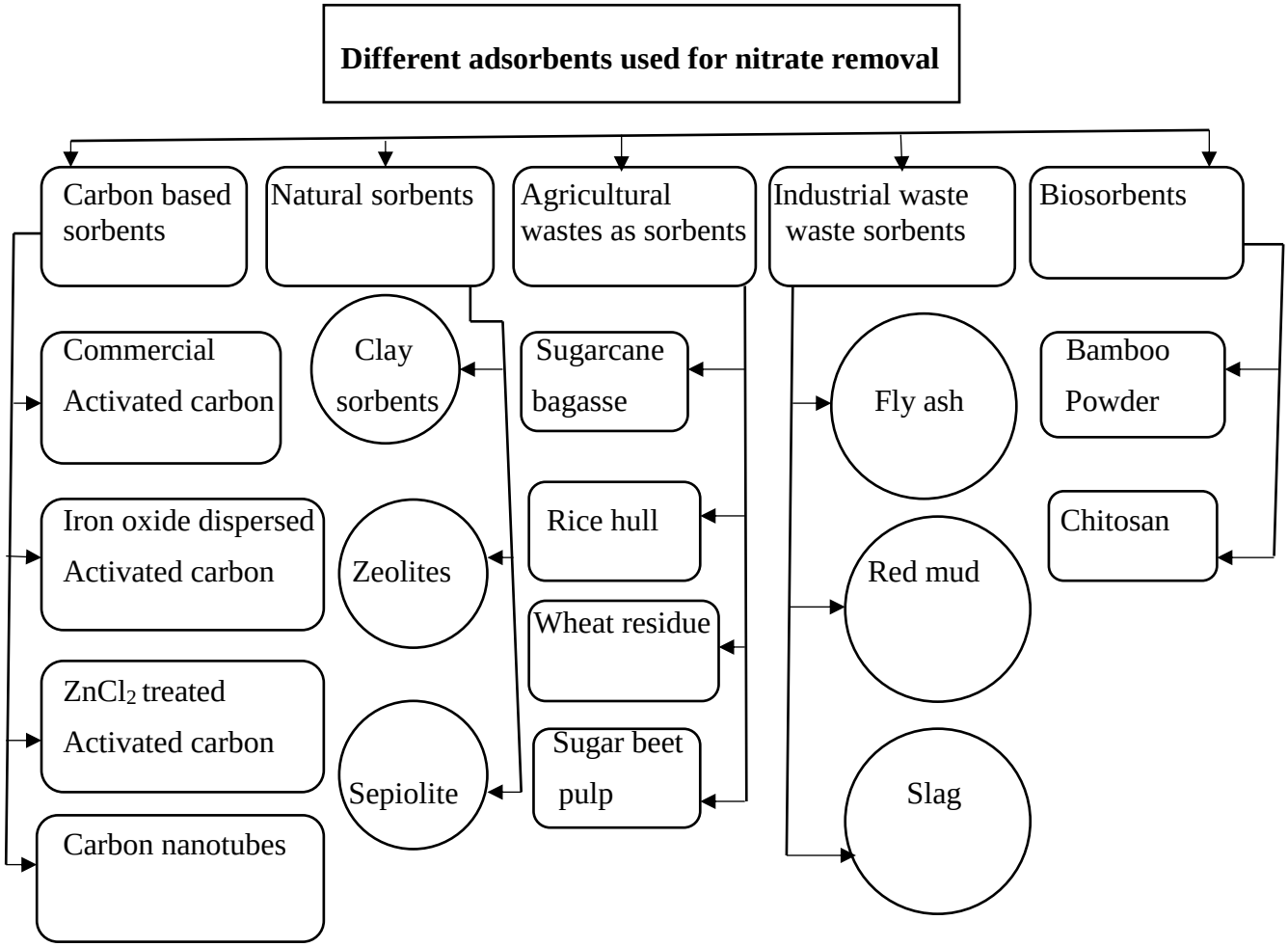

Figure 2. 3: List of different adsorbents used for the removal of nitrate from water

Figure 2.3 summarizes several adsorbents, which have been used for nitrate removal. In addition, adsorption capacity, pH, adsorbent dose, contact time, and initial nitrate concentration of different adsorbents for nitrate removal from water has been presented in Table 2.3.

2.16. Adsorption Regeneration

Regeneration is a very important aspect of adsorption from an economic and environmental point of view. The disposal of adsorbents is one of the problems associated with the adsorption methods. The regeneration can reduce the need for new adsorbents and additionally reduce the trouble of disposal of used adsorbents. Numerous regeneration methods were used with different degrees of success. The recovery of many solutes became viable with the aid of using solvent washing (Kulkarni & Kaware, 2014).

Table 2. 3: Adsorption capacities and other parameters for the removal of nitrate by different sorbents.

Adsorbents	pH	Initial NO_3^- concentration (mg/L)	Contact time (min)	Adsorbent dose	q_{max} (mg/g)	Reference
Natural Pumice	4-8	15-90	15-70	0.3-30 mg/L	167.37	(Helard et al., 2018)
Granular Ferric Hydroxide	3.8-7.8	50-150	30-90	0.625-3.75 g/50 mL	-	(Dehghani et al., 2015)
Local Clay	2-9	50-200	30-300	5-40 g/L	27.77	(Battas et al., 2019)
Solid waste from factory	2-12	13.29-84.17	10-120	4-32 g/L	0.065	(Berkessa et al., 2019)
Egg shell biowaste	3.5-9	50-1500	0.5-6 days	5-15 g/L	8.25	(El-ashgar, 2020)
Chitosan	2-10	25-500	5-120	0.5-10 g/L	-	(Moghadam et al., 2018)
Modified steel slag	1-10	20-300	30-420	0.2-2 g/100 mL	16.39	(Yang et al., 2017)
Zn-Al layered double hydroxide/Activated Carbon	2-12	100 mg per 50 mL	10-120	25-200 mg	73.74	(Karthikeyan & Meenakshi, 2019)
Zeolite supported zero-valent Iron nanoparticle	2-10	30-200	10-500	2-10 g/L	22.94	(Sepehri et al., 2014)
Modified rice husk	3-11	50-300	20-120	0.1-0.4 g/L	55.55	(Katal et al., 2012)

CHAPTER THREE

METHODOLOGY

3.1. Chemicals Reagents and Equipment's

The main raw material that was used to generate calcium silicate hydrate during the experimental work was Aluminium sulphate solid waste residue from Awash Melkassa chemical factory. SWR was reacted with NaOH to form sodium silicate solution. The produced product reacted with $CaCl_2$ to produce CSH. The $FeCl_3.6H_2O$ and $FeCl_2.4H_2O$ were reacted to form Fe_3O_4 product. Anhydrous potassium dihydrogen phosphate (KH_2PO_4), KNO_3, NaCl and Na_2CO_3 were dissolved in deionization water to form phosphates, nitrates, chloride and carbonate stock solutions in 1000 mg/L each, respectively. The diluted (0.1 M) of HCl and NaOH were used to adjust the pH of the solution. All chemicals reagents used were analytical grade.

Equipment that were used for experimental work includes; electronic balance, magnetic stirrer, ball mill, Autoclave Reactor, conical flask, beaker, funnel, water dispenser, measuring cylinder, magnetic stirrer, beaker, oven, filter paper, vacuum filter, burette, various mesh size sieves. NitraVer ® 5 Nitrate Reagent powder pillows, 10 mL, pk/100 also used for nitrate concentration measurement using UV/VIS Spectrophotometer (Hach DR6000 ^{TM} LPV441.99.00002, USA),

3.2. Methods

3.2.1. Calcium silicate hydrate (CSH) Synthesis

Calcium silicate hydrate (CSH) was synthesized using sol-gel method according to (Wakene et al., 2021) method as shown in figure 3.1. Fresh Aluminium sulphate solid waste residue from Awash Melkassa Chemical Factory was dried on oven at 105 ^oC overnight. Solid to liquid ratio of 1:10 was used. Based on this 100 g of powder dried Aluminium sulphate filter cake was mixed within 4 M NaOH (1000 ml) at 80 ^oC; stirred using heated magnetic stirrer and let reacted for 2 hr. followed by cooling. This solution was vacuum filtered to separate into the filter cake residue and the filtrate, which contains mainly sodium silicate (Na_2SiO_3). Balanced amount of calcium chloride ($CaCl_2$) which was computed from the material balance at Ca/Si ratio 1.2 was added in a drop wise into the Na_2SiO_3 at room temperature. Subsequently, a white semi-rigid porous gel was developed and aged for 24 hr. at static condition in the Teflon bottle followed by filtration

to remove the solvent. The formed gel were gently mixed with deionized water for an hour to remove free $Ca(OH)_2$; and dried at 80 ^oC for 24 hr. to obtain CSH. The produced CSH meshed at 90 µm and stored in the glass bottle prior to be use for the adsorption.

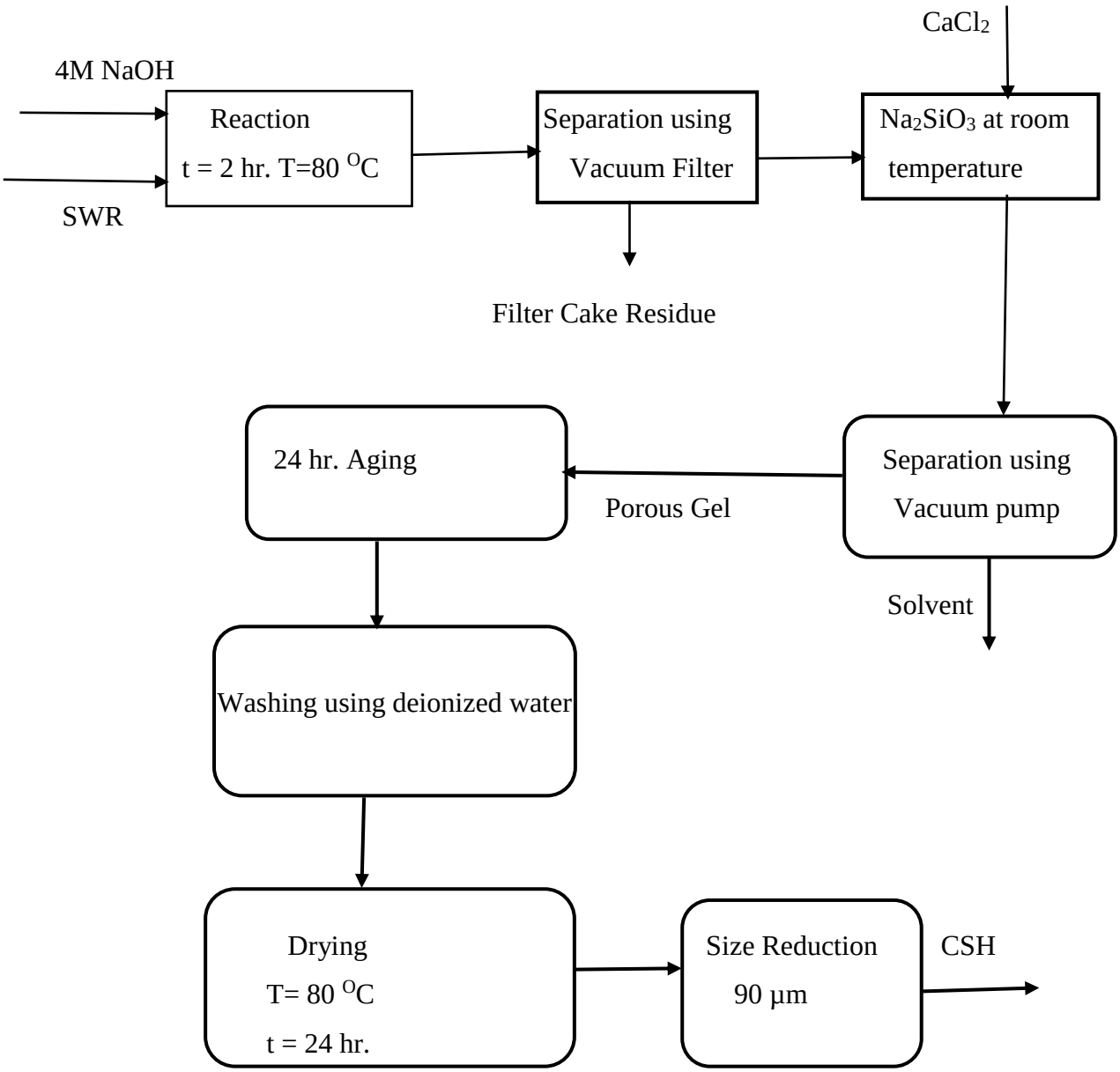

Figure 3. 1: Experimental framework of calcium silicate hydrate (CSH) synthesis

3.2.2. Fe_3O_4 Synthesis

Magnetic particle of magnetite was synthesized using of method co-precipitation of ferric and ferrous salts. According to (Wubishet et al., 2020) method 15.1 g $FeCl_3 \cdot 6H_2O$ and 5.55 g of $FeCl_2.4H_2O$ were dissolved in 100 ml of 0.3 M HCl. Then the solution of 120 mL of 3 M NaOH over a period of 2 hr. under vigorous stirring at 80 ^OC was added dropwise from separatory funnel. Precipitation was expected at pH between 8 and 14.

After the system cooled to room temperature, the precipitate separated by permanent magnet, and washed with distilled water until neutral pH. Finally Fe_3O_4 was washed with acetone and dried in oven at 65 ^oC overnight (Hariani et al., 2013). The relevant chemical reaction can be expressed as:

$$Fe^{2+} + 2Fe^{3+} + 8OH^- \rightarrow Fe_3O_4 + 4H_2O \quad 3.1$$

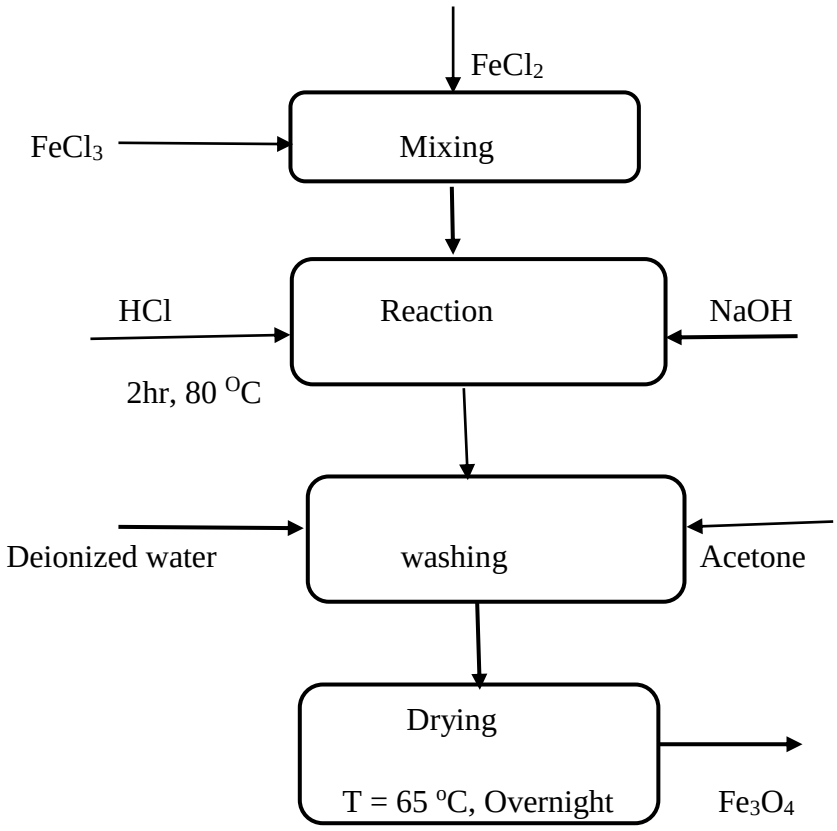

Figure 3. 2: Experimental framework of Fe_3O_4 synthesis by coprecipitation method

3.2.3. Fe_3O_4 Loaded CSH Composite Synthesis

The novel Fe_3O_4 loaded CSH composite were synthesized according to (Peng et al., 2017) by a dynamic hydrothermal synthesis method. Accordingly, 10-40 wt. % of Fe_3O_4 was added to CSH and dissolved in 100 ml of deionized water. To obtain uniform mixture it was ultra-sonicated for 30 min at room temperature. The product was removed after the temperature and pressure were reduced to atmospheric conditions followed by the uniform mixture reacted in autoclave hydrothermally at 170 ^OC for 7 hr. The produced particles were washed several times with distilled water to remove excess ions, and the washed precipitates were finally dried at 70 ° C over night as shown in figure 3.3.

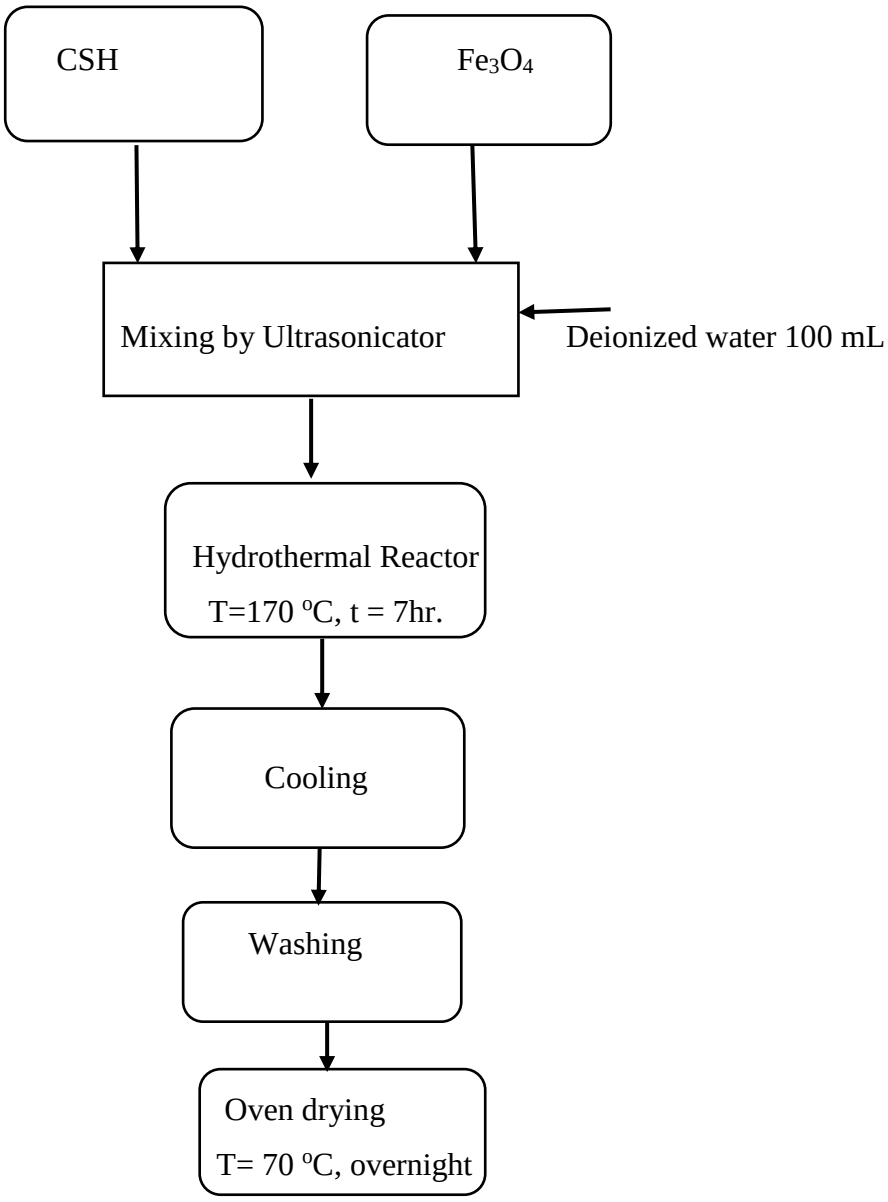

Figure 3. 3: Experimental framework for Fe_3O_4 loaded CSH composite

3.3. Material Characterization

3.3.1. Absorption Spectroscopy

To determine the chemical compositions of solid waste residue of Awash Melkassa chemical factory, Complete Silicate Analysis using analytical methods of Lithium Metaborate fusion ($LiBO_2$ Fusion), HF attack, Gravimetric, Colorimetric and Atomic Absorption Spectroscopy (AAS) were conducted. The analysis performed at Addis Ababa Ethiopian Geological survey.

3.3. 2. X-ray Diffraction (XRD)

X-ray diffraction (XRD) is one of the most considerably used techniques for characterization. Commonly, XRD gives information regarding the crystalline structure, nature of the phase, lattice parameters, and crystalline grain size. In this study the analysis of SWR of Aluminium sulphate plant, CSH and Fe_3O_4 loaded CSH composite were subjected to XRD machine model shimadzu XRD-7000 x-ray diffractometer using cu-kα radiation. The measurement condition for each test includes voltage = 40.0 (kV), current = 30.0 (mA) and scan range from 10.00 to 80.00 with 0.02 step size.

The average particles size are calculated by using Scherrer equation (Abraha, 2015).

$$D = \frac{K.\lambda}{\beta Cos\theta} \qquad 3.2$$

Where, D is crystalline size, K = (0.9) is a Scherrer constant, λ is the wavelength of the x-ray, θ is Bragg angle of corresponding diffraction peak and β is full width at half maximum (FWHM)

$$n\lambda = 2dsin\theta \qquad 3.3$$

Where n (an integer) is the "order" of reflection, λ is the wavelength of the incident X-rays, d is the interplanar spacing of the crystal and θ is the angle of incidence.

3.3.2. Fourier Transform Infrared Spectrometry (FTIR)

The functional group of CSH, Fe_3O_4 loaded CSH and solid waste residue of aluminium sulphate plant were detected using JASCO FT/IR-6600 type A model with Serial number A013861790. The FTIR spectrum from 4000-400 cm^{-1} in resolution 4 cm^{-1} recorded. Sample for the FTIR analysis were prepared by weighting the amounts of sample, 1 gm, and Potassium Bromide (KBr) powder, 100 gm into an agate mortar. The FTIR pattern is plotted within the FTIR machine by generating the transmittance peaks (%) as the Y-axis versus wavenumber (cm^{-1}) as the X-axis.

3.3.3. Brunauer-Emmett-Teller (BET)

The Brunauer-Emmett-Teller (BET) method is commonly applied to calculate the specific surface area based on nitrogen adsorption isotherm measurements at 77 K. In this study the specific surface area of the CSH and Fe_3O_4 loaded CSH were carried out using Horiba

Instruments, Inc SA-9600 Series surface area analyzer at 200 ^{O}C degassing temperature for 2 hr. in the presence of nitrogen gas.

3.3.4. Thermal gravimetric analysis (TGA)

Thermal gravimetric analysis (TGA) analysis was performed using (Beijing, HCT-1, TGA) analyzer. The Nitrogen gas used as carrier gas and the heating rate was set at 20^{o}C/min to determine the thermal stability of 10 mg of the solid waste residue of aluminium sulphate plant and Fe_3O_4 loaded CSH. The temperature was adjusted between 20 ℃ to 800 ℃ and the decomposition of sample weight (%) against temperature (℃) was recorded. This analysis resulted two types of curve, TGA curve and derivative Thermogravimetric (DTG) curve.

3.3.5. Scanning Electron microscope (SEM)

A scanning electron microscope (SEM) is a type of electron microscope that produces images of a sample by scanning the surface with a focused beam of electrons. The electrons interact with atoms in the sample, producing various signals that contain information about the surface topography and composition of the sample. In this study, the morphology of CSH before and after adsorption of nitrate ion as well as Fe_3O_4 loaded CSH before and after adsorption of nitrate ion was conducted using SEM analyzer of model: JCM-6000PLUS Bench Top SEM, JEOL, Japan. The procedure of analysis includes, 30 mg specimen is mounted on a metal stub using a sticky carbon tape, which increases conductivity. The clip holds the sample securely and that the clip was not obscuring any area that you intend to image. The specimen must be electrically grounded to the sample holder to minimize specimen charging. Specimen exchange, evacuation, and automatic adjustment of image carried out to photographing and finally the image saved.

3.4. Adsorption experiments

The nitrate removal by Fe_3O_4 based CSH adsorbent was carried out in a series of batch experiments. The experimental procedure was as follows. The Nitrate solution was prepared by dissolving known mass of KNO_3 (99.55% pure) in 1000ml deionized water. A number of parameters such as reaction time, the concentration of nitrate, adsorbent dose, and pH affecting the removal of nitrate ion were varied widely in order to optimize the removal process. The experiments were performed in several 500 mL plastic bottles, each including a different amount of nitrate solution. The solution pH was adjusted using the addition of 0.1 M HCl and NaOH.

3.5. Design of Experiment

3.5.1. Response surface method (RSM)

Response surface method (RSM) is used only when several a few factors are involved in the optimization process. Box and Wilson published it in 1951. The RSM determines the relation between different independent variables within one or more dependent variables (Response). The RSM, which is a special type of experimental design, can be described as a collection of both mathematical and statistical methods for designing, improving, optimizing, and formulating a product design, in which several variables can affect the characteristics of the product design. RSM is the most useful method for analyzing data, and is an effective statistical method for modeling optimization of several parameters affecting the response curve.

3.5.2. Central Composite Design (CCD)

CCD is an excellent design method for the process optimization and finding the best possible output from the experiments. It is an integral part of a response surface methodology. The biggest merit of this type of optimization model is its accurate and no need of 3 level factorial experiment for developing a quadratic model (Bhattacharya, 2021). Moreover, it turns out to be the extension of 2 level factorial or fractional factorial design and estimate nonlinearity of responses in the given data set. CCD is not the only used to estimate curvature in obtained continuous response, but also gives maximum information in a minimum experimental trial. Reduction in the number of trials required to estimate the squared terms in the second-order model. RSM based on CCD was adopted to study the interaction effect between five independent variables to optimize the bioremediation process of nitrate. The independent factor was coded at five levels: $-\alpha$, -1, 0, $+1$ and $+\alpha$ where, α (minimum) 1 (low), 0 (center), $+1$ (height) and $+\alpha$ (maximum) obtained from a preliminary experiment (M. E. E.-S. and S. S. Ibrahim, 2021).

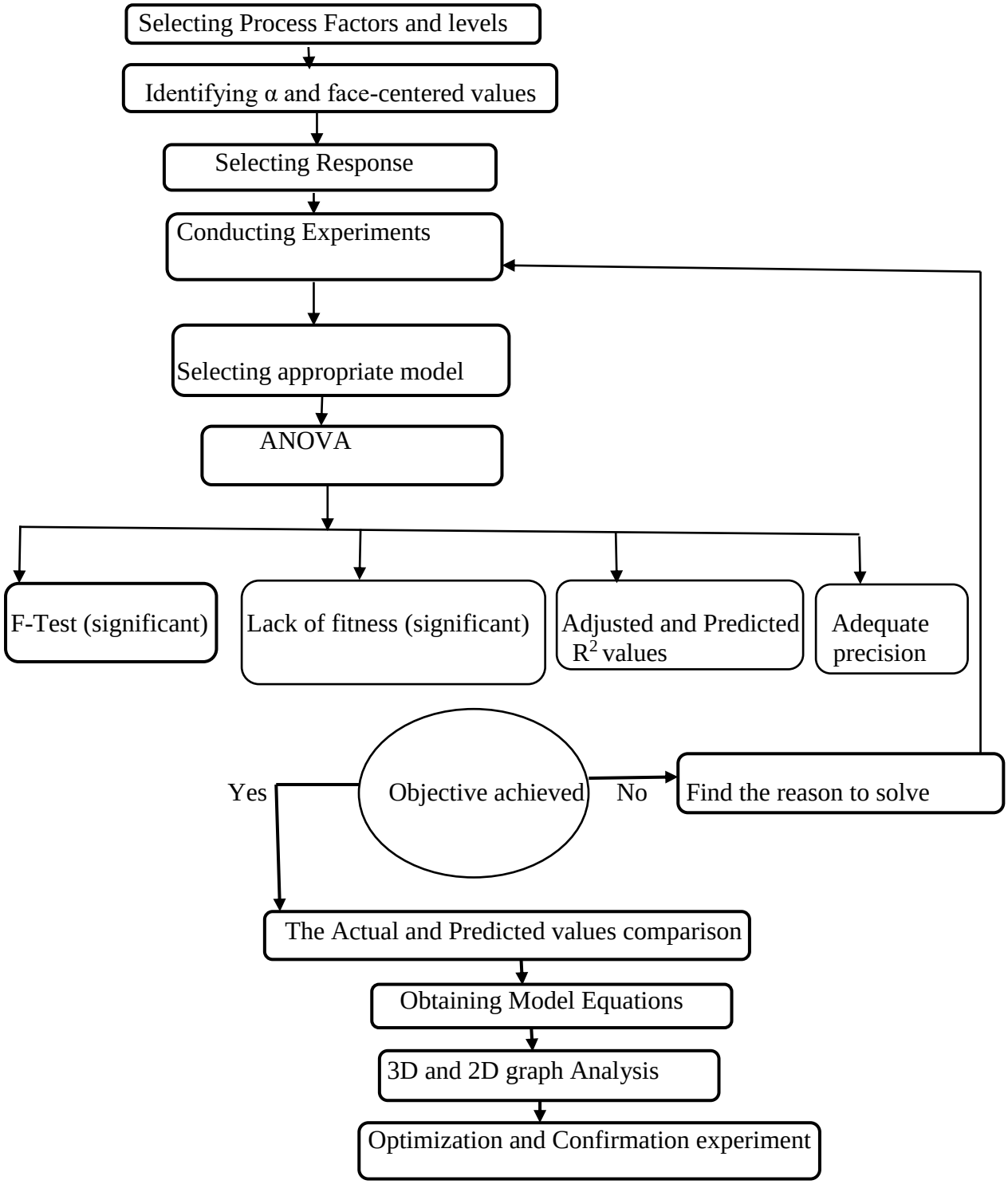

Figure 3. 4: Central Composite Design Analysis flow chart for optimization process

To perform optimization in process the fundamental tasks are screening, identifying the significant and important factors. The variable range and level are given in Table 3.1 in coded units resulting from RSM studies. The design was composed of 2k factorial points

augmented by 2^k axial points and a center point where k is the number of variables. Thus, 30 experiments ($2^k + 2k + 6 = 30$) were performed.

Table 3. 1: Experimental ranges and levels of the independent variables

Independent Variables	Units	- α	-1	0	+1	+ α
pH		2	4	6	8	10
Contact time	min	30	60	90	120	150
Initial nitrate Concentration	mg/L	10	35	60	85	110
Adsorbent Dose	g	0.8	1.6	2.4	3.2	4

The relation between the coded and actual values of a factor

$$\alpha = (2^k)^{1/4} \tag{3.4}$$

$$-\alpha = X_{min}\ and + \alpha = X_{max} \tag{3.5}$$

Where, Xmin and X_{max} represent the minimum and maximum level of factor.

$$-1 = \frac{(\alpha - 1)\text{Xmax} + (\alpha + 1)\,\text{Xmin}}{2\alpha} \tag{3.6}$$

$$0 = \frac{\text{Xmax} + \text{Xmin}}{2} \tag{3.7}$$

$$+1 = \frac{(\alpha - 1)\text{Xmin} + (\alpha + 1)\,\text{Xmax}}{2\alpha} \tag{3.8}$$

The nitrate removal efficiency (Re, %) the ratio of difference in nitrate concentration before and after adsorption calculated according the following formula given below:

$$Re = \frac{C0 - Ce}{\text{C0}}\ x\ 100\% \tag{3.9}$$

$$Rt = \frac{C0 - Ct}{\text{C0}}\ x\ 100\% \tag{3.10}$$

Nitrate adsorption Capacity at equilibrium (Qe) will calculated as:

$$Qe = \frac{(\mathrm{C0} - \mathrm{Ce})\mathrm{V}}{m} \qquad 3.11$$

Where C_0 is the initial nitrate concentration (mg/L), Ct nitrate concentration at given time t and Ce is the equilibrium concentration of nitrate (mg/L). V is the volume of working solution (L), and m is the dosage in (g)

The regression analysis was performed to estimate the response functions as a second order polynomial as shown below

$$\mathrm{y} = \beta_0 + \sum_{i=1}^{4} \beta\mathrm{i}\, xi + \sum_{i=1}^{4} \beta\mathrm{ii}\, x^2 + \sum_{i=1}^{3} \sum_{j=1+1}^{4} \beta\mathrm{ij}\ \mathrm{xij} + \varepsilon \qquad 3.12$$

Where y is percentage of Nitrate ion removed; Xi and Xj are the i^{th} and j^{th} coded independent variables; and β_0, Bi, Bii, and Bij denote the intercept, linear, quadratic, and interaction effect regression coefficients, respectively.

$$\mathrm{y} = \beta 0 + \beta 1\mathrm{A} + \beta 2\mathrm{B} + \beta 3\mathrm{C} + \beta 4\mathrm{D} + \beta 11\mathrm{A2} + \beta 22\mathrm{B2} + \beta 33\mathrm{C2} + \beta 44\mathrm{D2} + \beta 12\mathrm{AB} + \beta 13\mathrm{AC} + \beta 14\mathrm{AD} + \beta 23\mathrm{BC} + \beta 24\mathrm{BD} + \beta 34\mathrm{CD} \qquad 3.13$$

A, B, C, D are linear effects, A^2, B^2, C^2, D^2 are squared effects, AB, AC, AD, BC,BD, CD are interaction effects and Y is the predicted response. β_0 is constant coefficient, β_1,β_2,β_3,β_4 are linear coefficients, β_{11},β_{22},β_{33},β_{44} are squared coefficients, and β_{12},β_{13},β_{14},β_{23},β_{24},β_{34} are interactive coefficients, respectively.

Design expert version 11, was used for regression analysis of the data obtained as well as to estimate the coefficient of the regression equation. The equations were validated by the statistical test called ANOVA. The significance of each term in the equation is to estimate the goodness of fit in each case. Response surface used to determine the individual, square and interactive effects of test variable on percentage removal of nitrate ions.

3.6. Adsorption Kinetics

3.6.1. Pseudo-first-order kinetics

Lagergren presented a first-order rate equation to describe the kinetic process of liquid–solid phase adsorption that is expressed (Yifru Waktole Berkessa, 2019):

$$\frac{dq_t}{dt} = k1(q_e - q_{t)} \quad 3.14$$

Where q_e (mg/g) and q_t (mg/g) are the amounts of nitrate adsorbed on the adsorbent at equilibrium and at any time t, respectively, and k_1 (min^{-1}) is the rate constant of the first-order adsorption. After integration and applying boundary conditions q_t= 0 at t=0 and q_t=q_t at time=t, the integrated form:

$$\ln(q_e - q_t) = lnq_e - K_1 t \quad 3.15$$

The value of k_1 and q_e can be obtained from the slope and intercept of the linear plot of ln ($q_e - q_t$) versus t, respectively

3.6.2. Pseudo-second-order kinetics

The pseudo-second-order kinetic model can be expressed as the following equation

$$\frac{dq_t}{dt} = K_2(q_e - q_t)2 \quad 3.16$$

Where K_2 (g/mg min) is the rate constant of the second-order equation; qe (mg/g) is the maximum adsorption capacity; and qt (mg/g) is the amount of adsorbate adsorbed at time t (min). After integration:

$$\frac{t}{q_t} = \frac{1}{k_2\, q\mathrm{e}2} + \frac{t}{q_e} \quad 3.17$$

The value of q_e and k_2 will be obtained from the slope and intercept of the linear plot of t/qt versus t, respectively. The value of q_e and k_2 can be obtained from the slope and intercept of the linear plot of t/qt versus t, respectively.

3.6.3. Intraparticle diffusion

According to the intra-particle diffusion model, the plot of qt versus the square root of time ($t^{0.5)}$ should be linear if the intra-particle diffusion is involved inside the adsorption process. Moreover, if these lines pass through the origin when the intra-particle diffusion is the race-controlling step, and two or more slopes could occur in a multi-step adsorption process (Pan et al., 2017). Intraparticle diffusion model based on the theory proposed by Weber and Morris was used to determine whether particle diffusion was rate-limiting step

or not during adsorption of nitrate onto Fe_3O_4 loaded CSH. The mathematical equation for intraparticle diffusion model is given in Equation below

$$q_t = K_p t^{0.5} + C \quad (3.18)$$

Where qt is the amount of nitrate adsorbed (mg/g) at a given time t (min) and k_p (mg/g $min^{1/2}$) is the intraparticle diffusion rate constant and C is intercept. The kp and C value were obtained from plotting of qt versus $t^{0.5}$.

3.7. Adsorption isotherm

Adsorption isotherm is a curve describing the phenomenon governing the retention (release) or mobility of a substance from the aqueous porous media or aquatic environments to a solid phase at a constant temperature and pH (Yifru Waktole Berkessa, 2019).

3.7.1. Langmuir isotherm

A Langmuir isotherm model was originally used to describe gas sorption on monolayer homogeneous solid surface. The assumption for this model includes identical adsorption sites could be used to predict adsorbate–adsorbent interaction at liquid–solid interface.

$$q_e = q_{max} \frac{K_L C_e}{1 + K_L C_e} \quad (3.19)$$

$$\frac{C_e}{q_e} = \frac{1}{q_{max} K_L} + \frac{C_e}{q_{max}} \quad (3.20)$$

$$\frac{1}{q_e} = \frac{1}{q_{max} K_L} . \frac{1}{C_e} + \frac{1}{q_{max}} \quad (3.21)$$

Where, qe is the amount adsorbed (mg/g), C_e is the equilibrium concentration of adsorbate (mg/L), while q_{max} and K_L are constants related to adsorption capacity and energy of adsorption, respectively. In addition, a dimensionless constant, commonly known as separation factor (R_L) defined by Webber and Chakkravorti, is presented in in equation below.

$$R_L = \frac{1}{K_L C_0} \quad (3.22)$$

Where, K_L (L/mg) refers to the Langmuir constant and C_0 is the adsorbate initial concentration (mg/L). The computed R_L value suggests the adsorption nature to be either

unfavorable ($R_L > 1$), linear ($R_L = 1$), favorable ($0 < R_L < 1$) or irreversible ($R_L = 0$) (Foo & Hameed, 2010).

3.7.2 Freundlich isotherm

The Freundlich isotherm is empirical equations, which use to describe non-ideal sorption on heterogeneous surfaces and multilayer sorption; Freundlich isotherm summarized according to equation

$$q_e = k_f \ C_e^{1/n} \tag{3.23}$$

$$lnq_e = lnk_{f\,+} \left(\frac{1}{n}\right) lnC_e \tag{3.24}$$

Where Ce is the equilibrium concentration (mg/L), kf, and n are Freundlich isotherm constants related to adsorption capacity and adsorption intensity, respectively. The magnitude of the exponent, 1/n, gives an indication of the favorability of adsorption. Values of $n > 1$ represent favorable adsorption condition. Values of K_f and n are calculated from the intercept and slope of the plot.

3.7.3. Temkin Isotherm

Temkin isotherm model can relate the effects of indirect adsorbate/adsorbate interactions on the adsorption process; it is also assumed that the heat of adsorption of all molecules in the layer decreases linearly as a result of increase surface coverage (Ayawei et al., 2017). This isotherm consists of an aspect that explicitly takes into consideration of adsorbent–adsorbate interactions through ignoring the extremely low and huge value of concentrations, the model assumes that heat of adsorption (function of temperature) of all molecules within the layer would decrease linearly instead of logarithmic with coverage (Olalekan et al., 2012). The linear form of Temkin isotherm model is given by the following equations. The adsorption parameters (A_T and B) were determined from the slope and intercept of the qe versus ln Ce plot based on the linearized equation as presented in **Error! Reference source not found.**

$$\mathrm{qe} = \frac{\mathrm{RT}}{\mathrm{b}} \ln(\mathrm{A_T C_{e)}} \tag{3.25}$$

$$\mathrm{qe} = \frac{\mathrm{RT}}{\mathrm{b_T}} \ln \mathrm{A_T} + \frac{\mathrm{RT}}{\mathrm{b_T}} \ln \mathrm{C_e} \tag{3.26}$$

$$qe = \frac{RT}{b_T} \ln A_T + \frac{RT}{b_T} \ln C_e \quad (3.27)$$

$$qe = B \ln A_T + B \ln C_e \quad (3.28)$$

$$B = \frac{RT}{b_T} \quad (3.29)$$

Where A_T = Temkin isotherm equilibrium binding constant (L/g)

b_T = Temkin isotherm constant

R= Universal gas constant (8.314J/mol.k)

T = Temperature 298 k

B = Constant related to heat of sorption (J/mol)

3.8. Adsorption Thermodynamics

The thermodynamic reputation of the adsorption operation is important to study when the adsorption operation is favorable or unfavorable. This adsorption behavior can occur using thermodynamic factors involving the Gibbs free energy difference (ΔG), the enthalpy difference (ΔH), and the entropy change (ΔS). The units for ΔG and ΔH are joules, and the unit for ΔS is joules per kilogram. Gibbs free energy indicates the spontaneous character of the adsorption (ΔG< 0 for the spontaneous process), while enthalpy values determines the endothermic or exothermic nature of the process (ΔH< 0 is exothermic while ΔH> 0 is endothermic). Positive values of ΔS indicate increased randomness at solid-liquid interphase during the sorption processes, hence increased adsorption performance (Tsamo et al., 2019). The following equation is the main equation and that can be used to connect the between the adsorption factors.

$$\Delta G = \Delta H - T\Delta S \quad (3.30)$$

T assigned to the absolute temperature in Kelvin. The difference in Gibbs free energy can be also determined by the equation:

$$\Delta G = -RT \ln K_d \quad (3.31)$$

When; R assigned to the universal gas constant that equals 8.314 J/mol.K. Kd assigned to the thermodynamic equilibrium constant that equals (qe/Ce) with a unit of mol or (L/g). The combination of the last two equations will give this equation:

$$lnK_d = \frac{\Delta S}{R} - \frac{\Delta H}{RT} \quad 3.32$$

The plot of lnKd versus (1/T) will give a straight line with (-ΔH/R) as a slope and (ΔS/R) as an intercept. The resulting graph is known as Van't Hoff plot.

$$K_d = \frac{q_e}{C_e} \quad 3.33$$

These parameters can be obtained from experiments at various temperatures using the equations prior to the ΔHº and ΔSº values are determined from the slope and intercept of a linear plot of (ln Kd) versus (1/T).

3.9. The effects of co-existing ions

To study the co-existing of ions three different ions such as phosphate, chloride and carbonate were selected, which are commonly present in water, and competes with nitrate during the adsorption process (Loganathan et al., 2013). The sources of the ions includes anhydrous potassium dihydrogen phosphate (KH_2PO_4), Nacl and Na_2CO_3 respectively. For each ions, 20 mg/L of each initial concentration for optimum 85 mg/L of initial nitrate concentration conducted based on work (Berkessa et al., 2019). The adsorption of co-existing ions were involved at optimum operating parameters.

3.10. Desorption Experiments

The nitrate ions allowed to the adsorption process by Fe_3O_4 loaded CSH composite adsorbent. After adsorption, the supernatant was analyzed for residual adsorbate after separating the adsorbate by magnetic separation. The Fe_3O_4 loaded CSH composite adsorbent was treated with 1M NaOH. The gently agitated solution washed by deionized water. The treated and separated adsorbent was subjected to oven dry for six hour at 60 ºC. Then the adsorbent was ready for further adsorption and the adsorption-desorption was repeated for four cycles.

CHAPTER FOUR

RESULT AND DISCUSSIONS

4.1. Characterization of Materials

4.1.1. Atomic Absorption Spectroscopy

The analyses as indicated in (Table 4.1) show that the mass ratio of SiO_2/Al_2O_3 is 3.95. This high value suggests the presence of a large amount of free silica (Quartz). The solid waste residue showed 14.78 % of loss-on-ignition (LOI), and it may be due to the dehydroxylation of the sample and removal of its organic compounds. Loss on ignition (LOI) is a normally used technique to determine the organic matter content of clay by means of oxidation at an elevated temperature in a muffle furnace through measuring the weight loss. It is a check designed to measure the quantity of moisture or impurities lost while the sample is ignited under the situations targeted in the individual monograph (Battas et al., 2019).

Table 4. 1: Complete Silicate Analysis in (%) of elements determined for SWR

Components	%
SiO_2	65.44
Al_2O_3	16.57
Fe_2O_3	0.48
CaO	< 0.01
MgO	< 0.01
Na_2O	< 0.01
K_2O	1.60
MnO	< 0.01
P_2O_5	0.19
TiO_2	< 0.01
H_2O	1.22
LOI	14.73

Where, LOI indicates Loss on Ignition

4.1. 2. XRD Result Analysis

Figure 4.1 demonstrates the X-ray diffraction spectra of Awash Melkassa chemical factory, CSH before and after Adsorption. As shown from the figure CSH showed the intense peak at 29.5 ° it has been observed that there only exists one broad peak with a range of 10°~ 37°, amplifying its amorphous feature**.** There were clear diffraction peaks at 29.5°, 32.02° and 50.33° , which also confirmed within the result of that was done by (Kuwahara & Yamashita, 2017). The minor peaks at 18.05 and 34.1 degrees can be indexed to $Ca(OH)_2$ as observed from the XRD result which was the byproduct produced during calcium silicate hydrate formation. After nitrate adsorption, the diffraction peaks at 2θ values of 20.5^o, 22.9^o, and 35.8^o appeared suggesting that nitrate ion was adsorbed successfully on the positive layer of Calcium Silicate Hydrates (CSH) (H. Zhou et al., 2020).

From the complete silicate analysis of solid waste residue of Awash Melkassa chemical Factory, the major 65.44% of the component was SiO_2 and 16.57% of Al_2O_3 with other traces of minor oxides. As shown from figure 4.1 silica was found with the highest peak in a major constituent. As (Mor et al., 2016) studied, the sharp peak at 2θ from 20 - 40 degrees indicates the presence of a crystalline phase of SiO_2. The band at 2θ = 25^o indicates the presence of crystal silica component in solid waste residue (Peng et al., 2017). The well-defined diffraction at 2-Theta values of 12.4^o and 62.5^o corresponds to kaolinite. Moreover, the peaks corresponds to the 2θ values of 27.5 and 41.6 are typical characteristics of kaolinite. Components of quartz (SiO_2) are located at 2θ angles (^{o}) of 26.5, 39.5, and 45.7 (Zewdie et al., 2021).

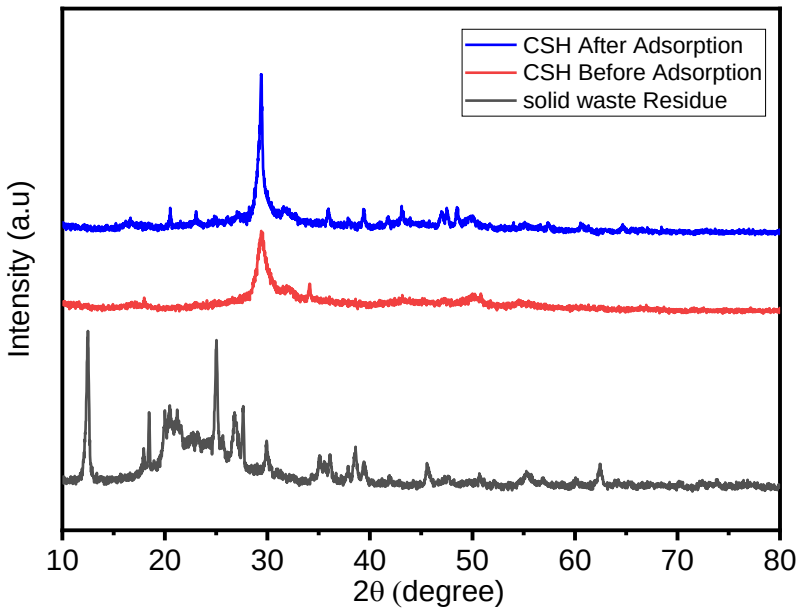

Figure 4. 1: The X-ray diffraction patterns of SWR, CSH Before and after adsorption

The crystal phase of Fe_3O_4 loaded CSH composite are investigated using X-ray diffraction. As observed from figure 4.2, the crystal structure of Fe_3O_4 has not changed after reaction with calcium silicate hydrates. The broad peak shown at $2\theta = 29.5^{o}$ because of a unique crystal structure of Calcium Silicate Hydrates (CSH) (Zhang et al., 2015).

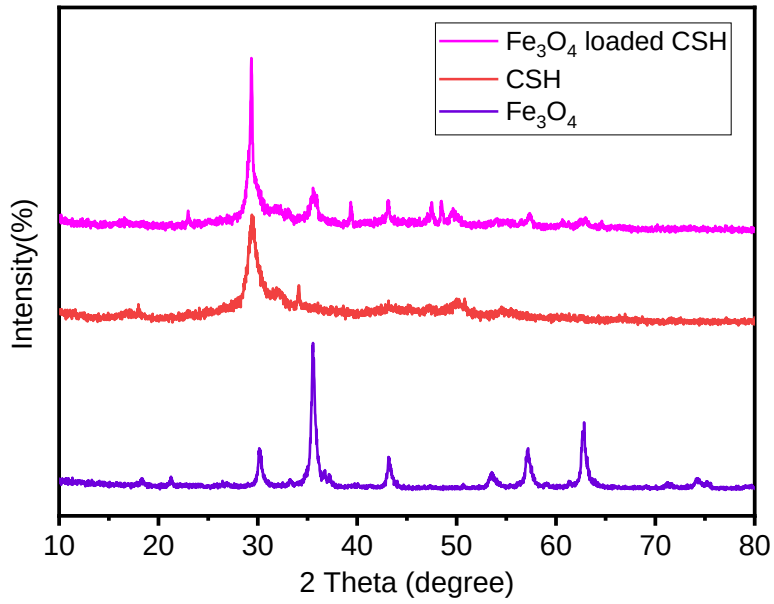

Figure 4. 2: The X-ray diffraction patterns of Fe_3O_4, CSH and Fe_3O_4 loaded CSH

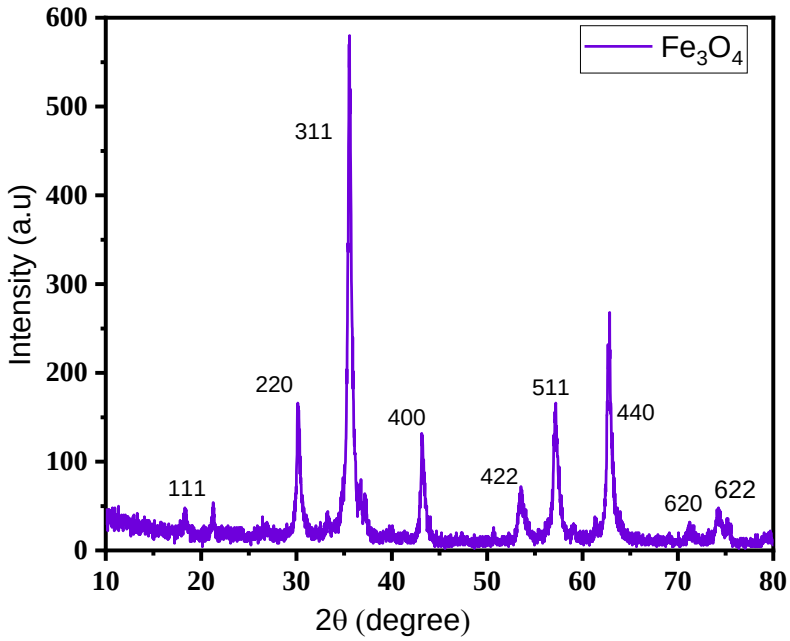

Figure 4. 3: The X-ray diffraction (XRD) patterns of Fe_3O_4

The XRD analysis was carried out to identify the crystal nature, phases, and average particle size of the dried powders of the magnetite. The pattern of XRD showed a number of Bragg's reflections that may be indexed based on the face-centered cubic structure of magnetite. The magnetite (Fe_3O_4) showed the angles corresponding to the peaks at 2θ of 18.3, 30.1, 35.5, 53.4, 57.1, 62.6, 71.1, and 74.4, which are represented the crystalline phase of magnetite. The XRD spectrum exhibited peaks corresponding to their crystal plane in a crystal lattice of 220, 311, 400, 422, 511, 440, 620, and 622 respectively. The result obtained was the same as magnetite found by (Loh et al., 2008). In addition, the results of phase analysis for magnetite Fe_3O_4 particles have a consistent result within peaks that appear in the sample with the literature Joint Committee on Powder Diffraction Standards (JCPDS file, No. 19-0629) (Byong Yong Yu, 2010). The extreme broad peaks indicating the ultra-fine as well as small crystallite size of the particle. Therefore, the observed peak positions and their relative intensities indicates, the formation of high purity crystalline Fe_3O_4 product (Ghandoor et al., 2012). Based on Scherer's equation the average crystallite size of 16.523 nm was obtained.

Table 4. 2: The crystallite size and d- spacing for magnetite (Fe_3O_4)

Peak position (2 Theta)	Theta	d-spacing	FWHM	Crystallite Size D (nm)	D nm (average)
18.3401	9.17005	4.833553	0.55861	14.40563857	16.52263349
21.26605	10.63303	4.174663	0.29627	27.28282428	
30.21297	15.10649	2.955715	0.52725	15.60672386	
35.58364	17.79182	2.52095	0.56335	14.81019792	
43.23819	21.6191	2.090739	0.49296	17.33493148	
53.58884	26.79442	1.708776	0.67052	13.2730874	
57.20798	28.60399	1.608972	0.67921	13.32236598	
62.80013	31.40007	1.478473	0.61428	15.15163809	
74.30147	37.15074	1.275513	0.56902	17.51629381	

4.1. 3. FT-IR Result Analysis

The spectra of Awash Melkassa Aluminium sulphate solid waste residue, CSH before and after adsorption are depicted in figure 4.4. The broad peak around 3438 cm^{-1} of Awash Melkassa Aluminium sulphate solid waste residue represents hydroxyl stretching vibration (Al-OH or Si-OH) (Aragaw & Angerasa, 2020). The broadband at 3530 cm^{-1} shown from the solid waste residue was as a result of –OH stretching that exists in the inner hydroxyl group between the tetrahedral and octahedral sheets (Sarma & Bhattacharyya, 2019). As (Balan et al., 2021) studied, the stretching frequencies of OH groups are mainly controlled by the strength of H bonding and by the nature of the neighboring cations. H_2O stretching was also found at 1650 cm^{-1}. The smaller peak around 574 cm^{-1} corresponds to Si-O-Al bending vibration that demonstrates the aluminium sulphate solid residue contains silicon dioxide and aluminium oxide. The peak around 986 cm^{-1} are corresponding to Si-O-Si stretching, which is the same result, which found by (Aragaw & Angerasa, 2020) and (M. S. Chen et al., 2004). On the other side, the sharp peak located at 457 cm^{-1} illustrates Si-O deformation.

Form the CSH sample before adsorption FTIR spectrum around 963 cm^{-1} can be responsible for the coupling of the vibrations of Si-O-Si, Si-OH and Si $(OSi)_3$ O-Ca groups. The absorption peak of CSH at 457 cm^{-1} could be assigned to the bending vibration of Si–O–Si. These two characteristic peaks demonstrated that the CSH had a Si-

O tetrahedron structure (Fang et al., 2018). On both CSH before and after adsorption, the broad and sharp peak observed around 3642 cm^{-1} corresponding to O-H of coordinated water molecules. The obtained result was confirmed within the result that was done by (Guan, Ji, Chen, et al., 2013). The band at 682 cm^{-1} is a characteristic of silicon dioxide and is possessed by the symmetric stretching vibration of Si-O-Si. In addition, the peak showed at 1658 cm^{-1}indicates the existence of hydroxyl groups (O-H stretch) that proofed the presence of water in the chemical structure of calcium silicate. The bands between 1443 and 1462 cm^{-1} are responsible for Ca-O. There have been two linkage kinds of hydroxyl groups in CSH such as Ca-OH with Si-OH linkages, and the Ca-OH linkage, which could react with nitrates accounted for the main proportion due to the low crystallinity of CSH (Fang et al., 2018).

The CSH after adsorption showed the broadband and sharp peak at 1443 and 870 cm^{-1} can be attributed to the characteristic peak of indicates the existence of a Ca-O (Guan, Ji, Cheng, et al., 2013). According to (Fang et al., 2018) reported CSH has the potential to release Ca^{2+} and OH^{-} ions to form precipitates with nitrates in the solution. The broad peak at 686 cm^{-1} corresponds to the vibrations of nitrate groups (Gensh et al., 2011). Moreover, the sharp peak showed around 800 cm^{-1} corresponding to symmetric stretching of nitrate ion, as supported by the literature (Vicente-mart et al., 2021). The presence of shoulder in a CSH after adsorption illustrates the overlapping peaks of Si-O-Si and SiO molecules adsorbing irradiation with the same ranges.

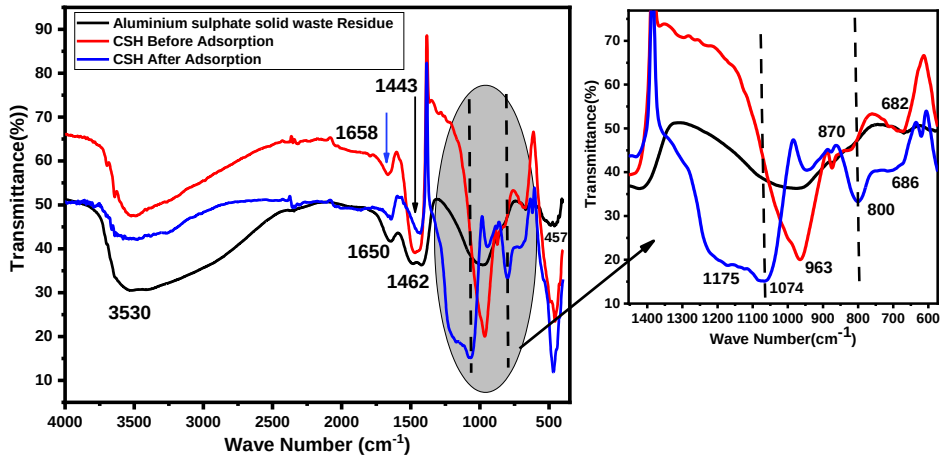

Figure 4. 4: FTIR spectra of solid waste residue, CSH before and after adsorption

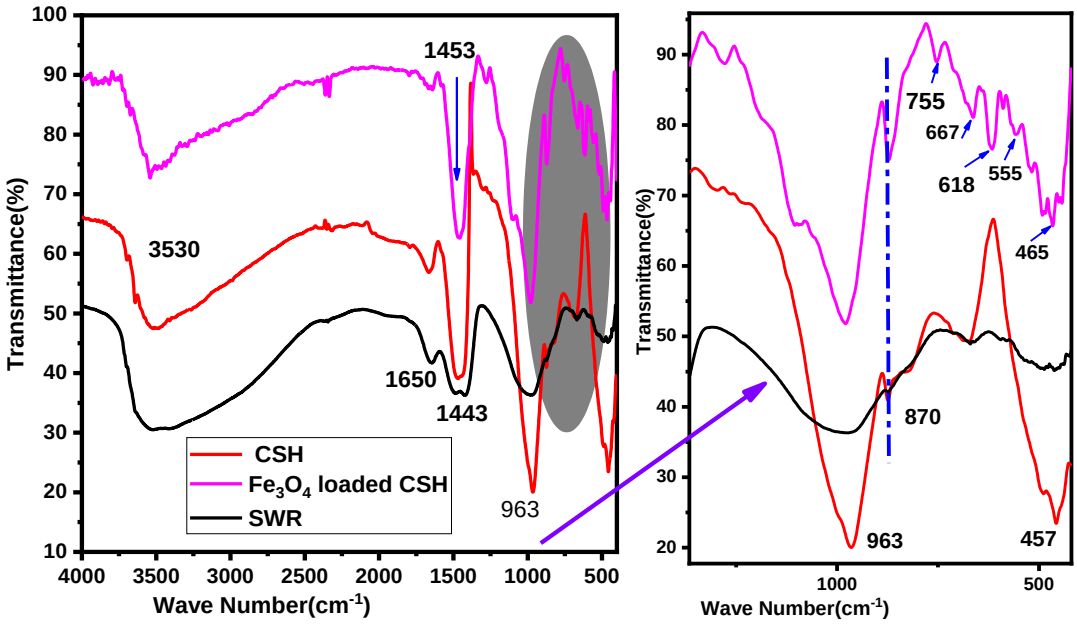

Figure 4. 5: FTIR Spectra of SWR, CSH and Fe_3O_4 loaded CSH composite

FTIR spectroscopy was conducted to identify the surface functional groups of Fe_3O_4 loaded CSH before and after the adsorption of nitrate ions from water. As figure 4.6 illustrates before adsorption the band at 981 cm^{-1} corresponds to the Si–O–H stretching vibration. The strong asymmetric stretching vibration of Si-O-Si was observed at 1092 cm^{-1}. The broadband centered around 3540 cm^{-1} designates the stretching vibration of the water molecules and O-H of CSH. On the Fe_3O_4 loaded CSH composite spectrum the broad OH absorption peaks possibly happened as a result of stretching vibration of water molecules on silica or magnetite. A large number of OH groups on the particle surface can contribute to the adsorption of nitrates. A similar results were reported by (Zhang et al., 2015). The band at approximately 1640 cm^{-1} indicated the bending vibration of water molecules, which point out the hydration of silicon dioxide and calcium oxide on the magnetite surface. The increase in the intensity of the OH stretching band could be due to the increase in the abundance of silanol (SiOH) as well as molecular water; the intensity increase of the H_2O bending mode certainly indicates the amount of molecular water. The absorption peaks from 465-618 cm^{-1} confirm the presence of stretching vibration of the Fe-O bond. A similar result was obtained by (Asab et al., 2020). Figure 4.5. Illustrates the FTIR spectra of aluminium sulphate solid waste residue, CSH and Fe_3O_4 loaded CSH. The different peaks formed because of Fe-O attachment on the Fe_3O_4 loaded CSH composite. Again a sharp peak at 755 cm^{-1} attributed to Fe-O-H bending vibrations (Mehrabi et al., 2015). From this FTIR result, it can be concluded that Fe_3O_4 loaded successfully to the

calcium silicate hydrates. The broadband at 1453 cm^{-1}, and sharp peak at 870 can be associated to the characteristic peak of CaO (Guan, Ji, Cheng, et al., 2013). The band at 667 is formed due to Fe-O-Si stretching (Azeddine et al., 2013).

After the adsorption of nitrate by Fe_3O_4 loaded CSH, the maximum band located at 1384 cm^{-1} can be assigned to the stretching vibration of NO_3^- ions intercalated in the interlayer. (Abdolmohammad-zadeh et al., 2012) on his study found the same result. The smaller peak at 804 cm^{-1} corresponding to symmetric stretching of nitrate ion. The bending vibration of water shifted to 1636 cm^{-1} by 4 cm^{-1} units from Fe_3O_4 loaded CSH before adsorption which implied a larger constraint as the result of water molecule association into the host structure.

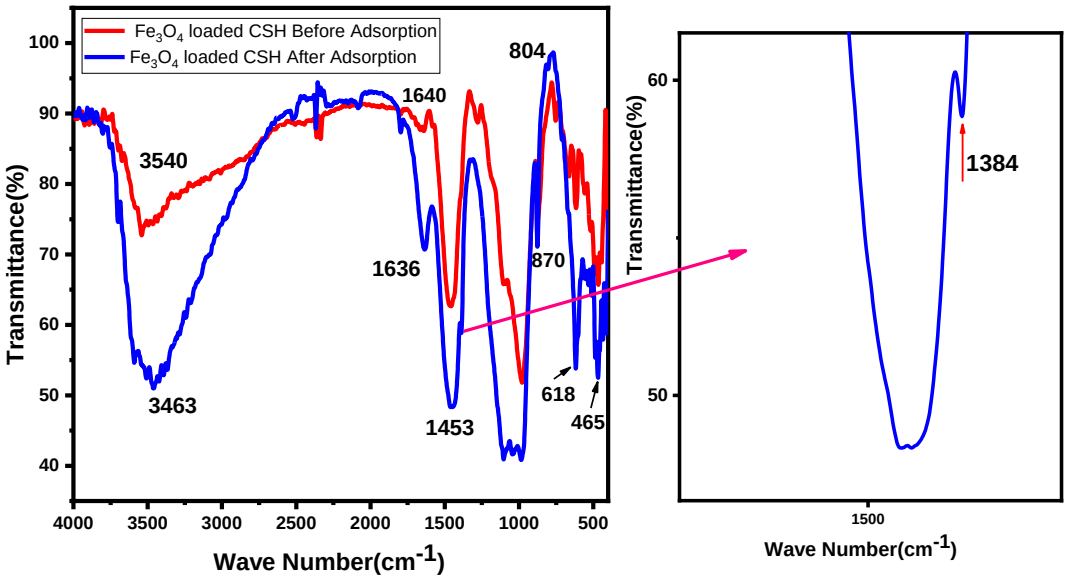

Figure 4. 6: FTIR spectra of Fe_3O_4 loaded CSH before and after adsorption

4.1.4. BET Result Analysis

The specific surface area of CSH and Fe_3O_4 loaded CSH were determined using the Brunauer–Emmett–Teller (BET). The specific surface area of Fe_3O_4 loaded CSH composite was found to be 163 m^2/g, which was higher than CSH of 91 m^2/g as observed from table 4.4. The increase of the specific surface area of Fe_3O_4 loaded CSH can be due to the presence of magnetic Iron oxide texture on the surface of CSH. The increased specific surface area provided a large number of active sites for the adsorption of the nitrate ion (S. Wang et al., 2021). In addition, materials with a higher surface area have excellent adsorption properties such as lack of internal diffusion, high surface binding

energy, and adsorption activity (Tyagi et al., 2018). The specific surface area result found by (Zhang et al., 2015) for magnetic calcium silicate hydrate was 196 m^2/g. The smaller amount of the surface area of Fe_3O_4 loaded CSH could be because of the agglomeration of the composite adsorbent to each other.

Table 4. 3: BET surface area result for CSH and Fe_3O_4 loaded CSH composite

Sample	**Surface area(m^2/g)**
Calcium silicate Hydrate	91
Fe_3O_4 loaded CSH composite	163

4.1. 5. Scanning Electron Microscope (SEM) Analysis

Scanning Electron Microscope (SEM) investigated the morphology nature of CSH before and after adsorption. As seen in figure 4.7 the vacant pores of CSH was observed before adsorption. The surface of CSH shows a highly porous structure, which enables a suitable diffusion channel for nitrate adsorption. In addition, it consist of smaller particles which had larger enough surface area to uptake nitrate (Xiaowen Tong et al., 2017). On the other side, as figure 4.7 depicted, CSH after adsorption appeared to have improved, smooth and homogenous surfaces. The porous structure of CSH loosed, and the irregular collective surface was observed after adsorption. After adsorption, the SEM images confirm that pores, and interstice were occupied by the solute molecules of nitrate ions. The external surface of CSH after adsorption is almost flat in the presence of agglomeration and cavities of the adsorbent observed. The nitrate molecule insert into the region of oxygen-silicon tetra hedron chain or layers of CSH (Guan, Ji, Chen, et al., 2013).

a) 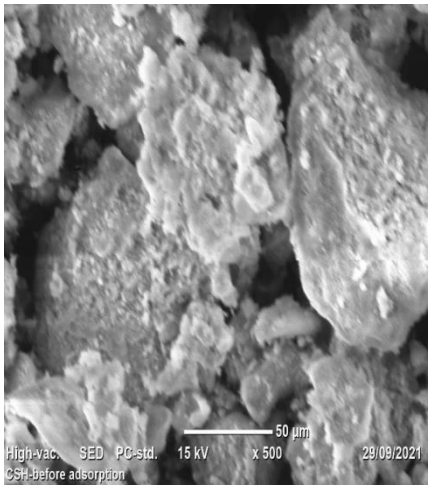

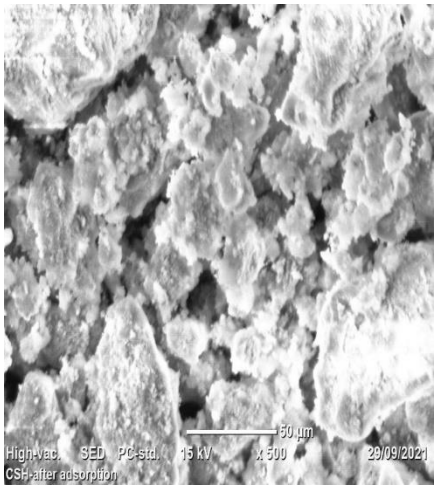

b)

Figure 4. 7: SEM images of a) CSH before adsorption b) CSH after adsorption

The dispersion of Fe_3O_4 into the surface of CSH was further illustrated by analyzing the surface morphology of the composite using the Scanning electron microscope. The SEM images figure 4.8 indicated CSH had a larger particle size of the heterogeneous structure, which constitute a smaller tiny particle surrounded in the whole surface. The morphology of CSH particles seems to have a non-spherical and irregular shape (Kuwahara & Yamashita, 2017). However, the addition of Fe_3O_4 to the surface of CSH leads to a smaller surface area of composite within homogenous and smooth surface morphology. The particles of Fe_3O_4 homogenously intercalated through the surface of CSH as observed. The improvement in surface area and structural properties of the composites enhance the removal efficiency of nitrate ions from the wastewater. According to (Zhang et al., 2015) work the Fe_3O_4 particles could be embedded in the CSH.

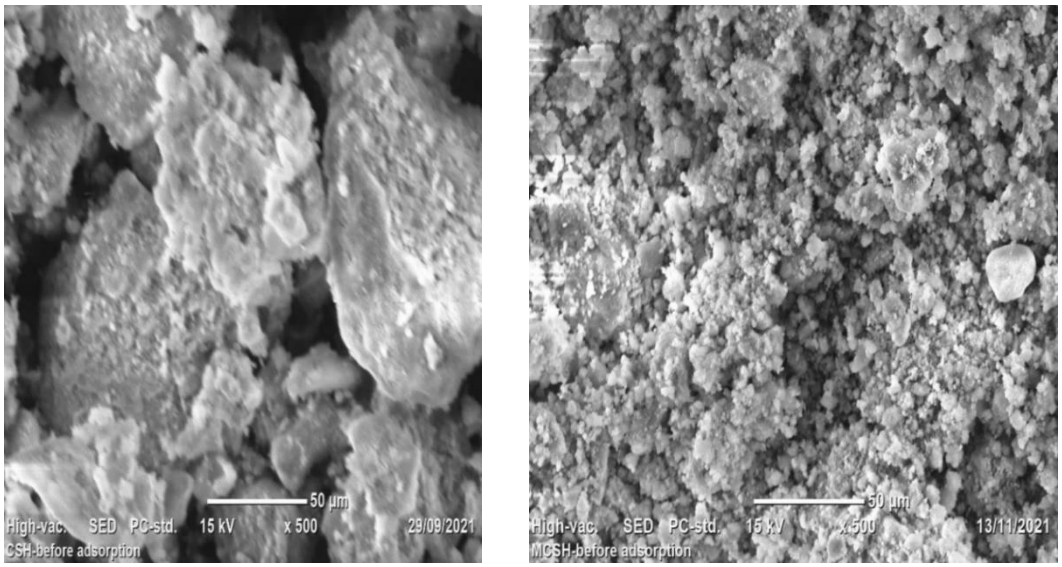

(a) **(b)**

Figure 4. 8: SEM images before adsorption for a) CSH b) Fe_3O_4 loaded CSH composite

The Fe_3O_4 loaded CSH before and after adsorption was illustrated by analyzing the surface morphology of the composite using the Scanning electron microscope. The typical SEM images presented in figure 4.9 shows Fe_3O_4 loaded CSH before adsorption with spherical agglomerated surfaces to each other (Peng et al., 2017). The SEM images indicated Fe_3O_4 loaded CSH after adsorption showed rougher, floc appeared and the number of pores increased. In addition, fine collective solute materials appeared after adsorption, which ensures the attachment of nitrate ions on the surface of Fe_3O_4 loaded CSH composite. The clear visible white color of uniform size distribution is located on the surface of the Fe_3O_4 loaded CSH composite. The nitrate-loaded composite adsorbent-

exhibited rougher surface than fresh sample before adsorption, this implied that the surface layer changed because of the interaction between nitrate ion and the functional groups on the adsorbent surfaces.

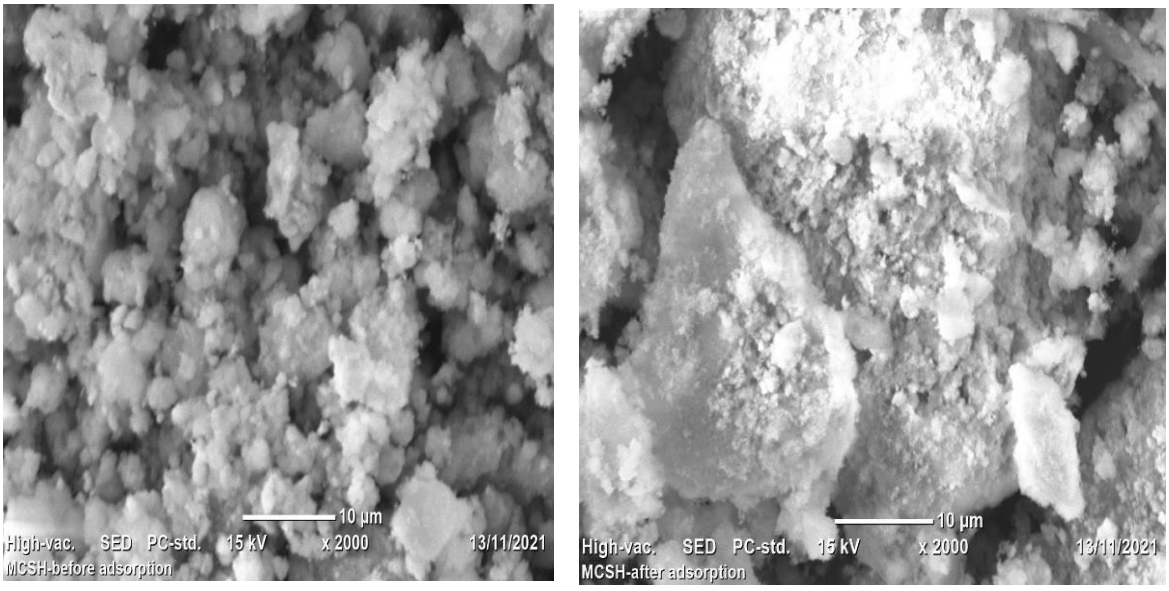

(a) **(b)**

Figure 4. 9: SEM images of Fe_3O_4 loaded CSH a) before adsorption b) after adsorption

4.1. 6. TGA analysis of Aluminium sulphate SWR of Awash Melkassa Chemical Factory

The solid waste residue of the aluminum sulfate plant of Awash Melkassa chemical Factory was subjected to Thermogravimetric analysis (TGA-DTA) to get the weight loss against temperature profile. Figure 4.10 depicts Thermogravimetric Analysis of Aluminium sulfate Solid waste Residue. The SWR shows three-step weight loss over the temperature range of TG analysis. The first endothermic mass loss from 30-200 ^oC is due to moisture loss and evaporation of surface adsorbed water. The second loss ranges from 200-500 ^oC corresponding to the decomposition of organic substances that exist in SWR. The stored solid waste residue over a long period may consist of different organic matters such as microorganisms like fungi, undecomposed plants, and stable organic matters (humus). The third weight loss in the range between 500-700 ^oC can be attributed to endothermic dehydroxylation (or alternatively, dehydration) to produce disordered metakaolin ($Al_2Si_2O_7$). In addition, at this range structure loses its crystallographic order.

According to (H. Wang et al., 2011) studied, endothermic mass loss of the kaolin from 450–600 ^{o}C was a result of metakaolin disordered and dehydroxylation continued up to 900 ^{o}C. Moreover, a previous study by (Kheshti, et al 2019) indicates that the decomposition of organic substances occurred at the range of 200-600 ^{o}C.

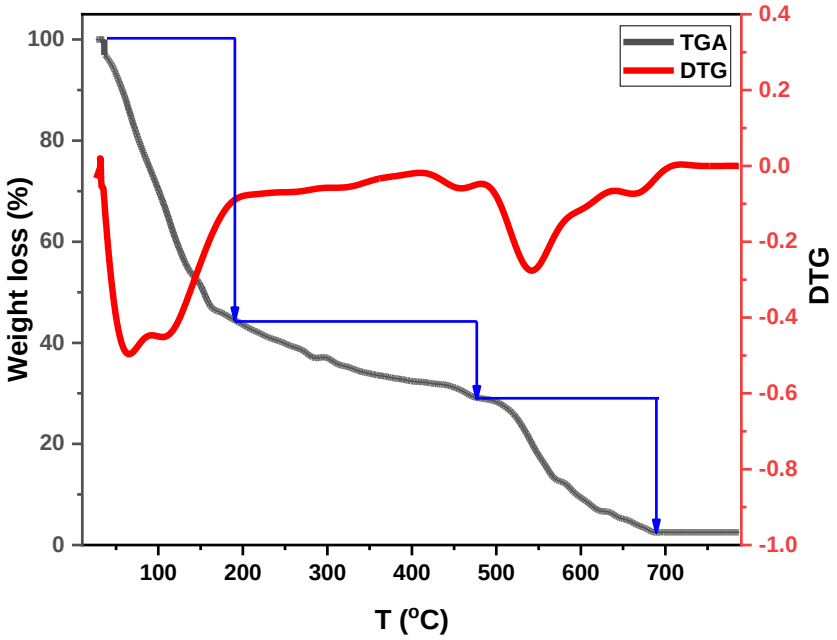

Figure 4. 10: Thermogravimetric Analysis of Aluminium sulphate Solid waste Residue

4.1.7. Thermogravimetric analysis of Fe_3O_4 loaded CSH composite

The stability of Fe_3O_4 loaded CSH composite adsorbent was determined by the Thermogravimetric analysis (TGA) and derivative Thermogravimetriy (DTG). The TGA curve Fe_3O_4 loaded CSH composite can be explained in figure 4.11, the TGA curve demonstrated that the major two regions of weight loss formed over the temperature range of TG analysis. The first region quick weight loss of up to 300 ^{o}C is occurred because of crystal and adsorbed water loss. The second region the major loss between 300-700 ^{o}C characterized by the weight loss due to dehydration of CSH and dehydroxylation of calcium hydroxide. Fe_3O_4 loaded CSH contains a large amount of water and hydroxyl groups in the structure is a result of its overall low crystallinity.

According to (Begaye, 2014) studied the Weight loss below 180 ^{o}C is associated with the evaporation of surface adsorbed water. In addition, the weight loss above 550 ^{o}C is attributed to the release structure of water. The result found by (Zhang et al., 2015) proved that the weight loss between 200-600 ^{o}C as a result of CSH dehydration. The

dehydroxylation of calcium hydroxide occurred in the range of 400- 600 ^{o}C according to (Begaye, 2014) studied. The TGA result found by (Noval & Universitaria, 2019) demonstrated that an increment of temperatures higher than 567.6 ^{o}C leads to magnetite-rich powder losing its magnetic properties and is not attracted by magnetic field effectively above this temperature.

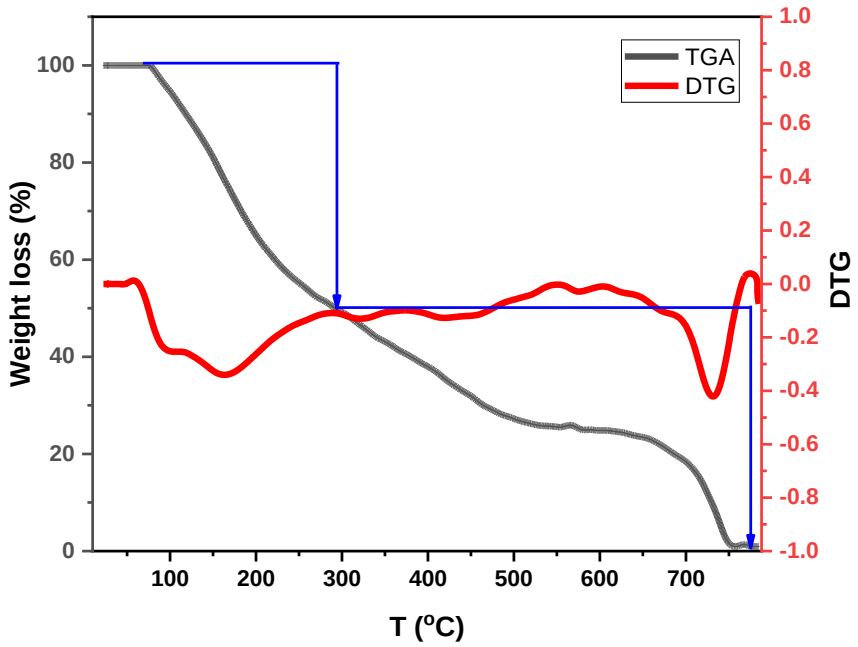

Figure 4. 11: Thermal Stability of Fe_3O_4 loaded CSH composite

4.2. Design of Experiment result Analysis

Table 4. 4: Experimental Result of Nitrate removal from aqueous solution

Run	pH	Contact time (min)	Adsorbent Dose (g/250ml)	C_o (mg/L)	C_e (mg/L)	Re(%) Actual	R_e (%) Predicted	Q_e (mg/g)
1	6	90	2.4	60	4.87	91.88	89.02	5.74
2	4	120	3.2	85	8.86	89.58	89.19	5.95
3	4	120	3.2	35	7.41	78.82	79.94	2.01
4	6	30	2.4	60	5.22	91.30	92.44	5.71
5	4	120	1.6	35	8.45	75.78	74.37	4.15
6	6	90	2.4	60	6.65	89.67	89.02	5.56
7	6	150	2.4	60	6.20	89.67	90.05	5.60
8	2	90	2.4	60	14.62	75.63	75.72	4.72

9	6	90	2.4	60	6.20	89.67	89.02	5.60
10	6	90	2.4	60	7.09	88.18	89.02	5.51
11	6	90	2.4	10	2.78	72.20	72.72	0.75
12	8	120	3.2	35	5.55	84.14	83.42	2.30
13	6	90	4	60	3.10	94.83	95.31	3.56
14	4	60	1.6	85	13.73	83.85	82.95	11.14
15	8	60	3.2	85	10.19	88.01	87.80	5.84
16	10	90	2.4	60	12.59	79.01	80.07	4.93
17	6	90	2.4	60	7.62	87.30	89.02	5.45
18	6	90	2.4	60	6.95	88.42	89.02	5.53
19	8	120	1.6	85	10.19	88.01	87.67	11.69
20	6	90	0.8	60	9.54	84.10	85.14	15.77
21	8	60	3.2	35	3.99	88.60	88.49	2.42
22	8	120	3.2	85	8.42	90.10	89.23	5.98
23	8	60	1.6	85	13.43	84.20	83.19	11.18
24	4	60	3.2	35	4.52	87.10	86.19	2.38
25	4	120	1.6	85	12.40	85.41	85.62	11.34
26	8	60	1.6	35	5.91	83.12	81.88	4.54
27	8	120	1.6	35	7.09	79.74	79.86	4.36
28	4	60	1.6	35	7.97	77.23	78.20	4.22
29	4	60	3.2	85	8.86	89.58	89.56	5.95
30	6	90	2.4	110	19.49	82.28	83.28	9.43

Where, C_o= initial nitrate concentration, C_e = equilibrium concentration of nitrate after adsorption, R_e = Removal efficiency of nitrate, and Q_e = Adsorption capacity

The adsorption performed by using CSH as an adsorbent of different factors: Time, pH, initial nitrate Concentration and adsorbent dose with constant particle size 90 µm, stirring speed of 200 rpm and 298k temperature.

Table 4. 5: Analysis of variance influence of the factors studied on NO_3^- Removal

Source	**Sum of Squares**	**Degree of Freedom**	**Mean Square**	**F-Value**	**P-Value Prob > F**	
Model	866.04	14	61.86	36.92	< 0.0001	significant

A	26.73	1	26.73	15.96	0.0012	
B	7.45	1	7.45	4.45	0.0522	
C	172.65	1	172.65	103.05	< 0.0001	
D	150.25	1	150.25	89.68	< 0.0001	
AB	2.43	1	2.43	1.45	0.2475	
AC	13.63	1	13.63	8.14	0.0121	
AD	3.09	1	3.09	1.84	0.1949	
BC	39.16	1	39.16	23.37	0.0002	
BD	7.83	1	7.83	4.67	0.00472	
CD	3.05	1	3.05	1.82	0.1970	
A^2	216.27	1	216.27	129.09	< 0.0001	
B^2	6.40	1	6.40	3.82	0.0694	
C^2	219.37	1	219.37	130.94	< 0.0001	
D^2	1.43	1	1.43	0.8528	0.3704	
Residual	25.13	15	1.68			
Lack of Fit	12.25	10	1.22	0.4754	0.8516	not significant
Pure Error	12.88	5	2.58			
Cor Total	891.17	29				

A = pH, B = Contact Time, C = Initial Nitrate Concentration, D = Adsorbent Dose

From the ANOVA (Analysis of Variance) Table, 4.2 results the higher F-Value and the lower P-value (<0.0001) indicates significance for the regression model. As the result demonstrates the model, the F-value of 36.92 implies it is significant. There is only a 0.01% chance that an F-value this large could happen due to noise. The p-value less than 0.05 implies that the model is statistically significant. They are extremely indispensable to understand the interaction among the independent variables. The result showed that Adsorbent dose (Factor D), initial nitrate concentration (Factor C), and pH (Factor A) are the major important variables in the adsorption process with P-value < 0.0001, < 0.0001, and 0.0012 respectively. Based on the value both the adsorbent dose and initial nitrate concentration are the best important factor. From the second polynomial model, A^2 and C^2 are significant models with P-values for both models < 0.0001. In the case of interaction effects, AC (pH and initial nitrate concentration), BC (contact time and initial nitrate concentration), and BD (Contact time and Adsorbent dose) are significant model terms for nitrate removal. Where there p-values are 0.0121, 0.0002 and 0.00472 respectively. The Lack of Fit of the F-value 0.48 implies the Lack of Fit is not significant relative to the pure

error. There is about 85.16% chance that a Lack of Fit F-value large could occur due to noise.

As shown from the ANOVA result, contact time indicates insignificant when compared with the other factors. This result confirmed that its contribution to nitrate removal adsorption was the lowest. In addition, the interaction effects of pH and contact time (AB), pH and Adsorbent Dose (AD), and initial nitrate concentration and Adsorbent Dose (CD) did not influence the adsorption process due to their highest P-value. Their P- values were 0.2475, 0.1949, and 0.1970 respectively that is greater than 0.1, which indicates the model terms are not significant. In the same way, quadratic terms B^2 and D^2 were insignificant factors within p values 0.0694 and 0.3704 that did not affect the adsorption process.

The model equations from the ANOVA result can be used to relatively comparing the removal efficiency of nitrates within factors and levels. The equation in terms of coded factors can be used to make predictions about the nitrate removal efficiency for the given levels of each factor. The coded equation is useful for identifying the relative impact of the factors by comparing the factor coefficients. The highest coefficients from the equation indicates the most influence factor that affect the adsorption process of nitrate removal. In other side, the equation in terms of actual factors can be used to make predictions about the Removal efficiency of Nitrate removal for given levels of each factors. The levels should be specified in the original units for each factor. This equation should not be used to determine the relative impact of each factor because the coefficients are scaled to accommodate the units of each factor and the intercept is not at the center of the design space.

The Final Coded Equations for nitrate removal from ANOVA result:

Removal Efficiency = 89.19 + 1.055* A - 0.56*B + 2.68*C + 2.50* D + 0.39*AB - 0.92*AC -0.44 *AD + 1.56*BC- 0.699375*BD - 0.44*CD - 2.81 *A^2 + 0.48 *B^2 - 2.83 *C^2 + 0.23 *D^2

Final Equation of Actual Factors

Removal Efficiency = +33.31708 + 10.13452PH - 0.209365 Contact Time + 0.625738 Initial Nitrate Concentration + 6.99682Adsorbent Dose + 0.006490pH * Contact Time - 0.018463 pH * Initial Nitrate Concentration - 0.274609pH * Adsorbent Dose + 0.002086 Contact Time * Initial Nitrate Concentration -0.029141Contact Time * Adsorbent Dose - 0.021844 Initial Nitrate Concentration * Adsorbent Dose -0.702005 pH^2 +

0.000537Contact Time² - 0.004525 Initial Nitrate Concentration² + 0.356608 Adsorbent Dose²

4.2.1 Model Adequacy

The regression model was found to be significant with the correlation coefficients of determination of R-Squared, adjusted R-Squared, and predicted R-Squared having a value 0.9718, 0.9455, and 0.9000 respectively as shown from table 4.3. The goodness fitness of the model was measured by a coefficient of determination R^2, which measured how well the real experimental data points have been approximated together with the regression model. As the result in a table, 4.3 expressed the value of $R^2 = 0.9718$ indicates the better fit of experimental data to that of predicted one. The value of larger Regression coefficient (R^2) approach to 1 illustrates, the validity of model in which it implies an acceptable agreement among the actual and predicted data. It implies 97.18% of the experimental variable studied attributed for the removal of nitrate. The Predicted R^2 of 0.9000 is in reasonable agreement with the Adjusted R^2 of 0.9455; i.e. the difference is less than 0.2. Therefore, this demonstrates that the measured data very well fitted with a quadratic model of the predicted value. Adeq Precision measures the signal-to-noise ratio. A ratio greater than 4 is desirable. Your ratio of 24.686 indicates an adequate signal. This model can be used to navigate the design space.

Table 4. 6: The model adequacy measures

Stad. Dev.	1.29	R^2	0.9718
mean	85.25	Adjusted R^2	0.9455
C.V%	1.52	Predicted R^2	0.9000
Press	89.10	Adeq Precision	24.6858

Generally, the smaller the value of Predicted residual sum of squares (PRESS) static obtained 89.1 indicates, better the experimental data points fits to the model. Moreover, the high R^2 value and p -value as well as not significant of fit indicating the best predicting of the experiment solution. Therefore, the result in both table 4.2 and 4.3 proved that, the best performance of the fitness of the model equations.

The figure 4.3 indicates the relationship of Actual and predicted value, which can be introduced from the regression model equations of a Design Expert chart based on

predicted and actual percent nitrate removal. The straight line shows the predicted values and the small rectangles represent the actual experimental values. The straight line is very close to the actual values and has a correlation coefficient R^2 equal to 0.9718, which confirms the accuracy of the model. The result confirmed that all the actual and predicted values are close to the line of perfect fit. Both of them showed the good agreement between them.

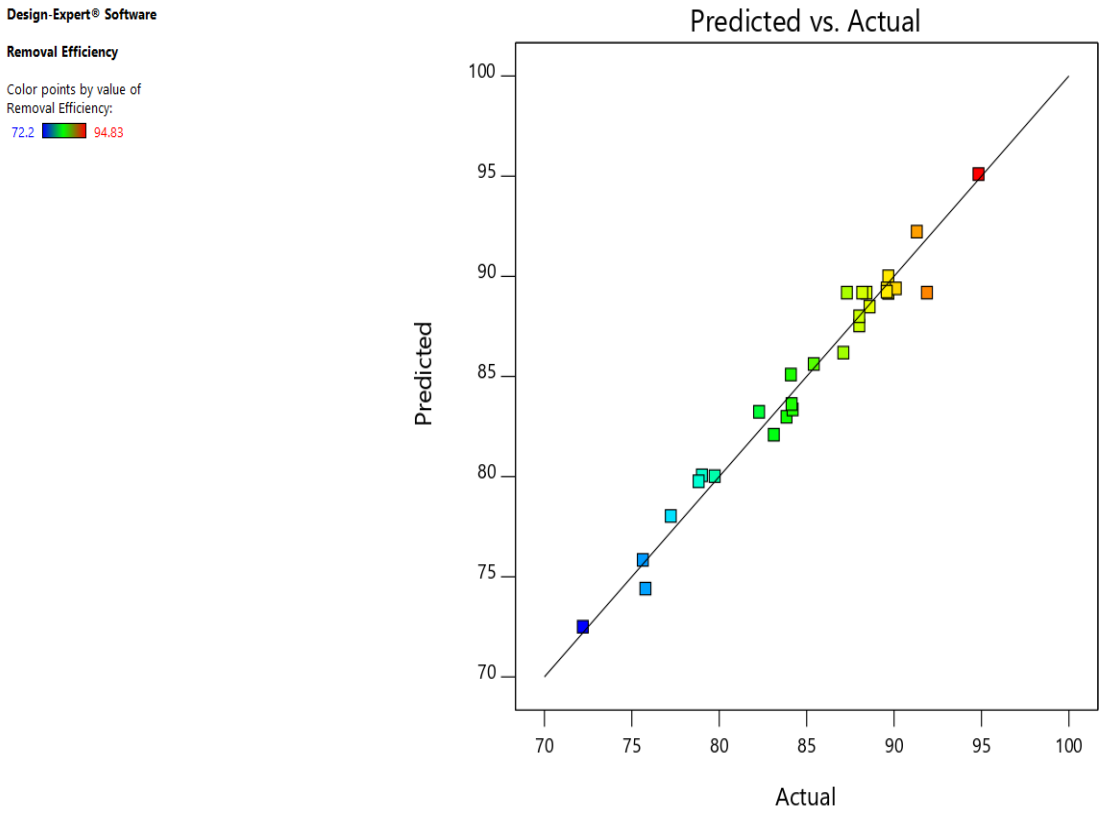

Figure 4. 12: Predicted vs Actual value nitrate removal adsorption plot

4.2.2. Optimization of the Response

In order to find the optimum value of each independent variables, four statistical metrics such as the larger regression coefficient (R^2), smaller lack of fit F-value, lower p-value and higher sum squares have been used. The response optimization was used to identify the combination of independent variables particularly, Contact time, PH, initial nitrate concentration, and adsorbent dose within the response of Nitrate removal efficiency. The goal of the process was to obtain high nitrate removal percentage. Therefore it has been set as maximum while the process parameters such as initial concentration, time and pH have been set as “within the range”, while adsorbent dose target at 2.4 g then response surface

method was used to optimize the process versus process parameters. According to the result obtained from optimizer Design-Expert version 11 software the maximum optimum removal efficiency of nitrate was achieved 93.06% by using 6.32 pH, 150 min contact time, 85 mg/L of initial nitrate concentration, and 2.4 g adsorbent dose.

4.2.3 Response Surface plots of Interaction Effects

The effect of the interactions between the four independent input and output variables and their interactions on the dependent variables can be seen using three-dimensional (3D) response surface plots. As observed from Figure 4.13- 4.18 it indicates the Plots of three-dimensional response surfaces of function of two variables with response and the remaining variables at the central level of the other variables. At lower pH values that indicates as acidic medium, the hydration surface of CSH underwent a protonation reaction. The dissolved nitrate ion was embedded in the adsorbent surface to obtain positive charge. However, an increase in PH of solution leads to OH^- concentration in the solution increased and as result deprotonation reaction takes place on the hydrated surface of the adsorbent to obtain a negative charge.

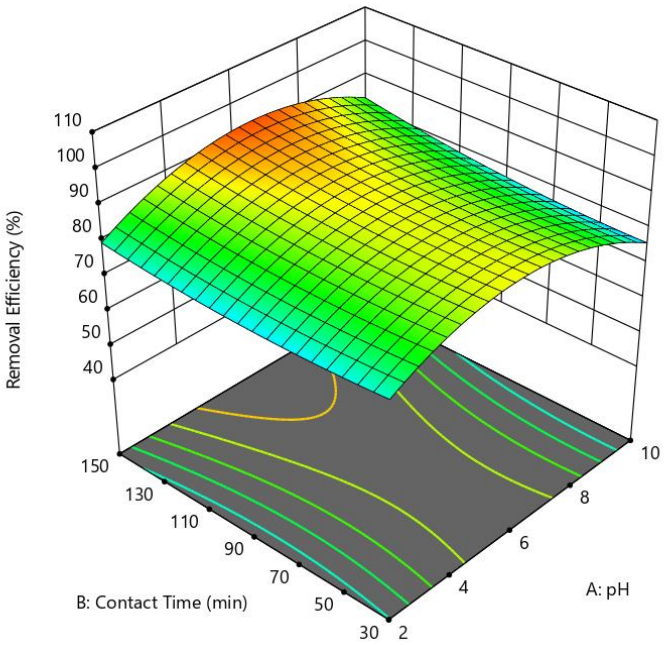

Figure 4. 13: 3D interaction effect of pH and time on nitrate removal efficiency.

Figure 4.13 shows the pH of aqueous solution is one of the important factor that affects the adsorptive removal of species at the adsorbent solution interfaces. In addition, the pH of the solution could influence the surface charges and degree of ionization of the adsorbate. As observed from the figure 4. 13 at the lower pH value the initial concentration increase

as the removal efficiency of nitrate decrease. In the other case, at lower initial nitrate concentration as pH was increased the removal efficiency also increased until pH reached 6.3. After that, the removal efficiency slightly decreases. As (Berkessa et al., 2019) reported decrease in nitrate removal after certain pH could be due to stronger competition of hydroxide ions. The influence of pH on anion exchange reaction was occurred because of the competition among the hydroxyl ions and anions. When pH increases, the negatively charged surface takes place and the adsorption capacities for nitrates decreases. This is due to negatively charged surfaces sites on the adsorbent could not favor the nitrate ion in the electrostatic repulsion. The protonated variable of the CSH surface, which commonly affect the electrical properties of the adsorbent and therefore pH of solution, had a basic influence on the adsorption of nitrate ion. The result also demonstrate that as the time increases the nitrate removal efficiency also increases. After two and half hour, the time reaches maximum value for adsorption process. After that, the percentage of nitrate removal decreases due to saturation of free adsorbents sites as well as because of an adsorbate releases from the adsorbent. Initially the faster rate may be due to availability of uncovered surface area of the adsorbents. However, as passage of time, the portion of the active sites of the adsorbents may be blocked and the rates becomes slower and reaches equilibrium when the surface becomes almost saturated.

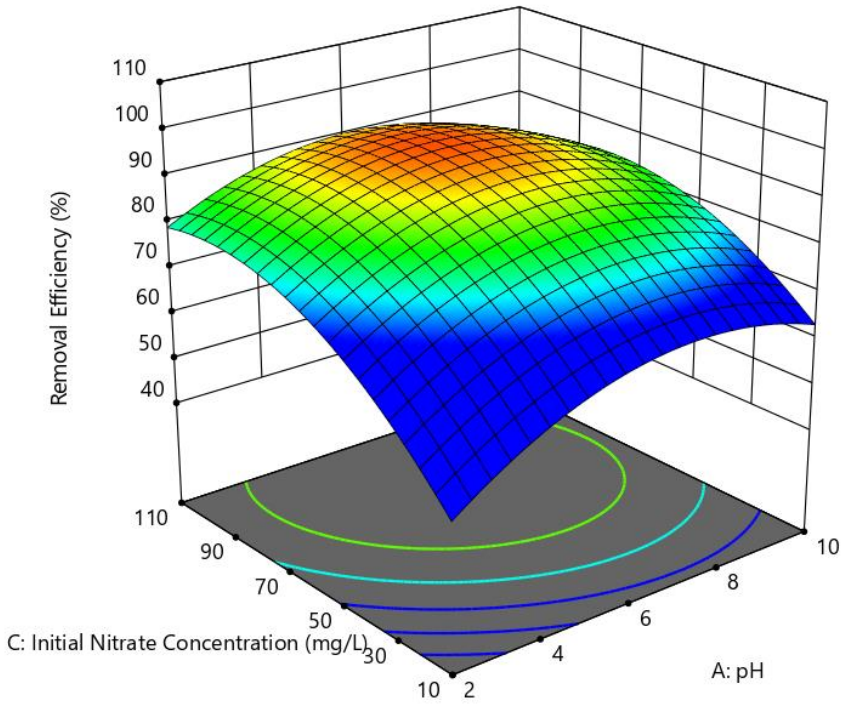

Figure 4. 14: RSM plot of 3D interaction effect of pH and initial nitrate

The figure 4.14 indicates the 3D interaction of pH and initial nitrate concentration on Nitrate removal efficiency at constant adsorbent dose and contact time. As the graph demonstrated, as both the initial nitrate concentration and pH increases the nitrate removal efficiency also increases. The rises of initial nitrate concentration leads to increments in the removal of nitrate ion from the solution due to the occurrences of large vacant places in the adsorbents. At the initial nitrate concentration of 85 mg/L, the removal efficiency reached maximum value of 93%. After that, the removal efficiency of the nitrate ions starting declined because of the vacant sites occupied by the nitrate ions. In the other case, the pH increases until 6.3 and the nitrate ion in the presence of anions can be adsorbed by the mechanism of electrostatic attraction through the positively charged surfaces.

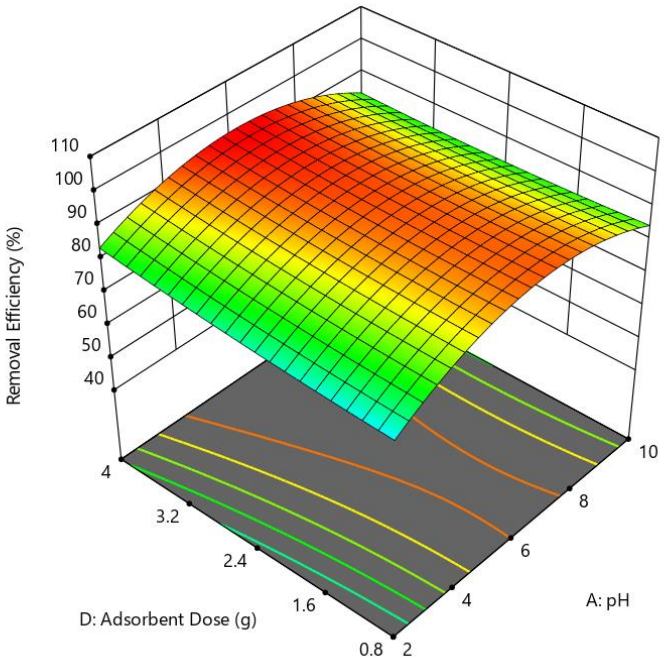

Figure 4. 15: 3D interaction effect of pH and dose on Nitrate removal efficiency

Figure 4.15 explained the 3D interaction effects of Adsorbent dose and pH on nitrate removal efficiency while both time and initial nitrate concentration remains constant. The sorption process was carried out on the molecules and surfaces of the CSH adsorbents. Therefore, the adsorbent amount had a meaningful effect on the nitrate removal efficiency. The adsorbent dose has a direct and indirect effect on the process and costs like the other parameters. As it can be observed from the graph as adsorbent dose of CSH increases, the nitrate removal efficiency also increases in the model. It is commonly understood that the

presence of larger surface area and exist of more active sites of the CSH adsorbent increase as larger adsorbent dose used in the sorption process. However, at higher concentrations of sorbate, the equilibrium uptake did not increase considerably with the rise within the CSH adsorbent. One more reason is also the particle interaction like aggregation, which ends from a high adsorbent dose. Such aggregation would cause a decrease within the total surface area of the adsorbent and a rise in diffusional path length.

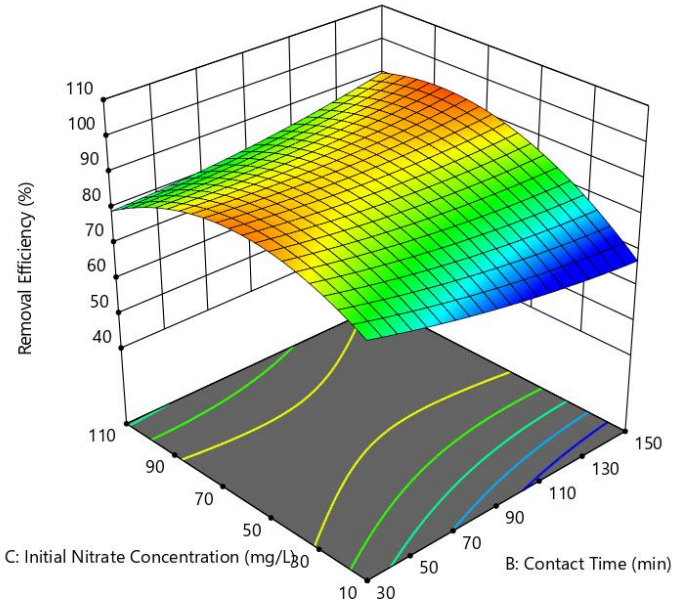

Figure 4. 16: 3D interaction effect of contact time and initial nitrate concentration

Figure 4.16 depicts the interaction effects of contact time and initial nitrate concentration on nitrate removal at fixed adsorbent dose and PH of solution. Initially as time increase, the removal efficiency of nitrate also increases. As the contact time increase after one hour, the removal efficiency nitrate decreases. In the other case the initial nitrate concentration increases leads to increase in removal efficiency and reached maximum 93.06 at 85 mg/L.

Figure 4.17 illustrates 3D interaction effect of Adsorbent dose and contact time on Nitrate removal efficiency at constant pH and initial nitrate concentration. As the adsorbent dose increases, there was an increment of nitrate removal efficiency. However, the percentage of nitrate removal did not increase with increasing contact time at any initial nitrate concentration. The adsorbent has reached the maximum adsorption capacity within or before one hour. In the other words, the surface coverage of the adsorbent was already saturated with nitrate in less than one hour. Therefore, it can be concluded that the

percentage of nitrate removal was highly dependent on the initial nitrate concentration, pH and weight of adsorbent but independent on contact time.

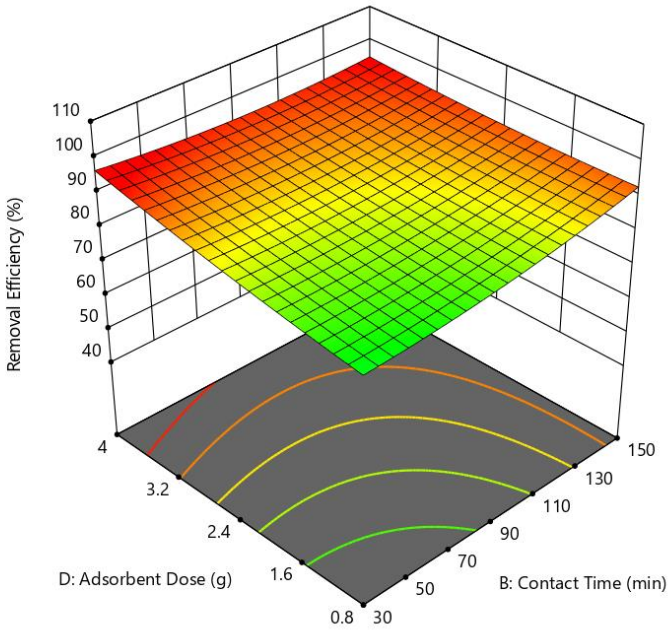

Figure 4. 17: 3D interaction effect of Adsorbent dose and time on Nitrate removal

The figure 4.18 showed the interaction between initial nitrate concentration and adsorbent dose. As it demonstrated increasing initial nitrate concentration, the percentage removal of nitrate removal increased in proportional manner. The process happened due to higher concentration gradient that performed as driving force to conquer the mass transfer between the bulk solution of nitrate ion and adsorbent surfaces of CSH. The adsorbent dose have no more effect on nitrate removal at lower value of initial nitrate concentration. As the initial nitrate concentration increased, the percentage of nitrate removal also increased as result of adsorbent dose increased. Therefore, adsorbent dose was the main independent variable that affects the adsorption of nitrates from the solution. The presence of high amount adsorbent dose in the adsorption process leads to increase in total available surface area, and site of adsorption (Loon & Fong, 2016).

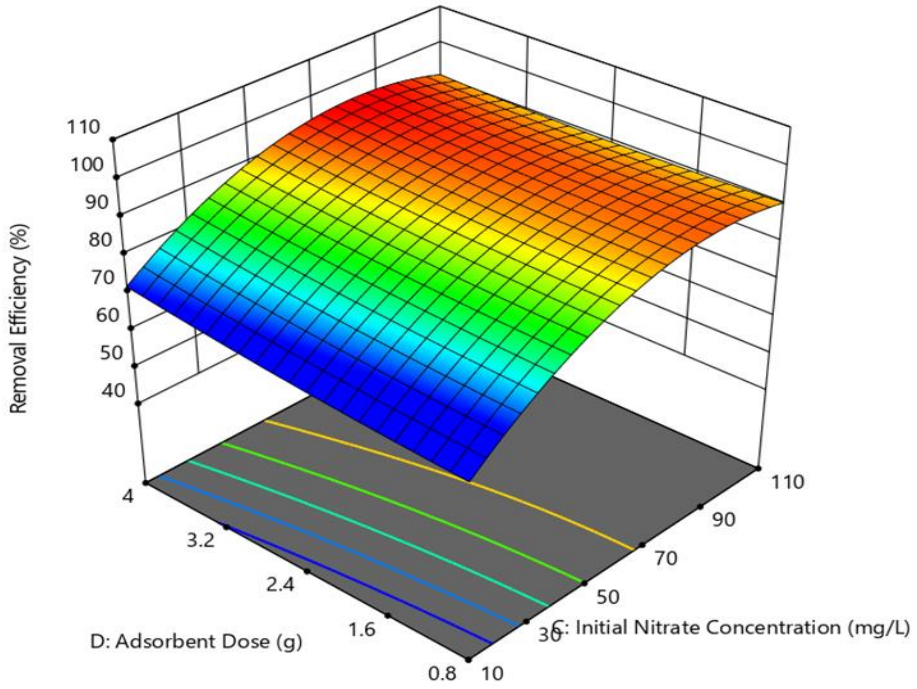

Figure 4. 18: 3D interaction effect of adsorbent dose and initial nitrate concentration

4.3. Fe_3O_4 loaded CSH Composite synthesis

The Fe_3O_4 Based CSH composite was synthesized at five different percent weight of Fe_3O_4 loaded to the prepared calcium silicate hydrate. The adsorption carried out at the optimum parameters obtained from optimization model such as 6.3 pH, 150 min contact time, 85 mg/L of initial nitrate concentration, and 2.4 g/250mL adsorbent dose. As Table 4. 7 indicated 25%, wt. of Fe_3O_4 loaded CSH composite was the best composite that resulted maximum nitrate removal efficiency as well as adsorption capacity of 92.71% and 8.21mg/g respectively. As percentage weight of Fe_3O_4 exceeds 25, the removal efficiency of nitrate decrease due to Fe_3O_4 have high surface free energy, and few functional groups subject to air oxidation. As result, aggregation formed in aqueous solution, which reduce the nitrate removal capacity (Peng et al., 2017). In addition, as percentage of Fe_3O_4 increases in the reaction, reduction in Ca/Si ratio occurred in Fe_3O_4 loaded Calcium Silicate Hydrate composite product. Consequently, active adsorption sites of Calcium silicate Hydrate reduced, which leads to decline in nitrate removal efficiency (Zhang et al., 2015). Therefore, for further adsorption isotherm, kinetics, thermodynamics, co-existing ions and regeneration studies 25% weight of Fe_3O_4 loaded CSH composite were used.

Table 4. 7: The effects of Fe_3O_4 loading on CSH for nitrate removal

% wt. of Fe_3O_4 loaded to CSH	Final Concentration of Nitrate ions C_e (mg/L)	Removal Efficiency of Nitrate ion (%)	Adsorption capacity Q_e (mg/g)
0	8.86	89.6	7.93
10	8.42	90.1	7.98
20	7.53	91.14	8.07
25	6.2	92.71	8.21
30	11.52	86.45	7.65
40	14.176	83.32	7.34

4.4. Equilibrium Isotherm

Adsorption system can be designed with the aid of adsorption isotherms typically referred to as equilibrium isotherms, which constitute the amount of solute adsorbed per unit weight of sorbent. These isotherms use equilibrium concentration of sorbent at a fixed temperature. To remove the nitrates ions from the wastewater, a particular design is optimized in order to generate proper correlations for experimental data, which is referred to as adsorption isotherm (Batool et al., 2018).

4.4.1. Adsorption Isotherm

The interaction of adsorbate with adsorbent can be identified by studying isotherm, which is a critical to optimizing and designing the desired adsorption system (Zhang et al., 2015). The equilibrium concentration of nitrate ion at constant optimized parameters of 150 min, 2.4 g/250 mL of Fe_3O_4 loaded CSH dose and, 6.3 pH at a room temperature were carried out. The adsorption of isotherm data for No_3^- ion was analyzed by applying three commonly used isotherms, Langmuir, Freundlich and Temkin Isotherms. Their correlation coefficients and constant parameters of sorption of NO_3^- by Fe_3O_4 loaded CSH were obtained from the slop and intercept of the graph for each equations of the isotherms.

4.4.1.1. Langmuir Isotherm

The adsorption isotherm determines the difference between the amounts of sorption and the solute concentration at equilibrium. The adsorption isotherm of nitrate ion using Fe_3O_4 loaded CSH composite was investigated. The concentration of nitrate ions in their

respective equilibrium phase at room temperature was studied to obtained maximum adsorption capacity of Fe_3O_4 loaded CSH for nitrate ion removal. The result obtained from Langmuir model indicates that the value of separation factor ($R_{L)}$ for all initial nitrate concentrations were greater than 0 and less than 1, which implies that the Langmuir isotherm is favorable. The values of R_L for initial nitrate concentration of 40, 55, 70, 85 and 100 mg/L were listed as 0.462, 0.385, 0.329, 0.288, and 0.256 respectively. The maximum adsorption capacity (q_{max}) can be determined from the intercept of Langmuir plots of $1/C_e$ vs $1/q_e$. The maximum adsorption capacity (q_{max}) and energy of adsorption (K_L) from Langmuir isotherm model were to be determined 27.933 mg/g and 0.0291 L/mg respectively. The values of correlation factor (R^2) gained for Langmuir isotherm equals to 0.99287.

Table 4. 8: Isotherm data for the removal of nitrate by Fe_3O_4 loaded CSH composite

C_o(mg/L)	C_e(mg/L)	ln (Ce)	$1/C_e$	q_e (mg/g)	$1/q_e$	Ln(q_e)	C_e/q_e
40	3.544	1.265	0.282	3.798	0.263	1.334	0.933
55	5.316	1.671	0.188	5.175	0.193	1.644	1.027
70	7.088	1.958	0.141	6.553	0.153	1.880	1.082
85	8.417	2.130	0.119	7.977	0.125	2.077	1.055
100	11.518	2.444	0.087	9.217	0.108	2.221	1.250

Table 4. 9: Isotherm parameters for the removal of nitrate by Fe_3O_4 loaded CSH

Isotherm	**parameters**	**Value**
Langmuir	q_{max} (mg/g)	27.933
	K_L (L/mg)	0.0291
	R^2	0.993
Freundlich	n	1.282
	1/n	0.78
	k_f (mg/g)$(1/mg)^{1/n}$	2.262

	R^2	0.985
Temkin	B (J/mole)	-2.464
	b_T	-1005.345
	A_T (L/mg)	0.145
	R^2	0.976

Table 4. 10: The values of R_L at various initial nitrate concentrations

C_o (mg/L)	R_L
40	0.462
55	0.385
70	0.329
85	0.288
100	0.256

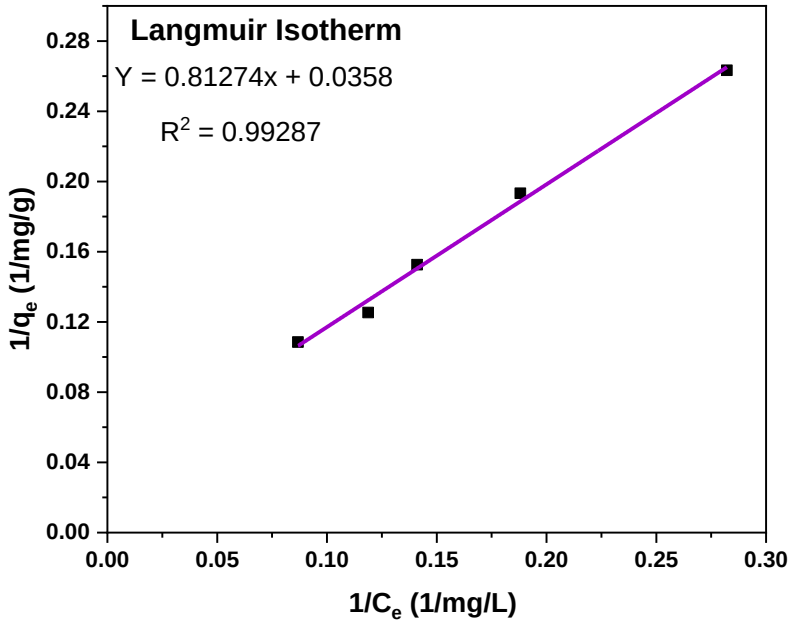

Figure 4. 19: Langmuir isotherm for nitrate adsorption by Fe_3O_4 loaded CSH

4.4.1.2. Freundlich Isotherm for nitrate adsorption by Fe_3O_4 loaded CSH composite

Freundlich isotherm is an empirical equation that can be employed to describe the heterogeneous systems. The linear form of the Freundlich isotherm model from Equation 3.24 was used to investigate the multi-layer adsorption of nitrate on the surface of the

adsorbents. The magnitude of the exponent 1/n indicates the favorability of the adsorption. 1/n is a heterogeneous factor, which is related to adsorption intensity or surface heterogeneity. The value of 1/n < 1 which equals to 0.78 indicates normal adsorption (Keshav et al., 2019). In order to reach a favorable adsorption process, the value of n should be in the range of 1 to 10. Table 4.9 depicts the value of n was 1.282, which confirmed favorable adsorption. From the Freundlich isotherm model the values of constant parameters such as K_f and n were determined by linear regression plot of log (q_e) and log (C_e). from the Freundlich isotherm model analyzed showed the equilibrium isotherm data fit to the experimental data which implies that adsorbed nitrate forms a monolayer surface coverage on the Fe_3O_4 loaded CSH composite and the chemisorption adsorption mechanism takes place. The values of correlation factor (R^2) gained for Freundlich isotherm equals to 0.9853.

As (Pan et al., 2017) studied in his research, The Langmuir and Freundlich adsorption isotherms relative parameters were calculated from their respective slope and intercept of the linear plots. High correlation coefficients (R^2 > 0.9205) indicated that both the Langmuir and Freundlich models were acceptably fit the experimental data in this study. The result obtained from adsorption equilibrium isotherm confirmed that the fitting the equilibrium data to both Langmuir and Freundlich isotherm models suggest that the presence of heterogeneous and homogenous adsorption surfaces on the adsorbent involved during the adsorption of nitrate ions. By comparing the values of correlation factor (R^2), the Langmuir models better suitable fits to with the equilibrium sorption which gives a larger R^2 equals to 0.993 and maximum adsorption capacity of 27.933 mg/g for nitrate ion adsorption.

4.4.1.3. Temkin Isotherm

Equilibrium constant of binding A_T provides information about binding energy, and β expresses heat of adsorption for a particular adsorption experiment. The correlation coefficient (R^2) obtained from this model was 0.9756. The result showed that the experimental data fitted to the model. However, when comparing with Langmuir and Freundlich the result found by Temkin model was the smallest correlation coefficient. The negative value of B (-2.464 J/mol) indicates the adsorption process was endothermic. According to previous study by (Keshav et al., 2019) for Temkin isotherm the following is predicted: a positive B (heat) value would indicate that nitrate ion binds to Fe_3O_4 loaded

CSH in an exothermic process, whereas a negative value would indicate an endothermic process.

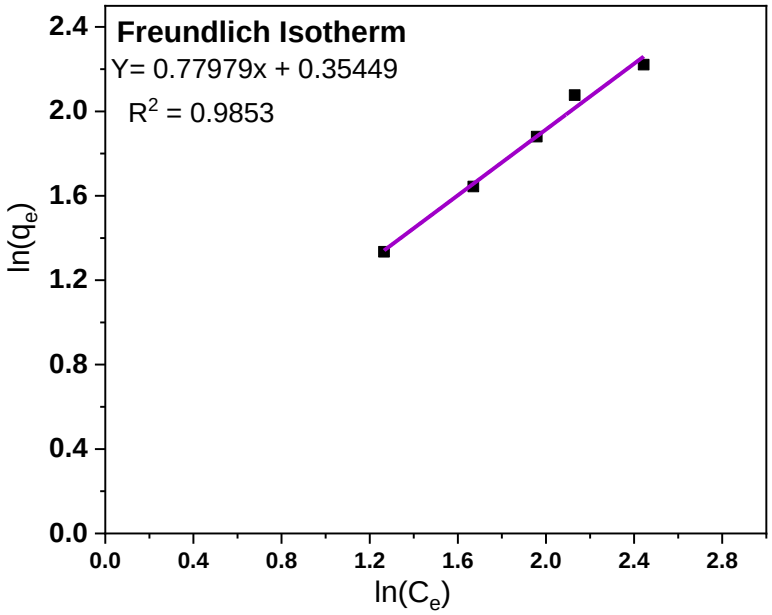

Figure 4. 20: Freundlich Isotherm for nitrate adsorption by Fe_3O_4 loaded CSH

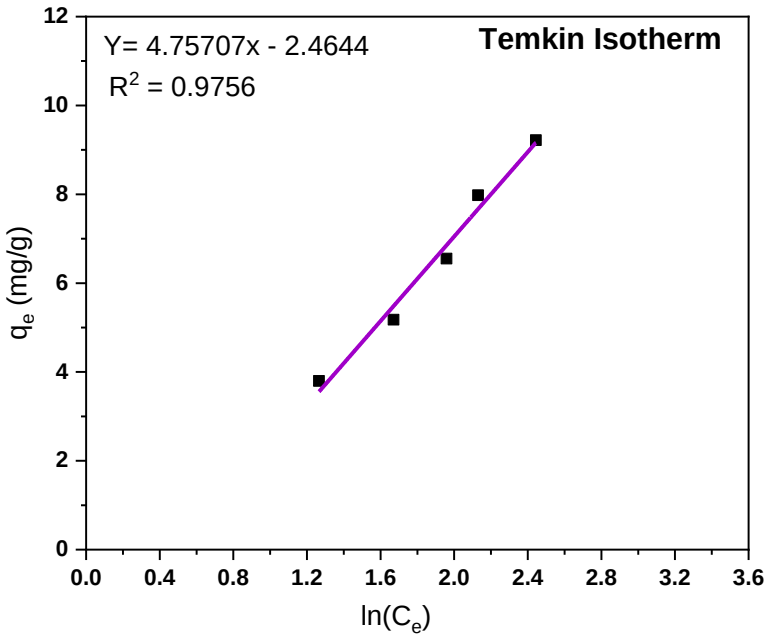

Figure 4. 21: Temkin isotherm model for nitrate sorption

4.5. Adsorption Kinetics

Kinetic experiment were investigated to examine the rate of nitrate adsorption on Fe_3O_4 loaded CSH adsorbent and the time required to reach equilibrium. The purpose of studying equilibrium kinetic is to identify the adsorbent retention time and provide

information about the specified time to reach the maximum capacity of adsorption and the controlling mechanism in the process that includes mass transfer or chemical reactions (Tohfegar et al., 2019). In this study Pseudo-first-order, Pseudo-second-order and Intraparticle diffusion kinetic models were analyzed to obtain the best kinetic models for nitrate removal. The kinetics study time dependence of nitrate were investigated from 30 to 210 min at constant room temperature, 85 mg/L initial nitrate concentration, pH =6.3, adsorbent dose = 2.4 g/250 mL.

Comparing the correlation coefficients of three kinetic models, it definitely revealed that the pseudo-second-order model best fit the adsorption kinetic of nitrate onto Fe_3O_4 loaded CSH and the adsorption processes were chemisorption. As shown in the figure 4.23 the Pseudo-second-order rate model show the best agreement with the experimental results, which implies that the whole process was controlled by chemical adsorption is the rate limiting steps of the process. Pseudo-second-order kinetic model predicts that adsorption behavior involves valance forces through sharing of electrons among nitrate ions and the Fe_3O_4 loaded CSH. In addition, the experimental adsorption capacity was in agreement with that of calculated adsorption capacity, which proved the model adopted is reasonable. The value of kinetic parameters were summarized in table 4.11.

Table 4. 11: Kinetics model parameters for Pseudo-first-order, Pseudo-second-order, and Intraparticle Diffusion

Kinetics	**parameters**	**Value**
Pseudo-First Order	q_e (mg/g)	0.777
	K_1 (min^{-1})	-0.013
	R^2	0.93
Pseudo-Second Order	$q_{e\ calc}$(mg/g)	8.24
	q_e exp(mg/g)	8.12
	q_e^2	67.88
	K_2 (g/mg.min)	0.036
	R^2	0.999
Intraparticle Diffusion	K_p ($mg/g.min^{1/2}$)	0.0558
	R^2	0.98

Table 4. 12: Pseudo first and second order kinetics and constant values

Time (min)	C_o (mg/L)	Ce(mg/L) NO_3^-	q_t (mg/g)	q_e (mg/g)	ln(qe-qt)	t/q_t (g.min/mg)
0	0	0	0	0	0	0
30	85	11.518	7.654	8.116	-0.773	3.919
60	85	10.632	7.747	8.116	-0.997	7.745
90	85	9.746	7.839	8.116	-1.284	11.481
120	85	8.86	7.931	8.116	-1.690	15.130
150	85	7.974	8.024	8.116	-2.383	18.695
180	85	7.088	8.116	8.116	-	22.179
210	85	7.088	8.116	8.116	-	25.875

Pseudo first order kinetics

$$\ln(q_e - q_t) = lnq_e - k_1 t$$

Intercept	**slope (k1)**	**q_e cal (mg/g)**	**K_1**	**R^2**
-0.252	-0.013	0.777	-0.013	0.93

Pseudo second order kinetics

$$\frac{t}{q_t} = \frac{1}{K_2 {q_e}^2} + \frac{t}{q_e}$$

Intercept	**slope**	**q_e cal (mg/g)**	**q_e^2**	**K_2**	**R^2**
0.439	0.121	8.24	67.886	0.033	0.999

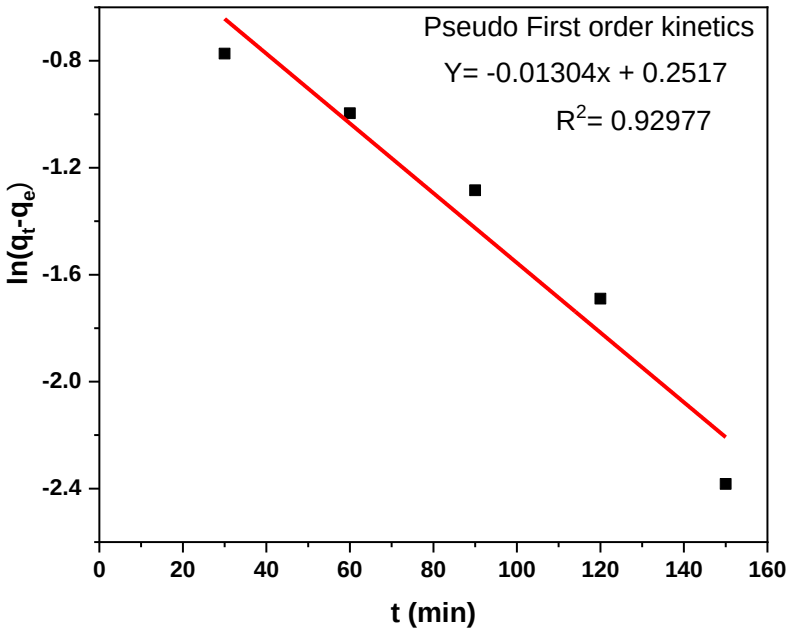

Figure 4. 22: Pseudo first order for sorption of nitrate ions

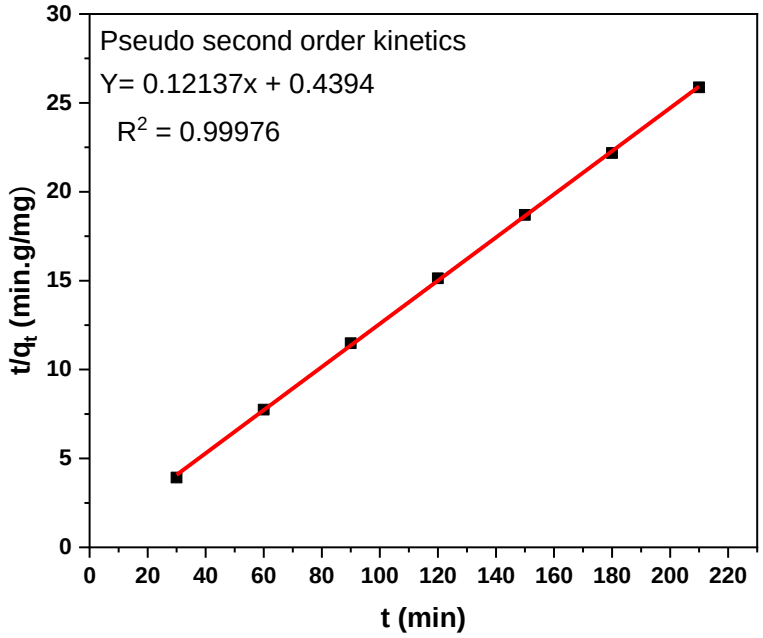

Figure 4. 23: Pseudo second order for sorption of nitrate ions

The intraparticle diffusion model can be describe the rate of adsorption process depends on the speed at which adsorbate diffuses towards adsorbent. The result analyzed from the adsorption equilibrium data of intraparticle diffusion model the graph $t^{0.5}$ versus q_t was linear which demonstrates that the intra-particle diffusion was involved inside the adsorption process. In the other case, the model expresses that intraparticle diffusion is not the only rate-determining step due to the graph $t^{0.5}$ versus q_t did not pass through the origin as observed from figure 4.24. This shows that intraparticle diffusion became not the only

rate-limiting step within the adsorption of nitrate. Consequently, other mass transfer processes like film diffusion and bulk diffusion could be there in determining the mass transfer mechanism of nitrate ions from the bulk solution to the Fe_3O_4 loaded CSH composite adsorbent surface. The diffusion process may affect the nitrate ion adsorption process on Fe_3O_4 loaded CSH composite as result of the porous structure of the adsorbent and the attractive effect of nitrate ions.

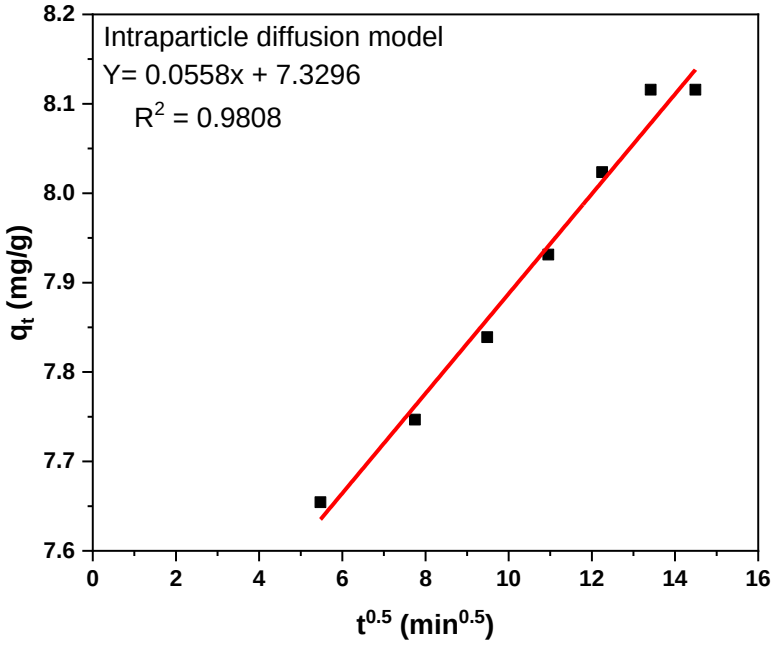

Figure 4. 24: Intraparticle diffusion model for nitrate sorption by Fe_3O_4 loaded CSH

4.6. Thermodynamics study

The thermodynamics parameters determined for nitrate adsorption on Fe_3O_4 loaded CSH at various three temperature of 298 K, 303 K and 313 K respectively. As it summarized in table 4.13, the values of Gibbs free change energy (ΔG^o) are found to be negative for adsorption of nitrate on Fe_3O_4 loaded CSH. The particular values ΔG^o to be found includes -0.015, -0.341 and -0.535 which confirms that the spontaneous and feasibility of adsorption process as result of negative values of Gibbs free energy changes at all temperatures.

As temperature increases, the magnitude of ΔG^o also more negative for nitrate adsorption, which implies that more spontaneity of the adsorption takes place at higher temperature. Higher temperature makes the adsorption easier due to higher driving force of adsorption. Similar results were found by (Singh et al., 2015). The positive value of change in

enthalpy ΔH^o (8.289 KJ/mol) confirms the endothermic nature of sorption process and indicates the adsorption of nitrate become more favorable at higher temperature. In the other case the positive values of ΔS^o (28.316 J/mol K) demonstrates that the process is entropy driven and the randomness between solid-solution interface increases throughout adsorption process. The report studied by (Ogata et al., 2015) found similar result. Increase in randomness of nitrate ion on Fe_3O_4 loaded CSH was as result of number of desorbed water molecules is larger than that of adsorbed nitrate ion and the adsorption of nitrate controlled by positive entropy change(Zhang et al., 2015). In addition, the presence of disorder state in the adsorption process is due to the combination of nitrate with a particle sites to form stable structures (Zhang et al., 2015).

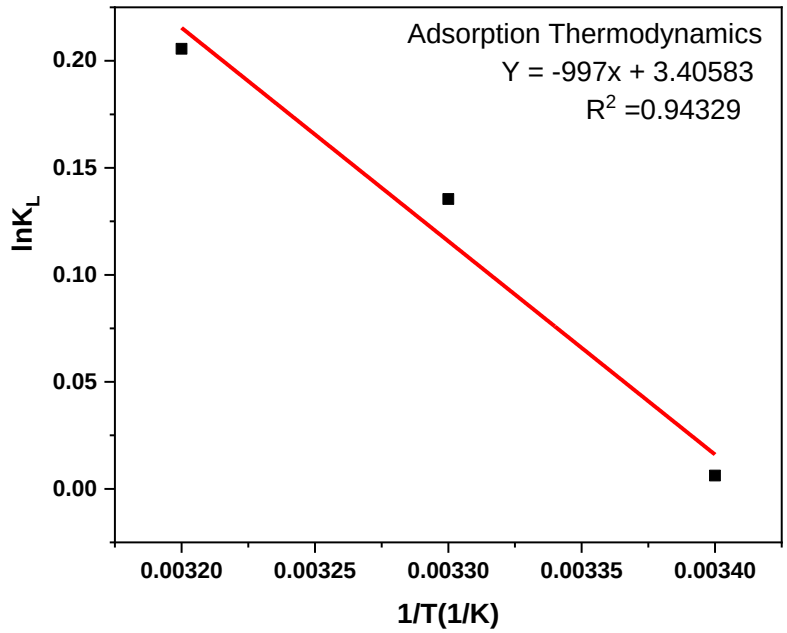

Figure 4. 25: Adsorption thermodynamics of nitrate on Fe_3O_4 loaded CSH composite

Table 4. 13: Thermodynamic parameters of nitrates adsorption on Fe_3O_4 loaded CSH

Adsorbent	qe (mg/g)	Temperature (K)	K_L	ΔG^o (KJ mol^{-1})	ΔH^o (KJ mol^{-1})	ΔS^o (J mol^{-1} K^{-1})	R^2
Fe_3O_4 loaded CSH	8.02	298	1.0062	-0.015	8.289	28.316	0.943
	8.12	303	1.145	-0.341			
	8.16	313	1.228	-0.535			

4.7. The Effect of Co-existing Ions

Normally, the common inorganic anions which include PO_4^{3-}, Cl^- and CO_3^- frequently coexist with NO_3^- in natural water sources, that can act as competing ions and strongly interfere with the sorption process of NO_3^-, resulting in inefficiency. Due to this reason, it is necessary to evaluate the effect of the competing anions. Increasing the coexisting anion would cause an obvious decrease in nitrate sorption capacity, which would result from the competitive effect of anions for available sorption sites of adsorbent. Therefore, the effects of these competitive anions were investigated in this study. As Figure 4.26 demonstrates the effect of three co-existing ion such as Phosphates, Chlorides and Carbonates of 20 mg/L of each on nitrate removal at optimum parameters were investigated. The results indicated that the anions have substantial effect on nitrate removal. The effect of carbonate was not prominent as compared to phosphates and chlorides. The presence of phosphate ion within nitrates reduce the percentages of nitrate removal from 92.71% to 73.94%. In addition, chloride were another influential ion, which reduce the nitrate removal efficiency to 79.15%. Therefore, Phosphate was the greatest competitor for nitrate followed by chlorides and carbonates. (Alighardashi, 2018) confirmed that phosphate ions were the most influential ions which compete with nitrate. These is as result of high concentration of phosphates leads to lack of available surface area on Fe_3O_4 loaded CSH adsorbent sites. The basic characteristics of anions to be considered for the selective adsorptions includes the solubility, ionic radius, hydration energy and bulk coefficient (Rafiee, 2014). The competing anions reduce the removal efficiency of nitrate in the order of carbonates > chloride > phosphate. The effect of chloride ion can be obtained from greater tendency of chloride to undergo ion exchange reaction.

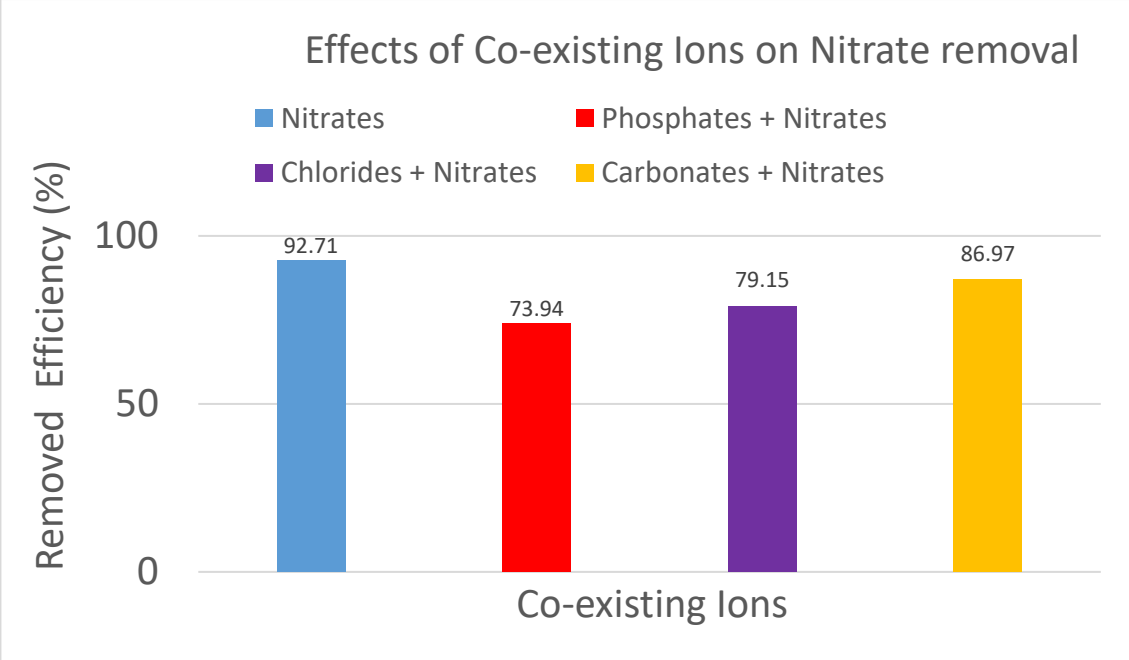

Figure 4. 26: Effects of Co-existing ions in nitrate removal by Fe_3O_4 loaded CSH

4.8. Regeneration Study

To assess the durability of this adsorbent, regeneration, and reuse studies were carried out for the adsorption of nitrate over four consecutive adsorption-desorption cycles. A solution of 1M of NaOH was chosen as the eluent in the desorption process. High reusability of adsorbent is very indispensable for any adsorbent, which significantly increase the economic value of the adsorption process. To study regeneration study 2.4 g of adsorbent dose, 6.3 of pH, 85 mg/L of initial nitrate concentration at 2:30 hr. with removal efficiency of 97.21% were used to regenerate Fe_3O_4 loaded CSH. As shown in bar graph figure 4.27, the removal efficiency of the first cycle was 86.44% while the second cycle resulted 82.8%. At the third and fourth cycle, the removal efficiency of nitrate ion were 74.98 and 68.73% respectively. This value ensures that the prepared adsorbent could be reused different times without any loss of adsorption ability. Therefore, Fe_3O_4 loaded CSH is a promising adsorbent for removal of nitrate ion from contaminant water.

After the adsorption-desorption process, the adsorbed nitrate ion was concentrated in a caustic solution. To recover the adsorbed nitrate from the solution, calcium based chemicals such as $CaCl_2$, $Ca(OH)_2$ should added to the alkaline solution to produce calcium nitrate fertilizer for agricultural use.

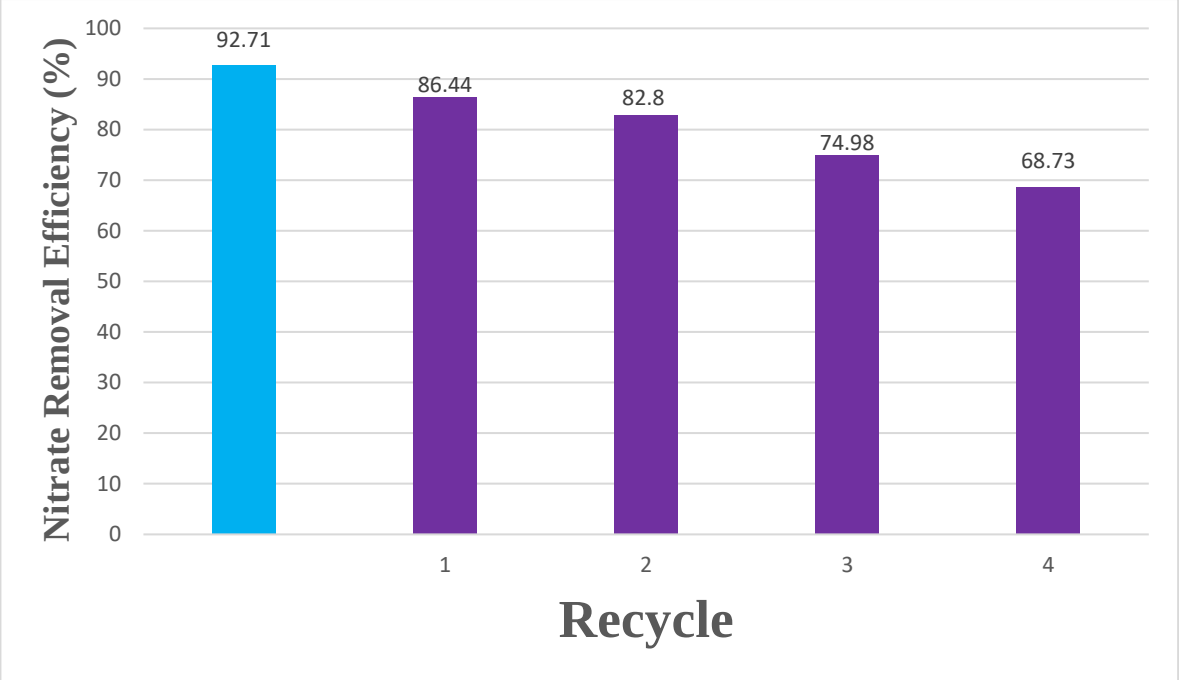

Figure 4. 27: Reusability performance of Fe_3O_4 loaded CSH composite

4.9. Removal of Nitrate from Real Waste water

In order to apply the laboratory experimental result in to the practical real world application, the investigation carried out by taking the real wastewater, which have highest amount of total Nitrogen from Adama Science and Technology University wastewater treatment plant. There is huge amount of total nitrogen contains wastewater from different sources flow in to the treatment plant. For experimental work, the wastewater at inlet of ASTU treatment plant selected for adsorption process. Average lab results from ASTU treatment plant indicates the influent contains total nitrogen of 125 mg/L and 75 mg/L of total phosphorus. Total Nitrogen is the addition of nitrate-nitrogen (NO_3-N), nitrite-nitrogen (NO_2-N), ammonia-nitrogen (NH_3-N) and organically bonded nitrogen. For the sorption of real wastewater contains NO_3^- -N the optimum parameter from batch adsorption of synthetic wastewater were used.

The optimum parameter includes, pH = 6.3, contact time =150 min, Fe_3O_4 loaded CSH dose = 2.4 g/300 mL. The initial NO_3^--N obtained from ASTU treatment plant from total nitrogen result, which was 52.5 mg/L.

Table 4. 14: The adsorption results of real wastewater of ASTU wastewater treatment

Initial Nitrate-Nitrogen (NO_3-N) (mg/L)	Final Nitrate-Nitrogen Concentration (NO_3-N) (mg/L)	Average	Removal Efficiency R_e (%)	Adsorption Capacity (mg/g)
52.5	15.0	15.8	69.9	4.59
	16.6			

The removal efficiency of nitrate-nitrogen on the Fe_3O_4 loaded CSH adsorbent was found 69.9%. This result was much slower than that of removal efficiency of synthetic wastewater containing nitrate-nitrogen. The reason behind this result could be the presence of a large amount of total phosphates, Nitrite-Nitrogen, ammonia-nitrogen and organic nitrogen. Those ions compete in the adsorption process, which leads decrement in the removal efficiency of nitrate-nitrogen. These huge decreases in nitrate-nitrogen removal may be due to the organic content and high electrical conductivity that might have halted the adsorption process through blocking and competition for the adsorbent sites, respectively. The maximum adsorption capacity and higher nitrate removal efficiency would be obtained by separating those ions at the influent of the plant.

4.10. Comparison study of Nitrate by different adsorbents

The synthesized Fe_3O_4 loaded CSH composite adsorbent was compared with different adsorbents reported in related works for nitrate removal from water. As Table 4.15 indicated, the optimum pH, isotherm model, kinetics models, and q_{max} were compared for nitrate removal.

Table 4. 15: Adsorption capacities and other parameters for removal of nitrate by different adsorbent

Adsorbent	**Optimum pH**	**Isotherm**	**kinetics**	**q_{max} (mg/g)**	**Reference**
Modified pumice	5	Langmuir	Pseudo-first order	27.66	(Rasuli et al., 2020)
Bio char from agricultural residue	3	Langmuir	Pseudo-second order	14.46	(Zhao et al., 2018)
Water glass-based silica Aerogel	6.7	Langmuir	Pseudo-second order	104.17	(Tohfegar et al., 2019)
Magnetic Mg/Fe hydrotalcite	6.3	Langmuir	Pseudo-first order	14.24	(J. Chen et al., 2021)
ZnCl-modified Coconut granular Activated Carbon	4.4	Langmuir	Pseudo-second order	14.01	(Khan et al., 2011)
Solid waste from Factory	7	Freundlich	Pseudo-second order	o.o65	(Berkessa et al., 2019)
Modified rice husk	7	Freundlich	Pseudo-second order	55.55	(Katal et al., 2012)
Fe_3O_4 loaded CSH	6.3	Langmuir	Pseudo-second order	27.93	This study

CHAPTER FIVE

CONCLUSIONS AND RECOMMENDATIONS

5.1. Conclusions

This research work focus on the synthesis and characterization of Fe_3O_4 loaded CSH composite adsorbent from Aluminum Sulphate solid waste residue of Awash Melkassa Chemical Factory as a raw material as silicate source to remove the nitrate ions from wastewater. The XRD, FTIR and SEM result analysis confirmed that nitrate ion was successfully adsorbed by Fe_3O_4 loaded CSH composite. The absorption peak from 465-618 cm^{-1} indicates the stretching vibration of Fe-O, which well-confirmed successful attachment of Fe_3O_4 to the Calcium silicate hydrate. In addition, the peak at 1384 cm^{-1} after adsorption was responsible for nitrate ion, which shows nitrate adsorption by Fe_3O_4 loaded CSH composite. Moreover, the diffraction peak at 2θ of 20.5º and 35.8º illustrated the adsorption of nitrate on the surface of Calcium Silicate Hydrate. The specific surface area of Fe_3O_4 loaded CSH obtained from BET analysis was 162 m^2/g.

The Response Surface Method (RSM) adopted to explore the model equation for nitrate removal efficiency. The central composite design was selected to study the effect of variation in pH, initial nitrate concentration, contact time, and adsorbent dose. The validation of the model using ANOVA analysis verified that the quadratic model selected is accurate, and statistically significant with a p-value less than 0.05. The optimum removal efficiency of 93.06% was obtained at pH= 6.3, C_o = 85 mg/L, t = 150 min, and dose = 2.4 g. The result shows the interaction effect of those parameters had a significant effect on the adsorption process.

The Langmuir isotherm model was in better agreement with the experimental data with maximum adsorption capacity and correlation coefficient (R^2) of 27.933 mg/g, and 0.993 respectively. This suggests that the adsorption process followed monolayer adsorption onto the surface of a finite number of identical adsorption sites. Nitrate adsorption kinetics was explained properly through the pseudo-second-order kinetics model (R^2 = 0.999), which indicated that the chemical adsorption became the controlling mechanism of the adsorption process. In addition, the thermodynamics parameters recommended that the nitrate removal is spontaneous and endothermic in nature.

The batch experimental studies for real wastewater by selecting Adama Science and Technology University treatment plant as nitrate-nitrogen source. The result investigated showed that 69.9% of NO_3-N was removed from wastewater. The reduction in removal efficiency from that of synthetic wastewater was due to large amount of total phosphates, nitrite-nitrogen, ammonia-nitrogen, and organic nitrogen were present in wastewater, which competes within nitrate ions during the adsorption process.

The effects of competing ion on nitrate adsorption by Fe_3O_4 loaded CSH composite was found to follow this order $CO_3^{2-} < Cl^- < PO_4^{3-}$. Adsorption regeneration study of Fe_3O_4 loaded CSH composite was investigated using 1M of NaOH as an eluent, which is the most prominent desorption agent. The adsorption- desorption of four cycle carried out successfully. According to this study, the result found indicates that the adsorbent is determined to be the best promising and effective for removal of nitrates ion from aqueous solution and wastewater.

5.2. Recommendation

For the future work, the following recommendations suggested based on the result obtained from this study.

- It is recommended that study the effects of adsorption parameters such as particle size, temperature and agitation speed.
- In this work batch equilibrium isotherm, kinetics and thermodynamics were conducted. However, the data obtained are not sufficient and feasible convert this batch experimental result in to the real wastewater. In order to get accurate adsorption result for industrial scale a continuous column adsorption study should be considered.
- The point of zero charge should be studied to obtain the possible attraction and repulsion between the adsorbent and adsorbate. Moreover, to identify information regarding ionization of functional groups and contact of ions with the adsorbent in the solution.
- The regeneration of the adsorbent was investigated by using NaOH as eluent agent. The determination of the most preferable regenerating solution is a very essential. Therefore, further studies on effectiveness of other regenerating solutions such as H_2SO_4, HCl, $NaNO_3$, NH_4Cl, HNO_3 and $CaCl_2$ should be investigated.

Grant Number: ASTU/SM-R/341/21

REFERENCE

Abdalla, M. M., Lung, C. Y. K., Neelakantan, P., & Matinlinna, J. P. (2020). A novel, doped calcium silicate bioceramic synthesized by sol–gel method: Investigation of setting time and biological properties. *Journal of Biomedical Materials Research - Part B Applied Biomaterials*, *108*(1), 56–66. https://doi.org/10.1002/jbm.b.34365

Abdolmohammad-zadeh, H., Tavarid, K., & Talleb, Z. (2012). *Determination of Iodate in Food , Environmental , and Biological Samples after The cientific WorldJOURNAL Research Article Determination of Iodate in Food , Environmental , and Biological Samples after Solid-Phase Extraction with Ni-Al-Zr Ternary Layered Double Hydroxide as a Nanosorbent*. *April*. https://doi.org/10.1100/2012/145482

Abegaz, M. T., & Midekssa, M. J. (2021). Quality and Safety of Rural Community Drinking Water Sources in Guto Gida District, Oromia, Ethiopia. *Journal of Environmental and Public Health*, *2021*. https://doi.org/10.1155/2021/5568375

Abraha, K. (2015). *Various sizes of the synthesized Fe_3O_4 nanoparticles assisted by mechanical vibrations*. *22*(April), 175–180.

Al-anber, M. A. (2011). *Thermodynamics Approach in the Adsorption of Heavy Metals*.

Alagha, O., Manzar, M. S., Zubair, M., Anil, I., Mu'azu, N. D., & Qureshi, A. (2020). Comparative adsorptive removal of phosphate and nitrate from wastewater using biochar-MgAl LDH nanocomposites: Coexisting anions effect and mechanistic studies. *Nanomaterials*, *10*(2). https://doi.org/10.3390/nano10020336

Ali, A., Shah, T., Ullah, R., Zhou, P., & Guo, M. (2021). *Review on Recent Progress in Magnetic Nanoparticles : Synthesis , Characterization , and Diverse Applications*. *9*(July), 1–25. https://doi.org/10.3389/fchem.2021.629054

Alighardashi, A. (2018). *Development and Application of Graphene Oxide / Poly-Amidoamines Dendrimers (GO / PAMAMs) Nano-Composite for Nitrate Removal from Aqueous Solutions*. 41–64.

Aragaw, T. A., & Angerasa, F. T. (2020). Heliyon Synthesis and characterization of Ethiopian kaolin for the removal of basic yellow (BY 28) dye from aqueous solution as a potential adsorbent. *Heliyon*, *6*(September), e04975. https://doi.org/10.1016/j.heliyon.2020.e04975

Asab, G., Zereffa, E. A., & Seghne, T. A. (2020). *Synthesis of Silica-Coated Fe 3 O 4 Nanoparticles by Microemulsion Method : Characterization and Evaluation of Antimicrobial Activity*. *2020*.

Asl, M. K., Hasani, A. H., & Naserkhaki, E. (2016). *Evaluation of Nitrate Removal from Water Using Activated Carbon and Clinoptilolite by Adsorption Method*. *13*(June), 1045–1054.

Ayawei, N., Ebelegi, A. N., & Wankasi, D. (2017). *Modelling and Interpretation of Adsorption Isotherms*. *2017*.

Azeddine, C., Djouadi, D., & Aksas, A. (2013). *Study of structural and optical properties of iron doped ZnO thin films prepared by sol-gel Study of structural and optical properties of iron doped ZnO thin films prepared by sol-gel*. *October*. https://doi.org/10.1051/epjap/2013130336

Balan, E., Fritsch, E., Radtke, G., Paulatto, L., Juillot, F., Baron, F., Petit, S., & Balan, C. E. (2021). *First-principles modeling of the infrared spectrum of Fe- and Al-bearing lizardite*. 647–657.

Batool, F., Akbar, J., Iqbal, S., Noreen, S., Nasir, S., & Bukhari, A. (2018). *Study of Isothermal , Kinetic , and Thermodynamic Parameters for Adsorption of Cadmium : An Overview of Linear and Nonlinear Approach and Error Analysis*. *2018*.

Battas, A., El Gaidoumi, A., Ksakas, A., & Kherbeche, A. (2019). Adsorption study for the removal of nitrate from water using local clay. *Scientific World Journal*, *2019*. https://doi.org/10.1155/2019/9529618

Begaye, M. (2014). *Synthesis and Multi-Scale Characterization of Calcium Silicate Hydrate at Multiple CaO / SiO2 Mixture Ratios*.

Berkessa, Y. W., Mereta, S. T., & Feyisa, F. F. (2019). Simultaneous removal of nitrate and phosphate from wastewater using solid waste from factory. *Applied Water Science*, *9*(2), 1–10. https://doi.org/10.1007/s13201-019-0906-z

Bhattacharya, S. (2021). *Central Composite Design for Response Surface Methodology and Its Application in Pharmacy*.

Brindha, K., Renganayaki, S. P., & Elango, L. (2017). Sources, toxicological effects and removal techniques of nitrates in groundwater: An overview. *Indian Journal of Environmental Protection*, *37*(8), 667–700.

Byong Yong Yu, and S.-Y. K. (2010). *Assembly of Magnetite Nanoparticles into Spherical Mesoporous Aggregates with a 3-D Wormhole-Like Porous Structure*. *c*, 1–9.

Chen, J., Wei, Y., Ji, H., Guo, P., & Wan, D. (2021). *Adsorption of nitrate and nitrite from aqueous solution by magnetic Mg / Fe hydrotalcite*. *21*(8). https://doi.org/10.2166/ws.2021.184

Chen, M. S., Santra, A. K., & Goodman, D. W. (2004). *Structure of thin SiO 2 films grown on Mo „ 112 …. November 2003*, 1–7. https://doi.org/10.1103/PhysRevB.69.155404

Chi Tei. (2019). In *Introduction to Adsorption*. https://doi.org/10.1016/b978-0-12-816446-4.09991-7

Crini, G., Lichtfouse, E., Wilson, L. D., & Morin-Crini, N. (2019). Conventional and non-conventional adsorbents for wastewater treatment. *Environmental Chemistry Letters*, *17*(1), 195–213. https://doi.org/10.1007/s10311-018-0786-8

Dehghani, M., Haidari, E., Shahsavani, S., & Shamsedini, N. (2015). *Removal of Nitrate in the Aqueous Phase Using Granular Ferric Hydroxide*. *7*(2). https://doi.org/10.5812/jjhs.7(2)2015.26419

Dey, S., Haripavan, N., Basha, S. R., & Babu, G. V. (2021). Current Research in Chemical Biology Removal of ammonia and nitrates from contaminated water by using solid waste bio-adsorbents. *Current Research in Chemical Biology*, *1*, 100005. https://doi.org/10.1016/j.crchbi.2021.100005

El-ashgar, N. M. (2020). *Removal of nitrate from groundwater by eggshell biowaste Ahmed H. Jendia, So fi ah Hamzah, A. A. Abuhabib and Nizam M. El-Ashgar*. 2514–2529. https://doi.org/10.2166/ws.2020.151

El Ouardi, M., Qourzal, S., Alahiane, S., Assabbane, A., & Douch, J. (2015). Effective Removal of Nitrates Ions from Aqueous Solution Using New Clay as Potential Low-Cost Adsorbent. *Journal of Encapsulation and Adsorption Sciences*, *05*(04), 178–190. https://doi.org/10.4236/jeas.2015.54015

Fang, D., Huang, L., Fang, Z., Zhang, Q., Shen, Q., Li, Y., Xu, X., & Ji, F. (2018). Evaluation of porous calcium silicate hydrate derived from carbide slag for removing phosphate from wastewater. *Chemical Engineering Journal*, *354*(July), 1–11. https://doi.org/10.1016/j.cej.2018.08.001

Fewtrell. (2004). *Children ' s Health | Review Drinking-Water Nitrate , Methemoglobinemia , and Global Burden of Disease : 112*(14), 1371–1374. https://doi.org/10.1289/ehp.7216

Foo, K. Y., & Hameed, B. H. (2010). *Insights into the modeling of adsorption isotherm systems*. *156*, 2–10. https://doi.org/10.1016/j.cej.2009.09.013

Ganesan, P., Kamaraj, R., & Vasudevan, S. (2013). Application of isotherm, kinetic and thermodynamic models for the adsorption of nitrate ions on graphene from aqueous solution. *Journal of the Taiwan Institute of Chemical Engineers*, *44*(5), 808–814. https://doi.org/10.1016/j.jtice.2013.01.029

Gensh, K. V, Kolosov, P. V, & Bazarnova, N. G. (2011). *Quantitative Analysis of Cellulose Nitrates by Fourier Transform Infrared Spectroscopy*. *37*(7), 814–816. https://doi.org/10.1134/S1068162011070077

German, T., Council, A., & Sru, E. (2015). *NITROGEN : Strategies ZUKUNFT environmental GESTALTEN problem*. *January*.

Ghadiri, S. K., Nasseri, S., Nabizadeh, R., Khoobi, M., Nazmara, S., & Mahvi, A. H. (2017). Adsorption of nitrate onto anionic bio-graphene nanosheet from aqueous solutions: Isotherm and kinetic study. *Journal of Molecular Liquids*, *242*, 1111–1117. https://doi.org/10.1016/j.molliq.2017.06.122

Ghandoor, H. El, Zidan, H. M., Khalil, M. M. H., & Ismail, M. I. M. (2012). *Synthesis and Some Physical Properties of Magnetite (Fe 3 O 4) Nanoparticles*. *7*, 5734–5745.

Gierak, A., & Łazarska, I. (2017). Adsorption of nitrate, nitrite, and ammonium ions on carbon adsorbents. *Adsorption Science and Technology*, *35*(7–8), 721–727. https://doi.org/10.1177/0263617417708085

Grassi, M., Kaykioglu, G., Belgiorno, V., & Lofrano, G. (2012). Emerging Compounds Removal from Water and Wastewater by Adsorption Process. *SpringerBriefs in Green Chemistry for Sustainability*, 15–37. https://doi.org/10.1007/978-94-007-3916-1

Guan, W., Ji, F., Chen, Q., Yan, P., & Pei, L. (2013). Synthesis and enhanced phosphate recovery property of porous calcium silicate hydrate using polyethyleneglycol as pore-generation agent. *Materials*, *6*(7), 2846–2861. https://doi.org/10.3390/ma6072846

Guan, W., Ji, F., Cheng, Y., Fang, Z., Fang, D., Yan, P., & Chen, Q. (2013). A novel synthesis method of porous calcium silicate hydrate based on the calcium oxide/polyethylene glycol composites. *Journal of Nanomaterials*, *2013*. https://doi.org/10.1155/2013/542109

Gul, S., Khan, S. B., Rehman, I. U., Khan, M. A., & Khan, M. I. (2019). *A Comprehensive Review of Magnetic Nanomaterials Modern Day Theranostics*. *6*(July), 1–15. https://doi.org/10.3389/fmats.2019.00179

Hai, T. H. I., & Bui, L. (2013). *REMOVAL OF NITRATE FROM WATER AND WASTEWATER BY AMMONIUM- FUNCTIONALIZED SBA-16 MESOPOROUS SILICA Résumé long*.

Hariani, P. L., Faizal, M., Ridwan, R., Marsi, M., & Setiabudidaya, D. (2013). Synthesis and Properties of Fe3O4 Nanoparticles by Co-precipitation Method to Removal

Procion Dye. *International Journal of Environmental Science and Development, November 2015*, 336–340. https://doi.org/10.7763/ijesd.2013.v4.366

Heck, K. N., Garcia-Segura, S., Westerhoff, P., & Wong, M. S. (2019). Catalytic Converters for Water Treatment. *Accounts of Chemical Research*, *52*(4), 906–915. https://doi.org/10.1021/acs.accounts.8b00642

Helard, D., Indah, S., Sari, C. M., & Mariesta, H. (2018). *The Adsorption and Regeneration of Natural Pumice as Low- Cost Adsorbent for Nitrate Removal From Water*. *03*(02). https://doi.org/10.24273/jgeet.2018.3.2.1545

Ho, Y. S., Porter, J. F., & Mckay, G. (2002). *DIVALENT METAL IONS ONTO PEAT : COPPER , NICKEL AND LEAD SINGLE COMPONENT SYSTEMS*. 1–33.

Ibrahim, I., & Bsharat, M. (2018). *The use of magnetic multiwalled carbon nanotubes functionalized with chitosan for nitrate removal from wastewater The use of magnetic multiwalled carbon nanotubes functionalized with chitosan for nitrate removal from wastewater*.

Ibrahim, M. E. E.-S. and S. S. (2021). *Application of central composite design approach for optimization nitrate removal from aqueous solution by immobilized Pseudomonas putida Marwa E. El-Sesy and Sabah S. Ibrahim*. 2931–2946. https://doi.org/10.2166/wst.2021.190

Ince, M. I. and O. K. (2019). *We are IntechOpen , the world ' s leading publisher of Open Access books Built by scientists , for scientists TOP 1 % Using Response Surface Methodology : Water / Wastewater Treatment*.

Jiang, D., Amano, Y., & Machida, M. (2017). Removal and recovery of phosphate from water by a magnetic Fe3O4@ASC adsorbent. *Journal of Environmental Chemical Engineering*, *5*(5), 4229–4238. https://doi.org/10.1016/j.jece.2017.08.007

Karthikeyan, P., & Meenakshi, S. (2019). Synthesis and characterization of Zn–Al LDHs/activated carbon composite and its adsorption properties for phosphate and nitrate ions in aqueous medium. *Journal of Molecular Liquids*, *296*, 111766. https://doi.org/10.1016/j.molliq.2019.111766

Katal, R., Baei, M. S., Rahmati, H. T., & Esfandian, H. (2012). Kinetic, isotherm and thermodynamic study of nitrate adsorption from aqueous solution using modified rice husk. *Journal of Industrial and Engineering Chemistry*, *18*(1), 295–302. https://doi.org/10.1016/j.jiec.2011.11.035

Keshav, V., Franklyn, P., & Kondiah, K. (2019). *Recombinant Fusion Protein PbrD Cross-Linked to Calcium Alginate Nanoparticles for Pb Remediation*.

https://doi.org/10.1021/acsomega.9b01624

Keskin, T. E. (2010). Nitrate and heavy metal pollution resulting from agricultural activity: A case study from Eskipazar (Karabuk, Turkey). *Environmental Earth Sciences*, *61*(4), 703–721. https://doi.org/10.1007/s12665-009-0385-x

Khan, M. A., Ahn, Y., Kumar, M., & Lee, W. (2011). *Adsorption Studies for the Removal of Nitrate Using Modified Lignite Granular Activated Carbon*. *March 2014*. https://doi.org/10.1080/01496395.2011.601782

Kheshti, Zeinab; Hassanajili, Shadi; Shahrashoob, Z. (2019). *Facile and Economic Method for the Preparation of Core-Shell Magnetic Mesoporous Silica*. *38*(5), 1–9.

Kulkarni, S., & Kaware, J. (2014). *Regeneration and Recovery in Adsorption- a Review*. *1*(8), 61–64.

Kuwahara, Y., & Yamashita, H. (2017). Phosphate removal from aqueous solutions using calcium silicate hydrate prepared from blast furnace slag. *ISIJ International*, *57*(9), 1657–1664. https://doi.org/10.2355/isijinternational.ISIJINT-2017-123

Lai, L., Xie, Q., Chi, L., Gu, W., & Wu, D. (2016). Adsorption of phosphate from water by easily separable Fe3O4@SiO2 core/shell magnetic nanoparticles functionalized with hydrous lanthanum oxide. *Journal of Colloid and Interface Science*, *465*, 76–82. https://doi.org/10.1016/j.jcis.2015.11.043

Li, J., Shi, X., & Shen, M. (2014). *Hydrothermal Synthesis and Functionalization of Iron Oxide Nanoparticles for MR Imaging Applications*. 1223–1237. https://doi.org/10.1002/ppsc.201400087

Loganathan, P., Vigneswaran, S., & Kandasamy, J. (2013). Enhanced removal of nitrate from water using surface modi fi cation of adsorbents e A review. *Journal of Environmental Management*, *131*, 363–374. https://doi.org/10.1016/j.jenvman.2013.09.034

Loh, K. S., Musa, A., & Ishak, Z. (2008). *Use of Fe3O4 Nanoparticles for Enhancement of Biosensor Response to the Herbicide 2,4-Dichlorophenoxyacetic Acid*. *September*. https://doi.org/10.3390/s8095775

Loon, Y., & Fong, Y. (2016). *Optimization of Nitrate Removal from Aqueous Solution by Amine- Functionalized MCM-41 using Response Surface Methodology*. *148*, 1239–1246. https://doi.org/10.1016/j.proeng.2016.06.485

Mehrabi, N., Soleimani, M., Yeganeh, M. M., & Shari, H. (2015). *RSC Advances Parameter optimization for nitrate removal from water using activated carbon and composite of activated carbon and Fe 2 O 3 nanoparticles*. 51470–51482.

https://doi.org/10.1039/c5ra03920g

Moghadam, F., Bagheri, S., & Khamar, M. (2018). *Evaluation of Chitosan Adsorbent Efficiency in Nitrate Removal from Aqueous Solutions and the Effect of Parameters on Adsorption Process*. *5*(5), 83–86.

Mohammed, L., Gomaa, H. G., Ragab, D., & Zhu, J. (2017). Magnetic nanoparticles for environmental and biomedical applications: A review. *Particuology*, *30*, 1–14. https://doi.org/10.1016/j.partic.2016.06.001

Mor, S., Chhoden, K., & Ravindra, K. (2016). Application of agro-waste rice husk ash for the removal of phosphate from the wastewater. *Journal of Cleaner Production*, *129*, 673–680. https://doi.org/10.1016/j.jclepro.2016.03.088

Nabhan, A. (2019). *Nitrate removal from water using activated carbon prepared from olive stone by microwave heating*.

Nigussie, W., Zewge, F., & Chandravanshi, B. S. (2007). *Removal of excess fluoride from water using waste residue from alum manufacturing process*. *147*, 954–963. https://doi.org/10.1016/j.jhazmat.2007.01.126

Noval, V. E., & Universitaria, C. (2019). *Fe 3 O 4 -TiO 2 and Fe 3 O 4 -SiO 2 Core-shell Powders Synthesized from Industrially Processed Magnetite (Fe 3 O 4) Microparticles*. *22*(3).

Nsami, J. N., & Mbadcam, J. K. (2013). *The Adsorption Efficiency of Chemically Prepared Activated Carbon from Cola Nut Shells by ZnCl 2 on Methylene Blue*. *2013*.

Ogata, F., Imai, D., & Kawasaki, N. (2015). Adsorption of nitrate and nitrite ions onto carbonaceous material produced from soybean in a binary solution system. *Journal of Environmental Chemical Engineering*, *3*(1), 155–161. https://doi.org/10.1016/j.jece.2014.11.025

Olalekan, A. P., Olatunya, A., Ekiti, A., & Dada, A. O. (2012). *Langmuir , Freundlich , Temkin and Dubinin – Radushkevich Isotherms Studies of Equilibrium Sorption of Zn 2 + Unto Phosphoric Acid Modified Rice Husk*. *January*. https://doi.org/10.9790/5736-0313845

Palko, J. W., Oyarzun, D. I., Ha, B., Stadermann, M., & Santiago, J. G. (2018). Nitrate removal from water using electrostatic regeneration of functionalized adsorbent. *Chemical Engineering Journal*, *334*, 1289–1296. https://doi.org/10.1016/j.cej.2017.10.161

Peng, L., Dai, H., Wu, Y., Dai, Z., Li, X., & Lu, X. (2017). Performance and adsorption

mechanism of a magnetic calcium silicate hydrate composite for phosphate removal and recovery. *Water Science and Technology*, *2017*(2), 578–591. https://doi.org/10.2166/wst.2018.184

Pizarro, A. H., Torija, I., & Monsalvo, V. M. (2018). *Enhancement of Pd-based catalysts for the removal of nitrite and nitrate from water*. 615–625. https://doi.org/10.2166/aqua.2018.024

Rafiee, R. N. J. and M. (2014). *Counterion Effects on Nitrate Adsorption from Aqueous Solution onto Functionalized Polyacrylonitrile Coated with Iron Oxide Nanoparticles - 287-293.pdf*.

Rajasulochana, P., & Preethy, V. (2016). Comparison on efficiency of various techniques in treatment of waste and sewage water – A comprehensive review. *Resource-Efficient Technologies*, *2*(4), 175–184. https://doi.org/10.1016/j.reffit.2016.09.004

Rakshitha R, Y. S. R. (2017). *Removal of Nitrate from Water by Chitosan , Clay and Activated Carbon as Adsorbents : A Mini Review Rakshitha R *, Yashas S R **. 7*(10), 46–51. https://doi.org/10.9790/9622-0710054651

Ranjan, S., Dasgupta, N., & Lichtfouse, E. (2016). *Nanoscience in Food and Agriculture*.

Rasuli, L., Nasseri, S., & Hadi, M. (2020). *Performance of surfactant-modified forms of clinoptilolite and pumice in nitrate removal from aqueous solution*. *180*, 227–236. https://doi.org/10.5004/dwt.2020.24861

Rezvani, F., Sarrafzadeh, M. H., Ebrahimi, S., & Oh, H. M. (2019). Nitrate removal from drinking water with a focus on biological methods: a review. *Environmental Science and Pollution Research*, *26*(2), 1124–1141. https://doi.org/10.1007/s11356-017-9185-0

Ruiz-Beviá, F., & Fernández-Torres, M. J. (2019). Effective catalytic removal of nitrates from drinking water: An unresolved problem? *Journal of Cleaner Production*, *217*, 398–408. https://doi.org/10.1016/j.jclepro.2019.01.261

S. P. Burghate1*, D. N. W. I. (2014). *Journal of Environmental Science , Computer Science and Engineering & Technology*. *February*.

Sadegh, H., Mazloumbilandi, M., & Chahardouri, M. (2019). Low-cost materials with adsorption performance. In *Handbook of Ecomaterials* (Vol. 5). https://doi.org/10.1007/978-3-319-68255-6_175

Sarma, G. K., & Bhattacharyya, S. S. G. K. G. (2019). Removal of hazardous basic dyes from aqueous solution by adsorption onto kaolinite and acid - treated kaolinite : kinetics , isotherm and mechanistic study. *SN Applied Sciences*, *1*(3), 1–15.

https://doi.org/10.1007/s42452-019-0216-y

Sato, T. (2016). *Structure of nanocrystalline calcium silicate hydrates : insights from X-ray diffraction , synchrotron X-ray absorption and nuclear magnetic resonance research papers*. 771–783. https://doi.org/10.1107/S1600576716003885

Sepehri, S., Heidarpour, M., & Abedi-Koupai, J. (2014). Nitrate removal from aqueous solution using natural zeolite-supported zero-valent iron nanoparticles. *Soil and Water Research*, *9*(4), 224–232. https://doi.org/10.17221/11/2014-swr

Singh, P. K., Banerjee, S., Srivastava, A. L., & Sharma, Y. C. (2015). *RSC Advances Kinetic and equilibrium modeling for removal of by a potential adsorbent , hydrous bismuth oxide*. 35365–35376. https://doi.org/10.1039/c4ra11213j

Soares, O. S. G. P. (2020). *Nitrate Catalytic Reduction over Bimetallic Catalysts : Catalyst Optimization*. *3*.

Sun, Y., Zheng, W., Ding, X., & Singh, R. P. (2020). Selective removal of nitrate using a novel asymmetric amine based strongly basic anion exchange resin. *Adsorption Science and Technology*, *38*(7–8), 271–285. https://doi.org/10.1177/0263617420945839

Suzaimi, N. D., Goh, P. S., & Malek, N. A. N. N. (2019). *Modified-Nano-Adsorbents for Nitrate Efficient Removal : A Review*. *23*(2), 65–81.

Teklu, K. T. (2018). *Spatial Distribution of Nitrate in the Drinking Water Sources Found in Ethiopia ; Retrospective Study*. *July*.

Temesgen Getahun. (2019). *Center for Environmental Science Zeolite-Zinc Oxide Nano composite for Removal of Nitrate from Spiked and Groundwater*.

Tohfegar, E., Moghaddas, J. S., Sharifzadeh, E., & Esmaeilzadeh–Dilmaghani, S. (2019). Synthesis and Characterization of Waterglass-Based Silica Aerogel Under Heat Treatment for Adsorption of Nitrate from Water : Batch and Column Studies. *Iranian Journal of Chemical Engineering*, *16*(4), 53–72.

Tsamo, C., Paltahe, A., Fotio, D., Vincent, T. A., & Sales, W. F. (2019). *Thermodynamic Evaluation of Co (II) Removal from Aqueous Solution Using Dead Neem Leaves*. *2019*.

Tyagi, S., Rawtani, D., Khatri, N., & Tharmavaram, M. (2018). *Journal of Water Process Engineering Strategies for Nitrate removal from aqueous environment using Nanotechnology : A Review*. *21*(September 2017), 2017–2019.

Velusamy, K., Periyasamy, S., Senthil, P., Dai, K., Nguyen, V., & Electrodialysis, E. D. (2021). Advanced techniques to remove phosphates and nitrates from waters : a

review. *Environmental Chemistry Letters*. https://doi.org/10.1007/s10311-021-01239-2

Vicente-mart, Y., Caravaca, M., Soto-meca, A., Miguel, Á., & Garc, C. (2021). *Adsorption Studies on Magnetic Nanoparticles Functionalized with Silver to Remove Nitrates from Waters*.

Wakene, A., Zewge, F., Chebude, Y., & Tesfaye, M. (2021). Phosphate abatement using calcium silicate hydrate synthesized from alum factory solid waste residue. *Separation Science and Technology*, *00*(00), 1–19. https://doi.org/10.1080/01496395.2021.1998125

Wang, H., Li, C., & Peng, Z. (2011). *Characterization and thermal behavior of kaolin Characterization and thermal behavior of kaolin*. *July*. https://doi.org/10.1007/s10973-011-1385-0

Wang, J., & Guo, X. (2020). Adsorption isotherm models: Classification, physical meaning, application and solving method. *Chemosphere*, *258*, 127279. https://doi.org/10.1016/j.chemosphere.2020.127279

Wang, S., Yao, S., Du, K., Yuan, R., Chen, H., Wang, F., & Zhou, B. (2021). *The mechanisms of conventional pollutants adsorption by modified granular steel slag*. *26*(1), 0–1.

Wu, J., Zhu, Y. J., & Chen, F. (2013). Ultrathin calcium silicate hydrate nanosheets with large specific surface areas: Synthesis, crystallization, layered self-assembly and applications as excellent adsorbents for drug, protein, and metal ions. *Small*, *9*(17), 2911–2925. https://doi.org/10.1002/smll.201300097

Wubishet, D. L., Abi, T. M., & Fekadu, D. T. (2020). *Al 2 O 3 / Fe 3 O 4 / ZrO 2 Ternary Nanosorbent : Synthesis and Characterization for Organic Dyes and Toxic Heavy Metals Removal from Wastewater*. *11*(8), 1341–1360.

Xiaowen Tong, Zhiquan Yang, Pan Xu, Y. L. and X. N. (2017). *Nitrate adsorption from aqueous solutions by calcined ternary Mg-Al-Fe hydrotalcite Xiaowen Tong , Zhiquan Yang , Pan Xu , Ying Li and Xiaojun Niu*. 2194–2203. https://doi.org/10.2166/wst.2017.082

Yang, L., Yang, M., Xu, P., Zhao, X., Bai, H., & Li, H. (2017). Characteristics of nitrate removal from aqueous solution by modified steel slag. *Water (Switzerland)*, *9*(10). https://doi.org/10.3390/w9100757

Zayat, D. L. and M. (2005). *Sol gel hand book.*

Zeng, L., & Yang, L. (2015). Preparation and characterization of Ni-doped calcium

silicate hydrate based on steel slag: Adsorption capacity for rhodamine B from aqueous solution. *Journal of Chemistry*, *2015*. https://doi.org/10.1155/2015/131050

Zewdie, T. M., Prihatiningtyas, I., Dutta, A., & Habtu, N. G. (2021). *Characterization and beneficiation of Ethiopian kaolin for use in fabrication of ceramic membrane Characterization and bene fi ciation of Ethiopian kaolin for use in fabrication of ceramic membrane*.

Zhang, H., Liu, Q., Wang, J., Liu, J., Yan, H., Jing, X., & Zhang, B. (2015). Preparation of magnetic calcium silicate hydrate for the efficient removal of uranium from aqueous systems. *RSC Advances*, *5*(8), 5904–5912. https://doi.org/10.1039/c4ra08678c

Zhao, H., Xue, Y., Long, L., & Hu, X. (2018). Adsorption of nitrate onto biochar derived from agricultural residuals. *Water Science and Technology*, *77*(2), 548–554. https://doi.org/10.2166/wst.2017.568

Zhou, H., Tan, Y., Gao, W., Zhang, Y., & Yang, Y. (2020). Selective nitrate removal from aqueous solutions by a hydrotalcite-like absorbent FeMgMn-LDH. *Scientific Reports*, *10*(1), 1–10. https://doi.org/10.1038/s41598-020-72845-3

Zhou, Y., Zheng, H., Qiu, Y., Zou, X., & Huang, J. (2020). *A Molecular Dynamics Study on the Structure , Interfaces , Mechanical Properties , and Mechanisms of a Calcium Silicate Hydrate / 2D-Silica Nanocomposite*. *7*(June), 1–14. https://doi.org/10.3389/fmats.2020.00127

Zhu, S., Fang, Y., Guo, Y., & Ma, X. (2019). Preparation of nano-calcium silicate hydrate and its application in concrete. *IOP Conference Series: Materials Science and Engineering*, *631*(2). https://doi.org/10.1088/1757-899X/631/2/022052

Zhu, Y. J., & Sham, T. K. (2014). The potential of calcium silicate hydrate as a carrier of ibuprofen. *Expert Opinion on Drug Delivery*, *11*(9), 1337–1342. https://doi.org/10.1517/17425247.2014.923399

Zia, M., Phull, A. R., & Ali, J. S. (2016). *challenges of iron oxide nanoparticles*. 49–67.

APPENDICES

Appendix A: BET specific surface area analysis of CSH and magnetic CSH (Fe_3O_4 loaded CSH)

Horiba Instruments, Inc.
SA-9600 Series Surface Area Analyzer

Analysis Report
Nov/08/2021

Customer	: Shimeles Nigussie	Operator ID	: SARA, CHEMO
Description	: Different Experiment	Analysis Date	: Nov/08/2021
Filename	: shimeles.sa2	Analysis Time	: 15:06:50

Condition Settings

Room Temp	: 27.0 (°C)	Atm. Pres	: 700.0 (mm)
Gas Used	: Nitrogen	Gas Conc	: 0.300, 0.002, 0.002 %

	Channel: 1	Channel: 2	Channel: 3
Sample Name	CSH	M CSH	
Tube Number	1	2	0
Tare Weight	10.1150 (gm)	9.9990 (gm)	0.0000 (gm)
Sample Weight	10.2240 (gm)	10.0720 (gm)	1.0000 (gm)
Degas Temp.	200 (°C)	200 (°C)	0 (°C)
Degas Time	120 (min)	120 (min)	0 (min)
Surface Area (M^2/gm)	91.294	162.887	-1.#IO
Slope	342.161	286.786	-1.#IO
Intercept	7.549	5.879	-1.#IO
Vm	0.003	0.003	-1.#IO
BET Const	46.326	49.782	-1.#IO
Pearson Coef	0.982	0.991	0.000
X[1] - 0.269	103.115	85.044	1.#IO
X[2] - 0.179	62.071	53.446	1.#IO
X[3] - 0.090	41.701	33.570	1.#IO

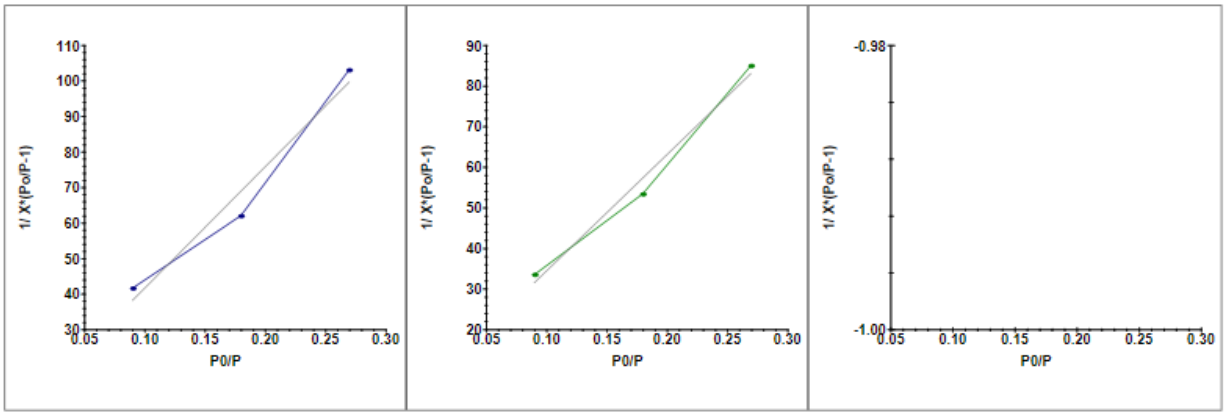

Appendix B: complete silicate analysis of aluminium sulphate solid waste residue

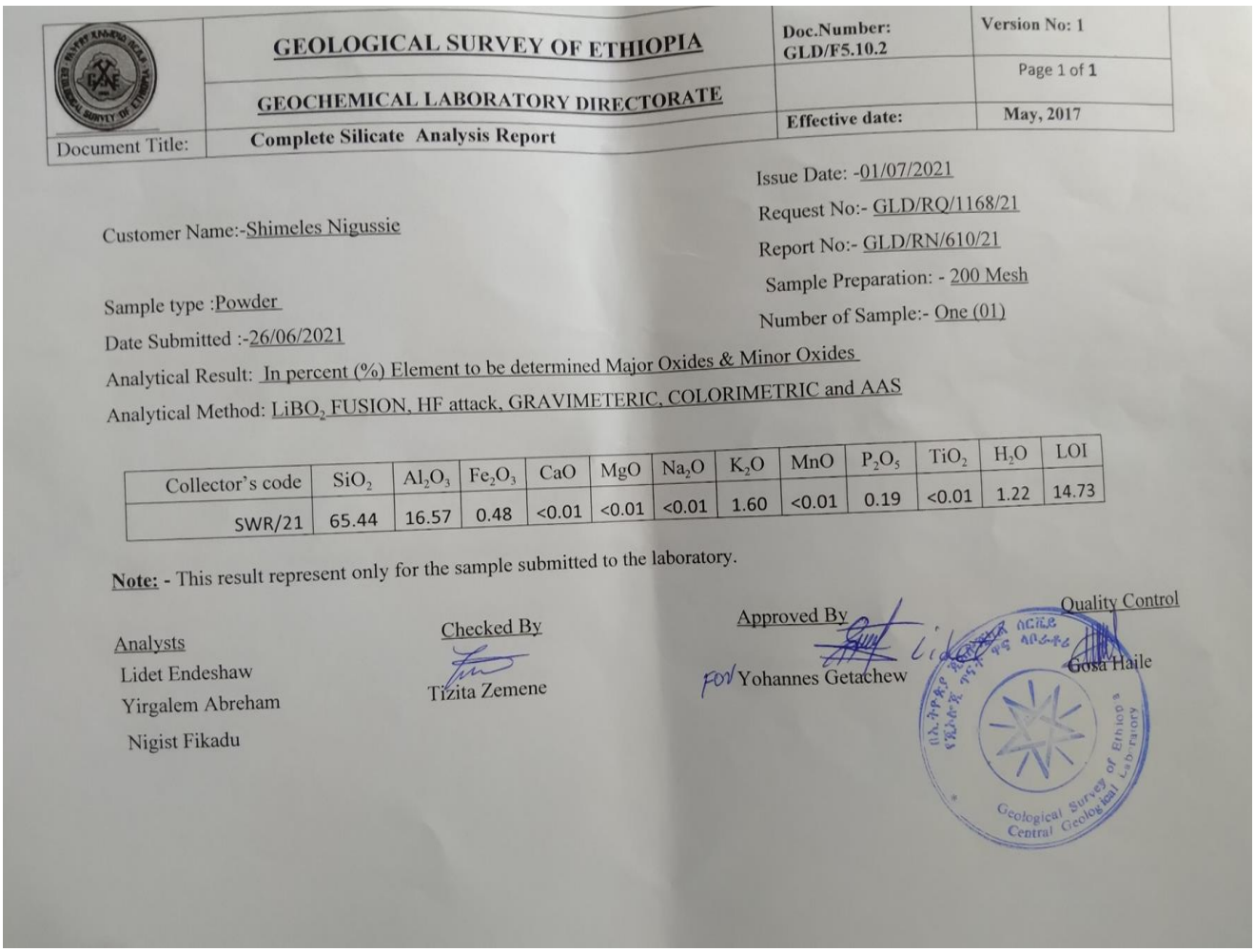

GEOLOGICAL SURVEY OF ETHIOPIA	Doc.Number: GLD/F5.10.2	Version No: 1
GEOCHEMICAL LABORATORY DIRECTORATE		Page 1 of 1
Document Title: Complete Silicate Analysis Report	Effective date:	May, 2017

Issue Date: -01/07/2021

Customer Name:-Shimeles Nigussie

Request No:- GLD/RQ/1168/21

Report No:- GLD/RN/610/21

Sample type :Powder

Sample Preparation: - 200 Mesh

Date Submitted :-26/06/2021

Number of Sample:- One (01)

Analytical Result: In percent (%) Element to be determined Major Oxides & Minor Oxides

Analytical Method: $LiBO_2$ FUSION, HF attack, GRAVIMETERIC, COLORIMETRIC and AAS

Collector's code	SiO_2	Al_2O_3	Fe_2O_3	CaO	MgO	Na_2O	K_2O	MnO	P_2O_5	TiO_2	H_2O	LOI
SWR/21	65.44	16.57	0.48	<0.01	<0.01	<0.01	1.60	<0.01	0.19	<0.01	1.22	14.73

Note: - This result represent only for the sample submitted to the laboratory.

Analysts
Lidet Endeshaw
Yirgalem Abreham
Nigist Fikadu

Checked By
Tizita Zemene

Approved By
FOR Yohannes Getachew

Quality Control
Gosa Haile

Geological Survey of Ethiopia Central Geological Laboratory

Appendix C: CSH Synthesis methods

Aluminium sulphate Solid Waste Residue

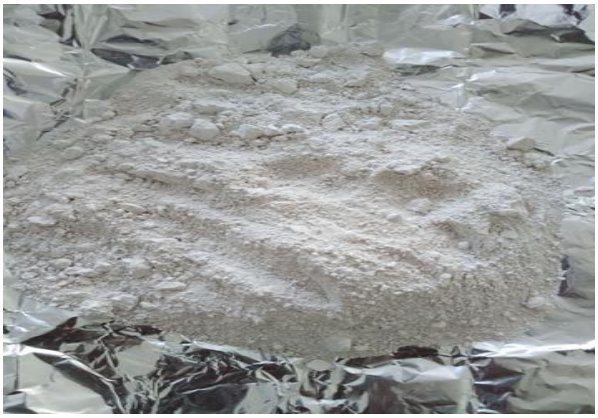

Prepared SWR

NaOH and SWR reaction

Separation of Na_2SiO_3 and Filter cake by Vacuum pump

Na_2SiO_3

Sized CSH product at 90 µm

CSH Product

Appendix D: Fe_3O_4 synthesis methods

Fe^{2+} and Fe^{3+}

NaOH droplet
to the mixture

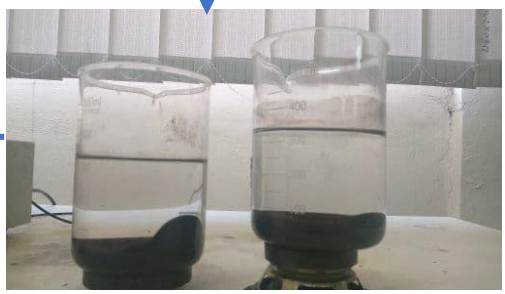

Washed Fe_3O_4

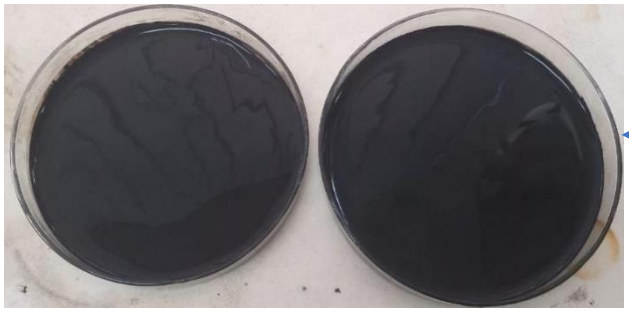

Fe_3O_4 product

Appendix E: Fe_3O_4 loaded CSH composite synthesis method

Fe_3O_4 and CSH

Ultrasonicator

Autoclave reactor

Fe_3O_4 loaded CSH Product

Fe_3O_4, Fe_3O_4 loaded CSH and CSH From left to right respectively.

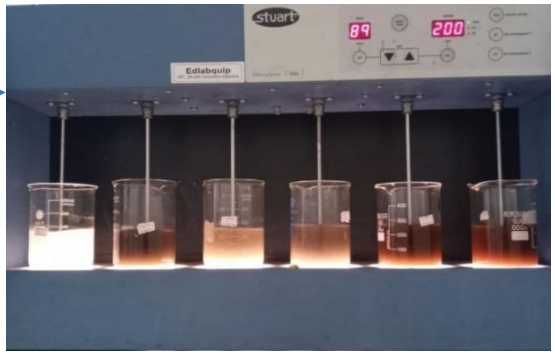

Adsorption process using CSH and Fe_3O_4 loaded CSH with different magnetite loading.

Appendix F: Band assignments of FTIR spectra of CSH and Fe_3O_4 loaded CSH

Functional Group	**Peak Position (cm^{-1})**	**Characteristics**
Ca-O	1402-1546, 870	Stretching vibration
Si-O-Si	760-850	Stretching or bending
	475	Asymmetric stretching vibration
	900-1180	Stretching vibration
Si-OH	3200-3390	Condensation of OH stretching vibration
	830-910	stretching vibration
H-O-H	1500-1680	Bending of water
	3000-400	Stretching vibration of water
$Si(OSi)_3O$-Ca	890-965	Stretching vibration
Si-O	1000-1250	Stretching of Si-O-Si cross-linked
Fe-O-H	795-900	Bending Vibration
NO_3^-	1340-1410	asymmetric stretching
	800-860	symmetric stretching
Fe-O	465-700	Stretching vibration
Al-O-Si	430-537	Skeletal vibration
Al-O	913	Bending Vibration
Fe-O-Si	667	Stretching vibration
Al-O-H	3620-3696	Stretching vibration

Appendix G: Solid waste Residue of Aluminium sulfate plant in Awash Melkassa Chemical Factory